Experimental and theoretical studies on the effects of smooth muscle on the mechanical response and remodeling of arteries

THÈSE N° 5793 (2014)

PRÉSENTÉE LE 7 MARS 2014

À LA FACULTÉ DES SCIENCES DE LA VIE
LABORATOIRE D'HÉMODYNAMIQUE ET DE TECHNOLOGIE CARDIOVASCULAIRE (SV/STI)
PROGRAMME DOCTORAL EN BIOTECHNOLOGIE ET GÉNIE BIOLOGIQUE

ÉCOLE POLYTECHNIQUE FÉDÉRALE DE LAUSANNE

POUR L'OBTENTION DU GRADE DE DOCTEUR ÈS SCIENCES

PAR

Aristotelis AGIANNIOTIS

acceptée sur proposition du jury:

Prof. M. Dal Peraro, président du jury
Prof. N. Stergiopulos, directeur de thèse
Prof. S. Greenwald, rapporteur
Prof. D. Pioletti, rapporteur
Prof. A. Rachev, rapporteur

ÉCOLE POLYTECHNIQUE
FÉDÉRALE DE LAUSANNE

Suisse
2014

The best way to predict the future is to invent it.

— Alan C. Kay

To my family for all their love and support…

ACKNOWLEDGEMENTS

I would like to acknowledge my co-workers, friends and family, who continuously supported me throughout my doctoral thesis.

Foremost, my advisor, Prof. Nikos Stergiopulos, was instrumental in providing a research atmosphere that encouraged independent thinking. Despite his independent approach, Prof. Stergiopulos would always provide consistent encouragement and a lot of time to discuss problems. I would like to thank the members of the jury for taking their time to read and discuss my research and for providing me with their suggestions regarding my thesis: Prof. Steve Greenwald, Prof. Dominique Pioletti, Prof. Alexander Rachev, and Prof. Matteo Dal Peraro. Finally, Prof. Rachev's incredible knowledge of mechanics was valuable in helping to develop the theories in this work. I thank him not only for the fruitful collaboration we have had, but also for his life lessons which were a constant source of inspiration.

I would like to thank Prof. Sokrates Tsangaris, my diploma thesis advisor and professor in the School of Mechanical Engineering of the National Technical University of Athens. He was an excellent source of scientific knowledge, he advised me to consider EPFL for graduate studies and he remains a real friend throughout the years.

I would like to thank Prof. Vassily Hatzimanikatis. He was my mentor at EPFL. I thank him for all the discussions we have had.

I owe certainly a great thanks to the former and current members of the Hemodynamics and Cardiovascular Technology Laboratory at EPFL. They made the lab a pleasant and challenging place to be. I will try to present them in the order that I met them. Dimitrios Kontaxakis, Stephan Bigler, Michel Bachman, Bryn Martin, Tamina Sissoko, Orestis Vardoulis, Alkiviadis Tsamis, Rana Saitta Rezakhaniha, Philippe Reymond, Adan Villamarin, Sylvain Roy, Tyler Thatcher, Rafaela Fernandez da Silva, Jelle Schrauwen, Martin Zulliger, Edouard Fonck, Mustapha Al Kharfane, Reda Hasballa, David Petiot, Aurélie Picquot, Prisci Briquez, Thiresia Giallourou, Christian Andrié, Luciano Capettini, Silvia Maia, Rodrigo Silva, Fabiana Fraga, Danielle Silva, Theodoros Papaioannou, Vanda Torrez Moya, Nicholas Metrakos.

Great thanks go to my friends in Lausanne and around the world. Without their help and support, my Ph.D. would not have been so enjoyable. I thank them not

only for their friendship, counsel and understanding, but also because they undertook the incredible task to distract me from my work and helped me have good time, relax and find new strength. My old-day friends Danis, Giannis, Alexandros, Sokratis, Spyros, my friends in Lausanne, Konstantinos, Aristeidis, Giannis, Polydeukis, Georgia, Aude, Ulli, Karoline, Emmanuelle, Diana, Rena, Fanny, Stefan, Gianluigi, Qingxia, my friends from Gent University, Patrick, Bram, Sander, Francesco. I would also like to give special thanks to Emilie.

I would like to acknowledge the financial support for this work by the Swiss National Science Foundation Grant 325230-125445.

Finally, I would like to thank my family, who have endlessly supported and encouraged me all the years. They have been a source of wisdom and motivation. Thank you so much!

Lausanne, 6.6.2013 Aristotelis Agianniotis

ABSTRACT

The purpose of this work is to contribute to the field of mechanics of the arterial wall. The role that each arterial wall constituent (elastin, collagen, vascular smooth muscle) plays in the mechanical properties and the remodeling of the arterial wall is experimentally investigated and mathematically modeled. The results are presented in the thesis in the form of an introduction, four chapters (a scientific article each) and a conclusion.

The introduction begins with the motivation for this work. A brief description and discussion of the arterial wall structure, the mathematical models for modeling the arterial wall and the remodeling of the arterial wall in response to changes in its mechanical environment are presented. Further, findings regarding two common vascular disorders (hypertension, atherosclerosis) are presented.

In the first work, we perform mechanical testing of mouse thoracic aortas at three different axial stretch ratios, namely at $\lambda_z = 1.6$, 1.8 and 2.0, and under maximally contracted or fully relaxed state of the vascular smooth muscle cells. The different values of axial stretch that we impose, allow each vessel to be tested below, near and above its *in vivo* axial stretch. Then, we present a methodology for the calculation of the active stresses in the circumferential and longitudinal direction. The study verifies the development of active axial stress in the wall of mouse aorta over a range of physiological loads when the smooth muscle cells are stimulated to contract. The results obtained show that the active axial stress is virtually independent of the magnitude of pressure, but it predominantly depends on the longitudinal stretch ratio. The dependence is non-monotonic and is similar to the active stress – stretch dependence in the circumferential direction reported in the literature. The expression for the active axial stress fitted to the experimental data shows that the maximum active stress is developed at longitudinal stretch ratio 1.81, and 1.56 is the longitudinal stretch ratio below which the stimulation does not generate active stress. Further, the study shows that the magnitude of active axial stress is smaller than the active circumferential stress. There is need for more experimental investigations on the active response of different types of arteries from different species and pathological conditions, and these results can promote building of refined constrictive models in vascular rheology.

In the second work, we analyze the mechanical properties of the thoracic aorta of the apolipoprotein E (apoE)-deficient mouse. The first goal of this study is to quantify the dysfunction of the aortic wall of the aorta. The second goal is to determine the mechanical properties, and to provide data that can be used in modeling the behavior of the arterial wall and in studying the growth and remodeling in the disease of atherosclerosis. For this study we perform inflation – extension mechanical tests at three different axial stretch ratios, namely at $\lambda_z = 1.6$, 1.8 and 2.0, and under maximally contracted or fully relaxed state of the vascular smooth muscle cells. Further, classical histology is performed on the arterial segments. The analysis of the data shows that a) the control aortas are generally more distensible than the (apoE)-deficient mouse aortas under both relaxed and contracted smooth muscle, b) aortas from (apoE)-deficient mice are stiffer than the control aortas, c) control aortas exhibit a higher active diameter response, despite the fact that vascular smooth muscle cell density is increased by approximately 15% in the (apoE)-deficient mouse aortas. We found substantial changes in the structural and elastic properties of the wall, in the active diameter response and in the histology of (apoE)-deficient mouse aortas compared to the control group. The data can be used in the development of constituent-based models of the arterial wall and in studying the changes in the arterial wall properties in the presence of disease, such as atherosclerosis.

In the third work, we build a constitutive model of the arterial tissue. The model considers a plausible link between part of elastin and the smooth muscle. The arterial tissue is considered as a constrained mixture of elastin, collagen, and smooth muscle cells. We consider two types of elastin that are involved in load bearing. One type of elastin is bonded to the smooth muscle cells, and the other part of elastin bears loads in concert with the collagen fibers. The opened-up configuration obtained from a circular ring after performing a radial cut is considered as a natural state of the vessel, but in this configuration the wall constituents are prestretched. We propose a method to quantify the prestretch ratios of the wall constituents by using data from normal and decellularized artery. We verify the model by comparing theoretically predicted against experimentally recorded pressure – radius curves of decellularized artery, and we perform sensitivity analysis of prestretch ratios.

In the fourth work, we perform theoretical simulations of modes of maladaptive remodeling in response to hypertension. We consider an artery to be a thick-walled cylindrical tube made of nonlinear, elastic, incompressible material. We

evaluate the relative importance of certain geometrical and mechanical factors. Given the values of hypertensive pressure and two parameters associated with vascular tone and arterial mass, we determine the outcomes of remodeling in terms of altered zero-stress state and deformed geometry from the conditions that the circumferential stress distribution and mean axial stress are restored to baseline values.

The conclusion section summarizes the main results of the thesis, presents improvements made over previous theoretical considerations and proposes future extensions of this work.

Keywords

Arterial remodeling; Adaptive remodeling; Maladaptive remodeling; Hypertension; Atherosclerosis; Material properties; Elastic properties; Elastin; Collagen; Vascular smooth muscle; Arteries; Apolipoprotein E; Mechanical test; Inflation – extension experiment; Histology

RÉSUMÉ

Cette thèse est destinée à contribuer au domaine de la mécanique de la paroi artérielle. Le rôle que joue chaque constituant de la paroi artérielle (élastine, collagène, muscle lisse vasculaire) dans les propriétés mécaniques et le remodelage de la paroi artérielle est étudié expérimentalement et modélisé mathématiquement. Les résultats sont présentés dans la thèse sous la forme d'une introduction, de quatre chapitres (quatre articles scientifiques) et d'une conclusion.

L'introduction commence par énoncer la motivation de ce projet. Une brève description et discussion de la structure de la paroi artérielle, des modèles mathématiques pour la modélisation de la paroi artérielle et le remodelage de la paroi artérielle en réponse au changement dans son environnement mécanique sont présentés. En outre, les résultats concernant deux pathologies vasculaires (hypertension, athérosclérose) sont présentés.

Dans le premier article nous effectuons des essais mécaniques aux aortes thoraciques de souris à trois différents rapports d'élongation axiale, à savoir à $\lambda_z =$ 1.6, 1.8 et 2.0, et sous l'état contracté au maximum ou sous l'état complètement relaxé des cellules musculaires lisses. Les différentes valeurs d'élongation axiale que nous imposons permettent à chaque vaisseau à être testé ci-dessous, près et au-dessus de son élongation axiale *in vivo*. Ensuite, nous présentons une méthodologie pour le calcul des contraintes actives en direction circonférentielle et longitudinale. L'étude confirme le développement de la contrainte axiale active dans la paroi de l'aorte de souris sur une plage de charges physiologiques lorsque les cellules musculaires lisses sont stimulées à se contracter. Les résultats obtenus montrent que la contrainte axiale active est pratiquement indépendante de l'amplitude de la pression, mais elle dépend essentiellement du rapport d'élongation longitudinale. La relation est non-monotone et est similaire à la relation de la contrainte active – élongation dans la direction circonférentielle rapportée dans la littérature. L'expression de la contrainte axiale active ajustée aux données expérimentales montre que la contrainte active maximale est élaborée à rapport d'élongation longitudinale 1.81, et 1.56 est le rapport d'élongation longitudinale au-dessous duquel la stimulation ne génère plus de contrainte active. En outre, l'étude montre que l'amplitude de la contrainte axiale active est inférieure à la contrainte circonférentielle active. Il est nécessaire d'effectuer des recherches expérimentales

sur la réponse active des différents types d'artères de différentes espèces et des conditions pathologiques. Ces résultats peuvent promouvoir la construction des modèles constrictives en rhéologie vasculaire.

Dans le deuxième article nous analysons les propriétés mécaniques de l'aorte thoracique de souris déficientes en apolipoprotein E (apoE). En particulier, le premier objectif de cette étude est de quantifier le dysfonctionnement de la paroi de l'aorte. Le deuxième objectif est de déterminer les propriétés mécaniques, et de fournir des données qui peuvent être utilisées dans la modélisation du comportement de la paroi artérielle et étudier la croissance et le remodelage à la maladie d'athérosclérose. Pour cette étude nous effectuons des essais mécaniques de gonflement – traction à trois différents rapports d'élongation axiale, à savoir à $\lambda_z =$ 1.6, 1.8 et 2.0, et sous l'état contracté au maximum ou sous l'état complètement relaxé des cellules musculaires lisses. En outre, histologie classique est effectuée aux segments artériels. L'analyse des données montre que a) les aortes de contrôle sont en général plus extensibles que les aortes de souris déficientes en apoE, b) des aortes de souris déficientes en apoE sont plus rigides que les aortes de contrôle, c) des aortes de contrôle présentent une réponse de diamètre active plus élevée, malgré le fait que la densité des cellules musculaires lisses est augmenté d'environ 15% dans les aortes de souris déficientes en apoE. Nous avons constaté des changements importants dans les propriétés structurales et élastiques de la paroi, dans la réponse de diamètre active et l'histologie des aortes de souris déficientes en apoE par rapport au groupe de contrôle. Les données peuvent être utilisées dans le développement des modèles structurels de la paroi artérielle et dans l'étude de changement des propriétés de la paroi artérielle en présence des maladies, telles que l'athérosclérose.

Dans le troisième article nous construisons un modèle structurel du tissu artériel et nous proposons une méthode permettant de déterminer les paramètres du modèle. Le modèle considère un lien plausible entre une partie de l'élastine et le muscle lisse. Le tissu artériel est considéré comme un mélange contraint d'élastine, de collagène et de cellules musculaires lisses. Nous considérons deux types d'élastine qui portent les charges. Un type de l'élastine est lié aux cellules musculaires lisses, et l'autre type de l'élastine porte des charges de concert avec les fibres de collagène. La configuration ouverte, obtenue d'un anneau circulaire après avoir effectué une coupe radiale, est considérée comme un état naturel du vaisseau, mais dans cette configuration les constituants de la paroi sont pré-étirés. Nous

proposons une méthode pour quantifier les rapports de pré-étirage des constituants de la paroi en utilisant des données d'une artère normale et d'une artère décellularisée. Nous vérifions le modèle en comparant des courbes de pression – rayon prédites théoriquement et enregistrés expérimentalement, et nous effectuons une analyse de sensibilité des rapportes de pré-étirage des constituants.

Dans le quatrième article nous effectuons des simulations théoriques des modes de remodelage inadapté en réponse à l'hypertension. Nous considérons une artère comme un tube cylindrique constitué d'un matériau non-linéaire, élastique et incompressible. Compte tenu de la pression d'hypertension et deux paramètres associés au tonus vasculaire et à la masse artérielle, nous déterminons les résultats de remodelage en termes de *zero-stress state* altéré et de géométrie déformée des conditions que la distribution de la contrainte circonférentielle et la contrainte axiale moyenne sont restaurées aux valeurs de base.

La conclusion récapitule les résultats principaux de la thèse, souligne les améliorations faites par rapport aux études théoriques précédentes et propose des perspectives de travaux futurs dans le domaine de la mécanique de la paroi artérielle.

Mots-clés

Remodelage artériel; Remodelage adaptatif; Remodelage inadapté; Hypertension; Athérosclérose; Propriétés de matériau, Propriétés élastiques; Elastine; Collagène; Muscle lisse vasculaire; Artère; Apolipoprotein E; Essai mécanique; Essai de gonflement – traction; Histologie

CONTENTS

Introduction

INTRODUCTION

Motivation

Cardiovascular disease

Cardiovascular diseases are the major contributors of morbidity and mortality worldwide [1]. The relative rate of death from 1999 to 2009 that is attributed to cardiovascular diseases, accounts for about one third of deaths in the United States [2]. On the basis of 2009 death rate data, one American dies every 40 seconds due to a cardiovascular disease [2]. In European Union, the cardiovascular diseases account for about forty percent of all deaths [3]. In addition to the mortality rates, the prolonged discomfort of the patients, the loss of productivity and the cost of expensive health care paid by the patients and the society in general are reasons to investigate the cardiovascular system and its failures. Overall cardiovascular disease is estimated to cost the European Union economy about €196 billion a year [3].

The rates of cardiovascular disease are high. Cardiovascular disease, however, is treatable and reversible. Patients are treated by drugs, surgical intervention, and encouragement of lifestyle changes by modifying risk factors, such as physical exercise, healthy eating, management of stress, and abstinence from smoking. In this way, physiological aspects of the cardiovascular system of the patient can be restored to normal values.

Biomechanics

A possible definition of biomechanics would be the following. “Biomechanics can be defined as the development, extension, and application of mechanics to answer questions of importance in biology and medicine.” [4] Through biomechanics we can address many of the biophysical phenomena that occur at different levels including molecular, cellular, tissue, organ and organism level.

Biomechanics is associated in part with the physiology of the cardiovascular system. The success or failure of various clinical interventions depends on the critical understanding of the mechanical behavior of the heart and the blood vessels. For instance, the geometrical and structural alterations that occur with aging cause a decrease in the arterial compliance [5], which leads to increase in systolic blood pressure. The increase in blood pressure is considered as the strongest predictor of cardiovascular mortality, because it augments the mechanical load on the left

ventricle and the whole systemic circulation [6]. Knowledge of the biomechanics of the cardiovascular system is important during cardiovascular surgical interventions, for the surgical tools may cause trauma to the tissue if there is no perception of the developed strains and stresses. The transplantation of a vessel and the implantation of an artificial tissue or a device can cause tissue damage and undesirable tissue growth and remodeling [7] due to the additional stresses that are borne by the contact of the native tissue and the artificial vessel or device. The mismatch of the compliance between the native and the artificial vessel can change locally the mechanical environment. The flow disturbances and the stress concentration that may occur at the native tissue can cause tissue proliferation, which is supposed to be the cause of long-term failure of the artificial graft [8]. Therefore, the long-term patency of arterial vein grafts when they are implanted for treating occlusive peripheral and coronary artery disease is done by minimizing compliance mismatch [9-10] and reducing acute overstretching [11-13]. Another important issue relates to the field of tissue engineering, where the goal is to develop grafts *in vitro*, whose mechanical and biological properties are similar to those of the native tissue [14].

In summary, a profound knowledge of vascular mechanics in both physiological and pathological conditions is important for the optimal treatment of cardiovascular diseases. There is a need for a) sophisticated theoretical ideas, because of the complexity of tissue structure and behavior, and b) new experiments, because of continuing lack of data. These provide the motivation for the present thesis, with the aim to contribute to the field of experimental studies and theoretical models of arterial wall modeling and remodeling in response to physiological and pathological conditions.

Background

Arterial structure

The arterial system serves as a conduit through which the blood is transported from the heart to the capillary networks. The arterial system is divided in pulmonic and systemic. The pulmonic arterial system consists of low-pressure vessels that transport blood poor in oxygen from the heart to the lungs, whereas the systemic consists of high-pressure vessels that transport blood rich in oxygen from the lungs to the rest of the body. The arterial structure and the mechanical behavior depend strongly on the specific location within the vasculature.

Arteries can be categorized according to the following general types. The elastic arteries, such as the aorta, the main pulmonary artery, the common carotid and the common iliac arteries tend to be larger-diameter vessels located closer to the heart. The muscular arteries, such as the coronary, the cerebral, the femoral and the renal arteries are smaller-diameter vessels closer to the organs.

The vascular wall consists of four main constituents: elastin, collagen, smooth muscle cells and endothelial cells [15-16]. The elastin of the arterial wall tends to be grouped in sheets forming layers called elastic laminae. The elastin is responsible for bearing loads at low pressures [16]. Vessels which have relatively high elastin content, such as the aorta, are relatively more compliant at physiologic pressures. The collagen forms wavy fibers in the arterial wall. The collagen fibers straighten and engage in bearing the load when the artery is subjected to higher pressures [16]. The artery resists excess inflation and is protected from bursting, for the collagen is very stiff. The vascular smooth muscle (VSM) cells are the contractile elements of the artery. The relaxation or the contraction of the VSM cells depends on neurological, mechanical and biochemical stimuli [17]. The VSM cells exist in different phenotypes in the arterial wall. In the normal mature vessels the contractile phenotype is the predominant phenotype. Its major function is the regulation of blood vessel diameter and blood flow. The altered functional demands can lead the VSM cells to change their phenotype to a relatively synthetic phenotype [18-20]. The endothelial cells form the endothelium, which is a thin layer of cells that lines the interior surface of blood vessels. The endothelium contributes little to the overall structural integrity of the wall, but it has a fundamental role in developmental biology and control of VSM tone.

The arterial wall consists of three layers: the intima, the media and the adventitia (Fig. 1). Therefore, the arteries are materially heterogeneous. It is

suggested that the intima does not contribute significantly to the load-bearing capability of the arterial wall and that the media and the adventitia are the most important layers structurally [21].

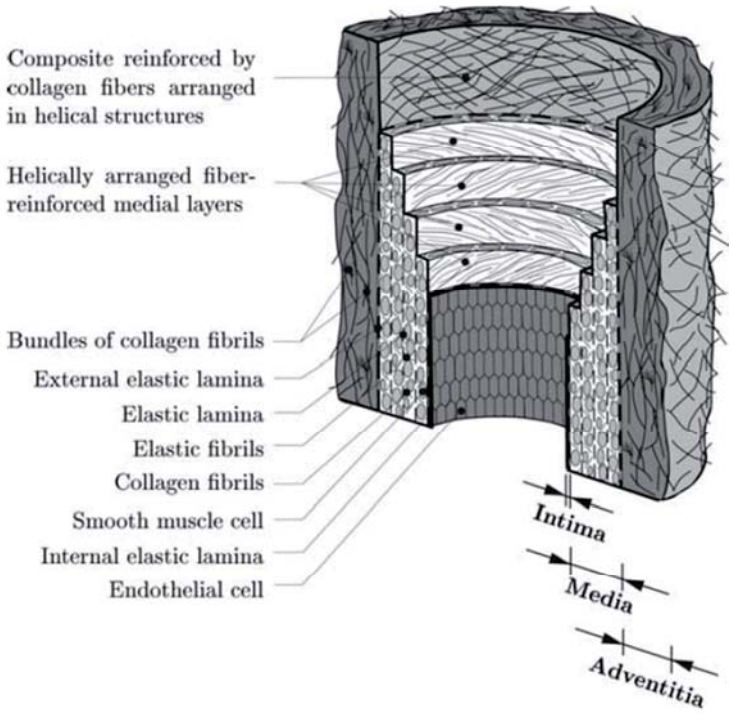

Figure 1. Schematic illustration of a healthy elastic artery composed of three layers: intima, media and adventitia [22].

Residual stress and strain

An artery free of external loads is not free of stresses due to the presence of residual strains. Chuong and Fung [23] and Vaishnav and Vossoughi [24] were the first who recognized the importance of arterial residual strains. The stress analysis that was performed on arteries subjected to physiologic loads prior to these studies predicted a large circumferential stress gradient across the arterial wall [25]. When the residual strains where incorporated into the stress analysis, however, the circumferential stress gradient was reduced to nearly homogenous level [26]. The important interpretation of this finding is that under normal conditions and loads, the cells that are situated across the arterial wall experience the same mechanical environment. Additionally, it was shown that the perturbation from the homogenous mechanical environment could initiate various growth and remodeling responses with

the aim to restore mechanical homeostasis [27-29]. The residual strains have been shown to change due to various diseases [28, 30-31] and during aging [32-34].

The residual strains of an arterial tissue are revealed by destructive cuts of the tissue. The most widely used method for revealing the residual strains is the single radial cut performed on an arterial ring [26]. In response to the radial cut, the ring springs open (Fig. 2). The (opening) angle formed by the open segment is considered as an experimental measure of the magnitude of the residual strain. This configuration is generally agreed to be a nearly stress-free configuration of the artery. However, cuts made in the axial and radial directions have revealed additional significant residual strains [35-37] showing that a single radial cut may not be sufficient to reveal the stress-free configuration of an artery.

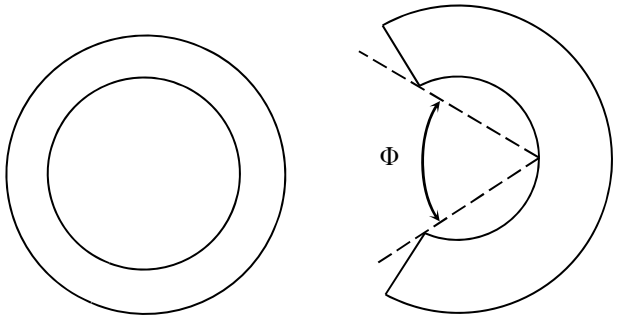

Figure 2. Schematic illustration of an arterial ring (left) and the opened-up configuration obtained in response to a radial cut (right). The opening angle Φ is considered as an experimental measure of the magnitude of the residual strain.

Finite elasticity

Constitutive relations describe the response of a material to applied loads. Soft-tissue behavior is generally non-linear over finite strains [38]. Wertheim [39] presented force-elongation data of various soft tissues including arteries and concluded that soft tissues do not obey Hooke's law. Fung [40] reported data from uniaxial tests on excised strips of mesentery. The results revealed a non-linear relationship between stress and stretch. Also, the data revealed that the response of the tissue to cyclic loading was relatively insensitive to strain rate and it was repeatable after a few initial preconditioning cycles. Fung called this behavior "pseudoelastic" and proposed that it can be separately assumed elastic in loading and unloading. Soft biological tissues typically exhibit non-linear pseudoelastic

responses over finite strains and the appropriate theoretical framework of finite elasticity is used for the quantification of their mechanical behavior.

The mechanical properties of soft tissues can be described through a strain-energy function (SEF) formulation [4, 41-42]. For an isothermal process, the stress can be determined directly from a SEF. The Cauchy stress is given from the equation

$$\boldsymbol{t} = -p\boldsymbol{I} + \boldsymbol{F} \cdot \frac{\partial W}{\partial \boldsymbol{E}} \cdot \boldsymbol{F}^T \tag{1}$$

where W is a SEF, $\boldsymbol{F}$ is the deformation gradient tensor, $\boldsymbol{F}^T$ is the transpose of the deformation gradient tensor, p is an unknown scalar function enforcing the kinematic constraint $det\boldsymbol{F}=1$, $\boldsymbol{I}$ is the unit tensor, $\boldsymbol{E} = \left(\boldsymbol{F}^T \cdot \boldsymbol{F} - \boldsymbol{I}\right)/2$ is the Green strain tensor. The arterial tissue consists largely of water [4] and responds incompressibly to loading, i.e., by preserving its volume [43-44]. We enforce the incompressibility condition in Eq. (1) via the Lagrange multiplier p, the value of which is determined from appropriate boundary conditions and equilibrium equations.

Material symmetry

If the response of a material to an applied loading is independent of the direction of loading, it is called isotropic. A non-isotropic response is called anisotropic. Examples of anisotropic behavior are the transversely isotropic and orthotropic behaviors. In transversely isotropic behavior, the response is the same in all directions transverse to a single preferred direction. Orthotropic behavior means that the material has three orthogonal preferred directions. The non-uniform distributions and orientations of the structural constituents of the wall suggest that the arterial wall is anisotropic [4]. It is suggested that the arterial tissue exhibits cylindrical orthotropy [25, 45], and the radial, circumferential and axial directions are the preferred directions [4]. Thus, if one applies equivalent loads in each of the three directions, the response of the material will be different. The anisotropic behavior of the arterial tissue has been suggested in various articles [26, 46-49].

Viscoelasticity

Biological tissues consist largely of water by wet weight and exhibit behavior that resembles both to fluid- and solid-like behavior [38, 50]. The biological tissues

have viscoelastic features. For examples, they creep under a constant load, they relax under a constant displacement and they exhibit hysteresis under cyclic loading [41]. Different approaches have been developed to study the viscoelastic behavior of soft biological tissues (cf. [51-53]).

Theoretical modeling of passive and active behavior of arteries

The main strain-energy functions that have been developed to describe the elastic material properties of arteries are divided in phenomenological and constituent based SEFs. Purely phenomenological SEFs have been proposed in the literature [23, 25-26, 47-49, 54-58]. The phenomenological SEFs have the following shortcomings. First, the elastic constants of the SEFs do not bear a clear physiological meaning, and second, the wall is assumed as a homogeneous medium. In order to overcome the shortcomings of phenomenological SEFs, constituent-based SEFs have been developed. These SEFs take into account the individual mechanical contribution of each arterial wall constituent [22, 59-66].

Most previous SEFs attribute the passive mechanical properties of the arterial wall to elastin and collagen. There are studies (cf. [67-68]) which have neglected the passive mechanical properties of the vascular smooth muscle under the assumption that its contribution to the circumferential wall stress is about one order of magnitude less than that of the SEF for elastin [69-70]. A limited number of studies have, however, included a description of the passive properties of the vascular smooth muscle [71-73].

It has been experimentally established that the active stress developed by the contraction of smooth muscle cells depends on two main factors, namely the intrinsic capability of the cells to generate stress when activated and the configuration of contractile proteins inside the cells [74-75]. The constitutive formulation of the active circumferential stress has been proposed in [76-77]. Fridez et al. [78] have proposed a phenomenological description of the circumferential active stress. A formulation for the active axial stress has been recently proposed in [79]. Cardamone et al. [80] and Wagner and Humphrey [81] have proposed that the active axial stress depends on the circumferential stretch. Zulliger et al. [82] have modeled the vascular smooth muscle as a structural element whose contribution to load bearing is modulated by the contraction of the cells. A mechanochemical finite strain model of smooth muscle

contraction is presented in the review paper [83]. The review paper [84] is concerned with the mathematical modeling of the mechanical behavior of arterial tissues.

Arterial remodeling

The arterial wall is continuously exposed to external loading. The blood pressure, the blood flow and the longitudinal extension result in wall stresses and shear stress on the inner arterial wall (Fig. 3). The arteries are sensitive to alterations in the mechanical loading, which may occur due to a) normal processes including angiogenesis, development and aging, b) diseases such as atherosclerosis, Marfan's syndrome, and aneurysms, c) injuries such as arterial denudation, wound healing, medial injury, and d) adaptations such as hypertension, altered flow and exercise. In response to the alteration in the mechanical loading, the artery exhibits changes in the geometry, structure and function of its arterial wall, a phenomenon called remodeling. Remodeling is a dynamic process. It appears to be due to delicate balance or imbalance in the production, removal and reorganization of the components of the vascular tissue at different rates, to different extents, and within different biomechanical states [73].

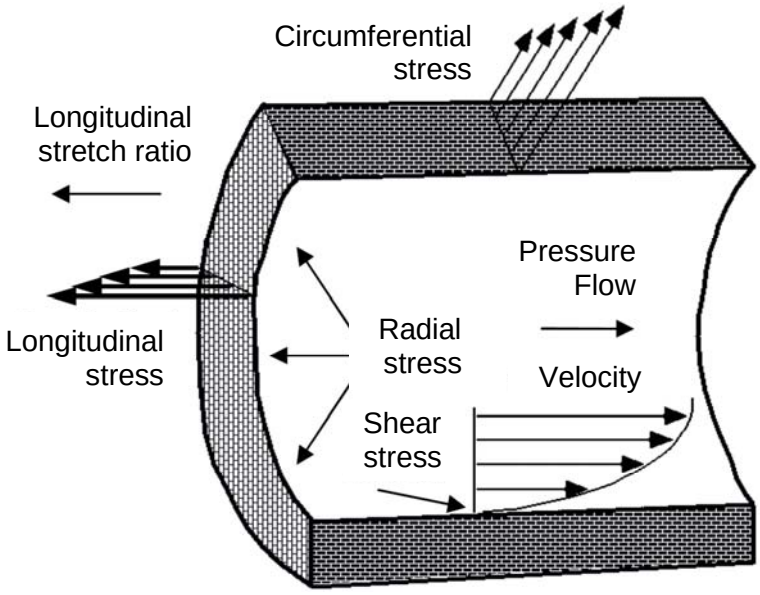

Figure 3. Stresses and loads acting on the arterial wall.

The sustained increase in pressure causes remodeling in arteries. The arterial wall thickens under sustained hypertension in order to restore the circumferential stress at the final adapted hypertensive state [27]. The circumferential stress is higher in the inner media and thus the thickening of the lamellar units is

primarily manifested there [27]. The adaptive pressure-induced remodeling results in the restoration of the magnitude of the media tensile stress and the intimal shear stress to their baseline values under normotensive conditions [51, 85]. The maladaptive pressure-induced remodeling, however, results in incomplete restoration of the baseline mechanical environment [86]. Hypertension is associated with increased deposition of extracellular matrix components which contributes to vessel wall thickening in hypertrophic remodeling or to reorganization of vessel wall cells in eutrophic remodeling [87]. The enhanced collagen deposition in the media and the adventitia results in thickening of the arterial wall [88-91]. Also, the VSM cell content is found to increase in the media.

When the local blood flow changes for more than few days, the arterial wall undergoes substantial remodeling [85]. The alteration of blood flow from its baseline value alters the flow-induced shear stress acting on the inner arterial surface. It has been experimentally shown that the increased blood flow induces arterial remodeling. It is manifested by an increase in lumen diameter in order to restore the shear stress to baseline values [91]. The arterial remodeling in response to increased blood flow might be accompanied by structural changes in medial elastin [85]. It is suggested that newly synthesized elastin is deposited in the inner and outer lamellar surfaces, accompanied by enzymatic digestion of highly cross-linked elastin fibers [92]. The remodeling due to increased flow appears to be associated with progressive removal of elastin [85, 93]. Further, the wall thickness increases due to the deposition of newly synthesized elastin in the inner and outer lamellar surfaces, possibly to restore circumferential stress.

Arteries also remodel when the flow decreases. Firstly, a VSM cell contraction takes place resulting in decrease of vessel diameter [94]. Further, VSM cells may migrate into the media and produce matrix proteins resulting in a structure that resembles the media (fibrocellular intimal hypertrophy) [95]. If the decrease in flow is relatively large, the proliferation process may form a stenosis or lumen obliteration, and the resultant tissue is poorly organized, matrix-free, and characterized by intimal hyperplasia [95].

Aging induces remodeling in large conduit arteries such as aorta and carotid arteries. The age-induced remodeling is associated with increased arterial volume [96], increased lumen area [97], intimal thickening [98], reduced axial stretch [99] and increased opening angle [100]. With progressing age, the content of collagen

increases [101], and the elastin is fragmented possibly due to mechanical fatigue failure caused by the pulsatile wall strain and the number of cardiac cycles [101-103].

The extension of arteries beyond their in vivo length causes them to grow lengthwise and to remodel [104]. The axial extension-induced remodeling has been associated with rapid accumulation of extracellular matrix [104]. Further, the alteration in the axial stress or strain appears to affect the orientation of the mitotic axis of the smooth muscle cells, and thus affect the orientation at which newly produced collagen is deposited in the extracellular matrix [105].

There exists an increasing need for physiologically motivated theoretical models to integrate the existing experimental observations into a consistent theoretical framework. Understanding the biomechanical remodeling laws will let us comprehend how the mechanical environment affects the remodeling of the cardiovascular tissue under physiologic and pathologic conditions. Additionally, it could help develop methods to construct tissues and organs *in vitro*, and promote new kinds of experiments and means of data analysis.

The theoretical models of remodeling facilitate the testing of hypothetical mechanisms that are involved in the arterial response and allow conducting parametric studies for evaluating the contribution of different factors to the remodeling process. Different approaches have been developed in order to study the adaptation of the vasculature. These approaches include the volumetric growth approach, the global growth approach and the constrained mixture approach.

In the volumetric growth approach the vessel is considered as a collection of infinitesimal elements which grow due to deviation of local stress or strain from certain baseline values (Fig. 4). The initial natural configuration of the artery $B_0(0)$ is a collection of infinitesimal elements each of which is in stress-free state. Each infinitesimal element grows according to a growth deformation tensor $\boldsymbol{F}_g$. The natural configuration of the artery $B_1(t)$ at time t of remodeling is a collection of grown infinitesimal elements each of which is in zero-stress state. Due to growth, the natural configurations $B_1(t)$ at time t of remodeling and the initial natural configuration $B_0(0)$ are different. If the grown elements are reassembled, they form the configuration $B_2(t)$, which can be a single opened ring due to radial cut or a pair of opened rings obtained by both circumferential and radial cuts (Fig. 4). If the elements of $B_1(t)$ are not geometrically compatible, the assembly to configuration

$B_2(t)$ requires the deformation $\boldsymbol{F}_{\mathrm{a}}$ which produces residual stress. The deformation $\boldsymbol{F}_{\boldsymbol{b}}$ bends the ring or rings closed, and the intact vessel is loaded by internal pressure and axially extended to give the final loaded configuration $b(t)$. The volumetric growth approach was first presented in [106] and then in [107]. Years later it was Rodriguez et al. [108] who focused on the kinematics of volumetric growth. The volumetric growth approach has been used in different studies of hypertension-induced remodeling [109-112]. Taber and Eggers [113] have used the volumetric growth approach to study the growth and remodeling during development, normal maturity and hypertension in the aorta.

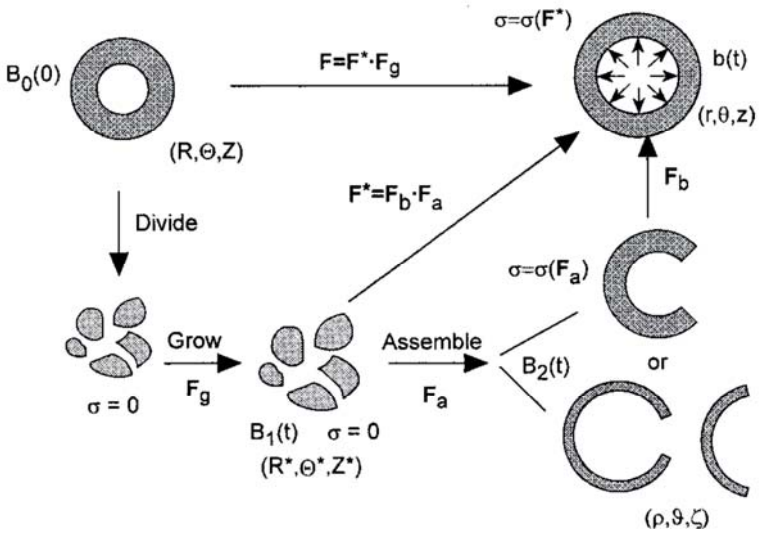

Figure 4. Schema showing the volumetric growth approach, where the vessel is considered as a collection of infinitesimal elements [110]. The natural configuration $B_1(t)$ at time t of remodeling is different than the initial natural configuration $B_0(0)$ due to growth. The assembling of the infinitesimal elements results in development of residual stresses in configuration $B_2(t)$. The loading configuration is $b(t)$.

The global growth approach is based on the assumption that remodeling manifests as a continuous change in the dimensions of the zero-stress configuration caused by the deviation of stress from homeostatic values [114]. The global growth approach is shown schematically in Fig. 5. The rates of change of the geometrical dimensions and the parameters that describe the stress/strain state of the arterial wall are related by appropriate evolution equations. The global growth approach is a particular case of the more general theory of volumetric growth. In the global growth approach, no deformation is needed to reassemble the grown elements into a

continuum body because it is assumed that all the changes of differential elements are mutually compatible [114]. The global growth approach has been used to study remodeling in hypertension [78, 115-117], in increased blood flow [77, 118], and in aging [67].

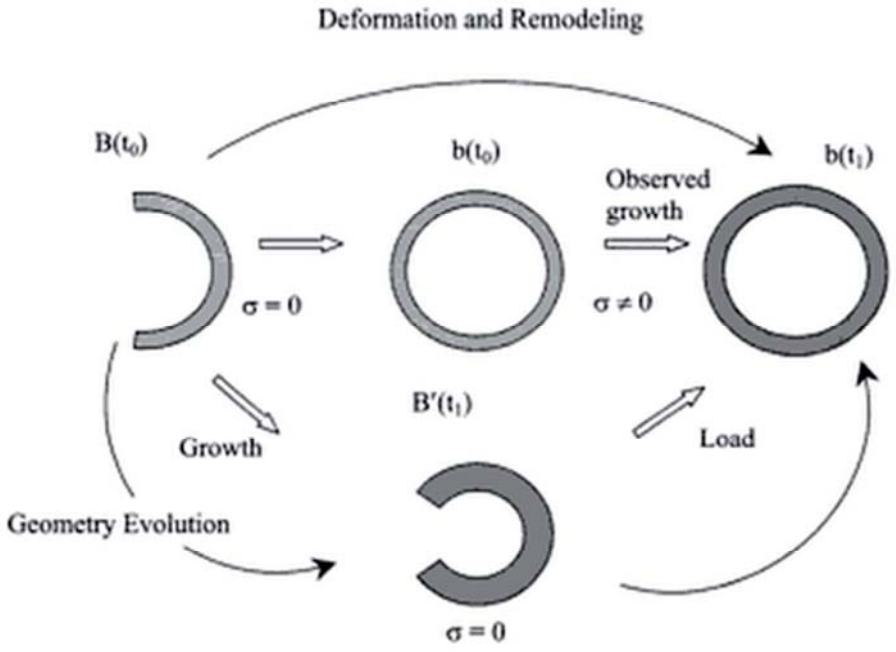

Figure 5. Schematic representation of the configurations of a growing artery in the global growth approach [114]. $B(t_o)$ is the original zero-stress state, $b(t_o)$ is the instantaneous deformed state, $B'(t_1)$ is the grown zero-stress state, and $b(t_1)$ is the grown deformed state.

The constrained mixture growth approach is based on the theory of constrained mixtures. The basic structural constituents (elastin, collagen, smooth muscle cells) of the mixture are considered to have individual mechanical properties, individual rates of production and removal, and individual evolving natural configurations (Fig. 6).The imbalances in the production and the removal of the individual constituents result in the observed remodeling. The constrained mixture growth approach was first proposed in [119]. It has been used to study remodeling in hypertension [71, 73, 120-122], in changes in blood flow [72-73, 119-122], and in axial extension-induced remodeling [73, 123-124]. Valentin and Humphrey [125] performed a sensitivity study using the constrained mixture approach. Humphrey [126] has written a brief review in the constrained mixture growth and remodeling.

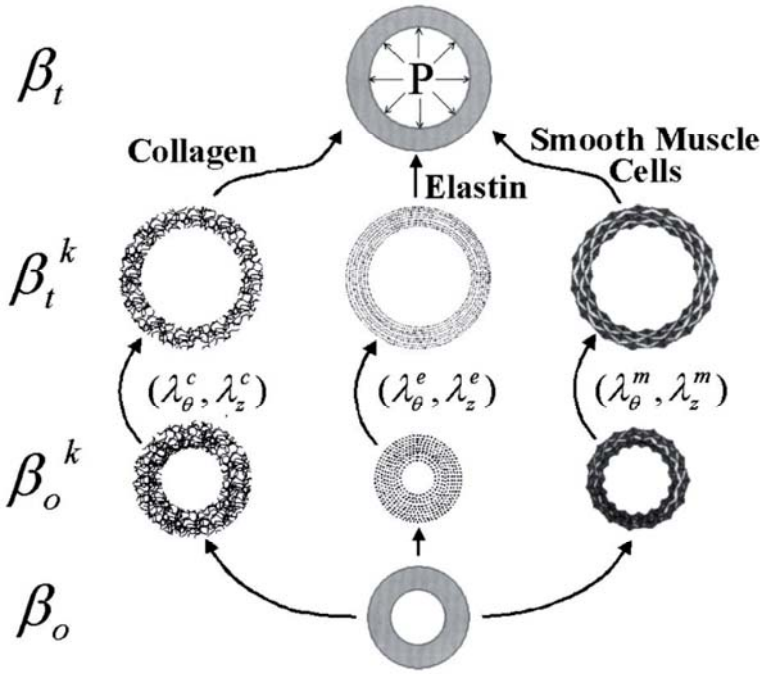

Figure 6. Schema showing the constrained mixture approach [72]. β_o is the natural configuration of the mixture. Each individual constituent (collagen, elastin, smooth muscle cells) has its own natural configuration β_o^k. β_t^k is the loaded configuration of each constituent. The loaded configuration β_t of the artery is the result of the contribution of the different wall constituents.

Vascular diseases

The diseases of the vasculature are a leading cause of morbidity and mortality. Due to the importance of these diseases, effort needs to be put in understanding their etiology; how they initiate and how they progress.

Two common vascular pathologies include hypertension and atherosclerosis. There is a large volume of literature related to hypertension and atherosclerosis and a number of theoretical and experimental studies that provide useful data that allow us to understand or test mechanisms involved in these pathologies.

Hypertension is the primary disease of the media. It is defined as the sustained elevation in arterial blood pressure. It is a chronic disease that is commonly observed in older individuals and has a close association with aging [127]. It has been found that mean aortic pressure gradually increases with advanced age [128]. The main causes of hypertension include genetics, improper diet, as well as abnormal functioning of the kidneys, the heart, the vasculature, or the nervous

system. Hypertension itself is a risk factor for many other cardiovascular disorders, such as atherosclerosis, stroke, aneurysms, and heart failure.

There are many studies in the literature that provide data of the geometry and the mechanical properties of the arterial wall of hypertensive subjects. Sharma [129] found stiffer rabbit aorta with increasing hypertension due to increased water uptake and possibly collagen [129]. Bashey at al. [130] found also increased stiffness, but with decreased mass fraction of collagen due to increase in smooth muscle content. Vaishnav et al. [131] did experiments in canine descending thoracic aortas. Hypertension did not affect the passive circumferential stress-strain response, but it increased the axial stiffness, with decrease in the *in vivo* stretch ratio. Similar decrease was found in the aorta by Wolinsky [132-133]. Hansen et al. [134] found a decrease in the generation of active stress in aortic strips. Arner and Uvelius [135] reported no difference in the generation of active stress despite the hyperplasia in the aorta of spontaneously hypertensive rats. Matsumoto and Hayashi [136-137] found increased wall thickness in hypertensive rat aortas, increased opening angle, and that the hypertensive aorta retracted less than the normotensive controls, i.e., they had lower in situ axial stretch.

Atherosclerosis is the primary disease of the intima. The risk factors for atherosclerosis include elevated cholesterol in serum, diabetes mellitus, smoking, genetic predisposition, stress, sedentary lifestyle and hypertension [4]. Atherosclerosis affects many different arteries of large and medium size. It causes ischemic heart disease, myocardial infarction and stroke, and it continues to be the leading cause of death in the western world.

Atherosclerosis is a highly progressive disease [4]. In humans it may begin in childhood but is manifested in middle-age or later [138]. Atherosclerosis increases overall stiffness of aorta [139-142], human cerebral arteries [143], iliac and carotid artery of dog [144]. Hudetz et al. [143], however, have shown that the normal anterior cerebral artery is stiffer than the atherosclerotic artery, and Newman et al. [145] have shown that aortas of normal cockerels are stiffer than atherosclerotic aortas in early stages of atherosclerosis, before increased calcification occurs. Hasegawa and Watanabe [142] found increased viscoelastic behavior of diseased thoracic aortas. Matsumoto et al. [146] found increased opening angle with increased intimal hyperplasia in the absence of significant calcification, but decreased opening angle with increased calcification which suggests that the opened calcified configuration may not be stress free.

Scope and overview

The intent of this thesis is to expand the knowledge on the role of each arterial wall constituent and particularly the VSM in the mechanical properties and the remodeling of the arterial wall. Aiming to that, a multi-scale approach has been applied. The approach includes theoretical modeling and remodeling of the arterial wall integrated in a constitutive framework, and experimental investigation including inflation – extension mechanical test of arterial samples under different vascular smooth muscle cell tones.

1st Chapter

In the study presented in the first publication, mechanical testing of mouse thoracic aortas is performed in three different axial stretch ratios, and under different state of contraction of the vascular smooth muscle cells. Then, a methodology is presented for the calculation of the active stresses in circumferential and longitudinal direction. In most previous theoretical studies, the contribution of the active stress was assumed to be only in the circumferential direction. There are histological findings that show in some arteries the existence of two main orientations of vascular smooth muscle cells in circumferential and longitudinal direction [147]. It has been reported that the isometric response of the muscle cells produced active tension in both the circumferential and axial direction [148]. Based on the observation that the VSM tone produces active stress in both the circumferential and axial direction, we develop a constitutive relation of the arterial wall, which appropriately takes into account the bi-axial contribution of active stress. The goal of the study is to describe experimentally the active stress under isometric conditions and propose an analytical expression for the active stress component in axial direction.

2nd Chapter

In the study presented in the second publication, we perform inflation – extension mechanical testing of mouse thoracic aortas at three different axial stretch ratios, and under different state of contraction of the vascular smooth muscle cells. It is difficult to determine with certainty the specific events that lead to atherogenesis in humans. There is evidence that local shear or wall stress may play a significant role. Many different animal models have been developed that mimic closely the human form of atherosclerosis. The characterization of the mechanical properties of arteries in animal models is a prerequisite for understanding the causal relationship between local stress and development of the disease. In this study, we quantify the dysfunction of the aortic wall, determine structural and elastic properties and provide

histological data of the thoracic aortas of apolipoprotein E-deficient mice which are used as experimental model of atherosclerosis.

3rd Chapter

In this study we propose a novel constitutive model of the arterial tissue and a method to quantify the prestretch ratios of the wall constituents by using data of normal and decellularized arteries. In the experimental study of Roy et al. [149], after the smooth muscle of porcine common carotid arteries has been functionally inactivated, the muscle cells were physically removed from the tissue by a detergent-enzymatic procedure that preserved the extracellular matrix scaffold. This resulted in geometrical changes between the intact and the decellularized artery. The geometrical changes are interpreted as elastic deformations that are released after the link between the smooth muscle cells and elastin is eliminated by the decellularization procedure. The model accounts for a plausible link between part of elastin and the smooth muscle. The arterial tissue is considered as a constrained mixture of elastin, collagen, and smooth muscle cells. We consider two types of elastin that are involved in load bearing. One type of elastin is bonded to the smooth muscle cells, and the other part of elastin bears loads in concert with the collagen fibers. Each type of elastin has a different prestretch ratio. The determination of the model parameters requires the minimization of the discrepancy between theoretically derived and experimentally recorded values of pressure, and at the same time to satisfy the condition that the total stress in the wall of an artery at its zero-stress state is equal to zero. It is therefore a problem of minimization with constraints. Finally, a sensitivity analysis of the prestretch ratios is performed.

4th Chapter

In this article we present theoretical simulations of modes of maladaptive remodeling in response to hypertension. An adaptive response of an artery manifests as preservation of the normotensive deformed diameter, change in residual strains and axial stretch ratio, and thickening of the arterial wall. As a result the tensile wall stress and the flow-induced shear stress remain at baseline values [51, 85]. A maladaptive response is characterized by the incomplete restoration of the baseline mechanical environment [86, 150-152]. This could result from a variety of dysfunctional biological processes. In our study we follow the methodology proposed in [153]. We formulate an inverse problem of vascular mechanics, in which the geometrical and mechanical properties of an artery are calculated from the prescribed deformed configuration, stress field, vascular smooth muscle cells tone

and mass. We then evaluate the relative importance of certain geometrical and mechanical factors in the remodeling response.

Suggested reading

The reader might want to refer to the following textbooks for an introduction to the basic principles of continuum mechanics, vascular wall constitutive modeling, and arterial remodeling.

Fung, Y. C., 1993, Biomechanics: Mechanical Properties of Living Tissue, Springer-Verlag, New York.

Holzapfel, G. A., 2000, Nonlinear Solid Mechanics: A Continuum Approach for Engineering, John Wiley & Sons, Sussex.

Humphrey, J. D., 2002, Cardiovascular Solid Mechanics: Cells, Tissues, and Organs, Springer-Verlag, New York.

References

[1] Roger VL, Go AS, Lloyd-Jones DM, et al. Heart Disease and Stroke Statistics—2011 Update: A Report From the American Heart Association. Circulation 2011;123:e18-e209.

[2] Go AS, Mozaffarian D, Roger VL, et al. Heart Disease and Stroke Statistics—2013 Update: A Report From the American Heart Association. Circulation 2013;127:e6-e245.

[3] Nichols M, Townsend N, Scarborough P, et al. (eds), European Cardiovascular Disease Statistics, Brussels, Sophia Antipolis, European Heart Network AISBL, European Society of Cardiology - The European Heart House, 2012.

[4] Humphrey JD, Cardiovascular Solid Mechanics: Cells, Tissues, and Organs, 2002.

[5] Westerhof N, Stergiopulos N, Noble MIM, Snapshots of hemodynamics an aid for clinical research and graduate education, In, Basic science for the cardiologist, New York, NY, Springer, 2005.

[6] Benetos A, Safar M, Rudnichi A, et al. Pulse Pressure: A Predictor of Long-term Cardiovascular Mortality in a French Male Population. Hypertension 1997;30:1410-5.

[7] Prendergast PJ, Lally C, Daly S, et al. Analysis of prolapse in cardiovascular stents: a constitutive equation for vascular tissue and finite-element modelling. J Biomech Eng 2003;125:692-9.

[8] Greenwald SE, Berry CL. Improving vascular grafts: the importance of mechanical and haemodynamic properties. The Journal of Pathology 2000;190:292-9.

[9] Abbott WM, Megerman J, Hasson JE, et al. Effect of compliance mismatch on vascular graft patency. J Vasc Surg 1987;5:376-82.

[10] Walden R, L'Italien GJ, Megerman J, et al. Matched elastic properties and successful arterial grafting. Arch Surg 1980;115:1166-9.

[11] Liu SQ, Moore MM, Yap C. Prevention of mechanical stretch-induced endothelial and smooth muscle cell injury in experimental vein grafts. J Biomech Eng 2000;122:31-8.

[12] Dobrin PB, Littooy FN, Golan J, et al. Mechanical and histologic changes in canine vein grafts. J Surg Res 1988;44:259-65.

[13] Shuhaiber JH, Evans AN, Massad MG, et al. Mechanisms and future directions for prevention of vein graft failure in coronary bypass surgery. Eur J Cardiothorac Surg 2002;22:387-96.

[14] Sonoda H, Takamizawa K, Nakayama Y, et al. Small-diameter compliant arterial graft prosthesis: Design concept of coaxial double tubular graft and its fabrication. J Biomed Mater Res 2001;55:266-76.

[15] Clark JM, Glagov S. Transmural organization of the arterial media. The lamellar unit revisited. Arteriosclerosis 1985;5:19-34.

[16] Roach MR, Burton AC. The reason for the shape of the distensibility curves of arteries. Can J Biochem Physiol 1957;35:681-90.

[17] Dingemans KP, Teeling P, Lagendijk JH, et al. Extracellular matrix of the human aortic media: an ultrastructural histochemical and immunohistochemical study of the adult aortic media. Anat Rec 2000;258:1-14.

[18] Harmon KJ, Couper LL, Lindner V. Strain-dependent vascular remodeling phenotypes in inbred mice. Am J Pathol 2000;156:1741-8.

[19] Owens GK. Regulation of differentiation of vascular smooth muscle cells. Physiol Rev 1995;75:487-517.

[20] Williams B. Mechanical influences on vascular smooth muscle cell function. J Hypertens 1998;16:1921-9.

[21] Burton AC. Relation of structure to function of the tissues of the wall of blood vessels. Physiol Rev 1954;34:619-42.

[22] Holzapfel GA, Gasser TC, Ogden RW. A new constitutive framework for arterial wall mechanics and a comparative study of material models. Journal of Elasticity 2000;61:1-48.

[23] Chuong CJ, Fung YC. Three-dimensional stress distribution in arteries. J Biomech Eng 1983;105:268-74.

[24] Vaishnav RN, Vossoughi J, Estimation of residual strains in aortic segments, In: Hall CW (ed), Biomedical Engineering II, Recent developments, New York, Pergamon Press, 1983:330 - 3.

[25] Demiray H, Vito RP. A layered cylindrical shell model for an aorta. International Journal of Engineering Science 1991;29:47-54.

[26] Chuong CJ, Fung YC. On residual stresses in arteries. J Biomech Eng 1986;108:189-92.

[27] Matsumoto T, Hayashi K. Stress and strain distribution in hypertensive and normotensive rat aorta considering residual strain. Journal of Biomechanical Engineering 1996;118:62-73.

[28] Liu SQ, Fung YC. Relationship between hypertension, hypertrophy, and opening angle of zero-stress state of arteries following aortic constriction. J Biomech Eng 1989;111:325-35.

[29] Humphrey JD. Vascular adaptation and mechanical homeostasis at tissue, cellular, and sub-cellular levels. Cell Biochem Biophys 2008;50:53-78.

[30] Lu X, Zhao JB, Wang GR, et al. Remodeling of the zero-stress state of femoral arteries in response to flow overload. Am J Physiol Heart Circ Physiol 2001;280:H1547-59.

[31] Zhao J, Lu X, Zhuang F, et al. Biomechanical and morphometric properties of the arterial wall referenced to the zero-stress state in experimental diabetes. Biorheology 2000;37:385-400.

[32] Valenta J, Vitek K, Cihak R, et al. Age related constitutive laws and stress distribution in human main coronary arteries with reference to residual strain. Biomed Mater Eng 2002;12:121-34.

[33] Valenta J, Svoboda J, Valerianova D, et al. Residual strain in human atherosclerotic coronary arteries and age related geometrical changes. Biomed Mater Eng 1999;9:311-7.

[34] Badreck-Amoudi A, Patel CK, Kane TP, et al. The effect of age on residual strain in the rat aorta. J Biomech Eng 1996;118:440-4.

[35] Greenwald SE, Moore JE, Jr., Rachev A, et al. Experimental investigation of the distribution of residual strains in the artery wall. J Biomech Eng 1997;119:438-44.

[36] Vossoughi J, Hedjazi Z, Borris FS, Intimal residual stress and strain in large arteries, In, ASME advances in Bioengineering, New York, ASME, 1993:434 - 7.

[37] Holzapfel GA, Sommer G, Auer M, et al. Layer-specific 3D residual deformations of human aortas with non-atherosclerotic intimal thickening. Ann Biomed Eng 2007;35:530-45.

[38] Humphrey JD. Review Paper: Continuum biomechanics of soft biological tissues. Proceedings of the Royal Society of London. Series A: Mathematical, Physical and Engineering Sciences 2003;459:3-46.

[39] Wertheim MG. Memoire sur l' eastocote et la cohesion des principaux tissues du corp humain. Ann. Chim. Phys 1847;21:385-414.

[40] Fung YC. Elasticity of soft tissues in simple elongation. Am J Physiol 1967;213:1532-44.

[41] Fung YC, Biomechanics: Mechanical Properties of living tissues, New York, Springer, 1993.

[42] Spencer AJM, Continuum Mechanics, London, Longman, 1980.

[43] Carew TE, Vaishnav RN, Patel DJ. Compressibility of the arterial wall. Circ Res 1968;23:61-8.

[44] Chuong CJ, Fung YC. Compressibility and constitutive equation of arterial wall in radial compression experiments. J Biomech 1984;17:35-40.

[45] Patel DJ, Fry DL. The elastic symmetry of arterial segments in dogs. Circ Res 1969;24:1-8.

[46] Doyle JM, Dobrin PB. Finite deformation analysis of the relaxed and contracted dog carotid artery. Microvasc Res 1971;3:400-15.

[47] von Maltzahn WW, Warriyar RG, Keitzer WF. Experimental measurements of elastic properties of media and adventitia of bovine carotid arteries. J Biomech 1984;17:839-47.

[48] Takamizawa K, Hayashi K. Strain energy density function and uniform strain hypothesis for arterial mechanics. J Biomech 1987;20:7-17.

[49] Holzapfel GA, Weizsacker HW. Biomechanical behavior of the arterial wall and its numerical characterization. Comput Biol Med 1998;28:377-92.

[50] Roy CS. The elastic properties of the arterial wall. Philos Trans R Soc Lond B 1880;99:1-31.

[51] Fung YC, Biomechanics: Motion, Flow, Stress, and Growth, New York, Springer Verlag, 1990.

[52] Pioletti DP, Rakotomanana LR. Non-linear viscoelastic laws for soft biological tissues. European journal of mechanics A 2000;19:749-59.

[53] Holzapfel GA, Gasser TC, Stadler M. A structural model for the viscoelastic behavior of arterial walls: Continuum formulation and finite element analysis. European Journal of Mechanics, A/Solids 2002;21:441-63.

[54] Fung YC, Fronek K, Patitucci P. Pseudoelasticity of arteries and the choice of its mathematical expression. Am J Physiol 1979;237:H620-31.

[55] Vaishnav RN, Young JT, Patel DJ. Distribution of stresses and of strain-energy density through the wall thickness in a canine aortic segment. Circ Res 1973;32:577-83.

[56] Moritake K, Handa H, Okumura A, et al. Quantitative analysis of microstructural components of human cerebral arteries. Neurol Res 1981;3:67-82.

[57] Humphrey JD. Mechanics of the arterial wall: review and directions. Crit Rev Biomed Eng 1995;23:1-162.

[58] Kas'yanov VA, Rachev AI. Deformation of blood vessels upon stretching, internal pressure, and torsion. Mechanics of Composite Materials 1980;16:76-80.

[59] Driessen NJB, Bouten CVC, Baaijens FPT. A structural constitutive model for collagenous cardiovascular tissues incorporating the angular fiber distribution. Journal of Biomechanical Engineering 2005;127:494-503.

[60] Gasser TC, Ogden RW, Holzapfel GA. Hyperelastic modelling of arterial layers with distributed collagen fibre orientations. Journal of the Royal Society Interface 2006;3:15-35.

[61] Gundiah N, Ratcliffe MB, Pruitt LA. The biomechanics of arterial elastin. J Mech Behav Biomed Mater 2009;2:288-96.

[62] Zulliger MA, Fridez P, Hayashi K, et al. A strain energy function for arteries accounting for wall composition and structure. J Biomech 2004;37:989-1000.

[63] Watton PN, Ventikos Y, Holzapfel GA. Modelling the mechanical response of elastin for arterial tissue. J Biomech 2009;42:1320-5.

[64] Rezakhaniha R, Fonck E, Genoud C, et al. Role of elastin anisotropy in structural strain energy functions of arterial tissue. Biomech Model Mechanobiol 2010.

[65] Lokshin O, Lanir Y. Micro and macro rheology of planar tissues. Biomaterials 2009;30:3118-27.

[66] Agianniotis A, Rezakhaniha R, Stergiopulos N. A structural constitutive model considering angular dispersion and waviness of collagen fibres of rabbit facial veins. Biomed Eng Online 2011;10:18.

[67] Tsamis A, Rachev A, Stergiopulos N. A constituent-based model of age-related changes in conduit arteries. Am J Physiol Heart Circ Physiol 2011;301:H1286-301.

[68] Tsamis A, Stergiopulos N, Rachev A. A structure-based model of arterial remodeling in response to sustained hypertension. J Biomech Eng 2009;131:101004.

[69] Bergel DH. The static elastic properties of the arterial wall. J Physiol 1961;156:445-57.

[70] VanDijk AM, Wieringa PA, van der Meer M, et al. Mechanics of resting isolated single vascular smooth muscle cells from bovine coronary artery. Am J Physiol 1984;246:C277-87.

[71] Gleason RL, Humphrey JD. A Mixture Model of Arterial Growth and Remodeling in Hypertension: Altered Muscle Tone and Tissue Turnover. Journal of Vascular Research 2004;41:352-63.

[72] Gleason RL, Taber LA, Humphrey JD. A 2-D model of flow-induced alterations in the geometry, structure, and properties of carotid arteries. J Biomech Eng 2004;126:371-81.

[73] Gleason RL, Jr., Humphrey JD. A 2D constrained mixture model for arterial adaptations to large changes in flow, pressure and axial stretch. Math Med Biol 2005;22:347-69.

[74] Dobrin PB. Influence of initial length on length-tension relationship of vascular smooth muscle. Am J Physiol 1973;225:664-70.

[75] Dobrin PB, Vascular mechanics. In: Handbook of Physiology. The Cardiovascular System. Vascular Smooth Muscle, In: Bohr DF, Somlyo AP, Sparks HV, et al. (eds), MD: Am. Physiol. Soc., 1983:65-104.

[76] Rachev A, Hayashi K. Theoretical study of the effects of vascular smooth muscle contraction on strain and stress distributions in arteries. Ann Biomed Eng 1999;27:459-68.

[77] Rachev A. A Model of Arterial Adaptation to Alterations in Blood Flow. Journal of Elasticity 2000;61:83-111.

[78] Fridez P, Rachev A, Meister JJ, et al. Model of geometrical and smooth muscle tone adaptation of carotid artery subject to step change in pressure. Am J Physiol Heart Circ Physiol 2001;280:H2752-60.

[79] Agianniotis A, Rachev A, Stergiopulos N. Active axial stress in mouse aorta. J Biomech 2012;45:1924-7.

[80] Cardamone L, Valentin A, Eberth JF, et al. Modelling carotid artery adaptations to dynamic alterations in pressure and flow over the cardiac cycle. Math Med Biol 2010;27:343-71.

[81] Wagner HP, Humphrey JD. Differential passive and active biaxial mechanical behaviors of muscular and elastic arteries: basilar versus common carotid. J Biomech Eng 2011;133:051009.

[82] Zulliger MA, Rachev A, Stergiopulos N. A constitutive formulation of arterial mechanics including vascular smooth muscle tone. Am J Physiol Heart Circ Physiol 2004;287:H1335-43.

[83] Stalhand J, Klarbring A, Holzapfel GA. Smooth muscle contraction: mechanochemical formulation for homogeneous finite strains. Prog Biophys Mol Biol 2008;96:465-81.

[84] Holzapfel GA, Ogden RW. Constitutive modelling of arteries. Proceedings of the Royal Society A: Mathematical, Physical and Engineering Science 2010;466:1551-97.

[85] Langille BL, Blood Flow-Induced Remodeling of the Artery Wall, In: Bevan JA, Kaley G,Rubanyi GM (eds), Flow-Dependent Regulation of Vascular Function, New York, Oxford University Press, 1995:277-99.

[86] Heagerty AM, Aalkjaer C, Bund SJ, et al. Small artery structure in hypertension. Dual processes of remodeling and growth. Hypertension 1993;21:391-7.

[87] Intengan HD, Schiffrin EL. Structure and mechanical properties of resistance arteries in hypertension: role of adhesion molecules and extracellular matrix determinants. Hypertension 2000;36:312-8.

[88] Hu JJ, Fossum TW, Miller MW, et al. Biomechanics of the porcine basilar artery in hypertension. Ann Biomed Eng 2007;35:19-29.

[89] Hu JJ, Ambrus A, Fossum TW, et al. Time courses of growth and remodeling of porcine aortic media during hypertension: a quantitative immunohistochemical examination. J Histochem Cytochem 2008;56:359-70.

[90] Xu C, Zarins CK, Pannaraj PS, et al. Hypercholesterolemia superimposed by experimental hypertension induces differential distribution of collagen and elastin. Arterioscler Thromb Vasc Biol 2000;20:2566-72.

[91] Walker-Caprioglio HM, Trotter JA, Little SA, et al. Organization of cells and extracellular matrix in mesenteric arteries of spontaneously hypertensive rats. Cell Tissue Res 1992;269:141-9.

[92] Kagan HM, Vaccaro CA, Bronson RE, et al. Ultrastructural immunolocalization of lysyl oxidase in vascular connective tissue. J Cell Biol 1986;103:1121-8.

[93] Langille BL, Hemodynamic factors and vascualr disease, In: Silver MD (ed), Cardiovascular Pathology, New York, Churchill-Livingstone, 1991.

[94] Langille BL. Remodeling of developing and mature arteries: endothelium, smooth muscle, and matrix. J Cardiovasc Pharmacol 1993;21 Suppl 1:S11-7.

[95] Glagov S, Zarins CK, Masawa N, et al. Mechanical functional role of non-atherosclerotic intimal thickening. Front Med Biol Eng 1993;5:37-43.

[96] Bader H. Dependence of wall stress in the human thoracic aorta on age and pressure. Circ Res 1967;20:354-61.

[97] Virmani R, Avolio AP, Mergner WJ, et al. Effect of aging on aortic morphology in populations with high and low prevalence of hypertension and atherosclerosis. Comparison between occidental and Chinese communities. Am J Pathol 1991;139:1119-29.

[98] Nejjar I, Pieraggi MT, Thiers JC, et al. Age-related changes in the elastic tissue of the human thoracic aorta. Atherosclerosis 1990;80:199-208.

[99] Wenn CM, Newman DL. Arterial tortuosity. Australas Phys Eng Sci Med 1990;13:67-70.

[100] Saini A, Berry C, Greenwald S. Effect of age and sex on residual stress in the aorta. J Vasc Res 1995;32:398-405.

[101] Sans M, Moragas A. Mathematical morphologic analysis of the aortic medial structure. Biomechanical implications. Anal Quant Cytol Histol 1993;15:93-100.

[102] Greenwald SE. Ageing of the conduit arteries. J Pathol 2007;211:157-72.

[103] Avolio A, Jones D, Tafazzoli-Shadpour M. Quantification of alterations in structure and function of elastin in the arterial media. Hypertension 1998;32:170-5.

[104] Jackson ZS, Gotlieb AI, Langille BL. Wall tissue remodeling regulates longitudinal tension in arteries. Circ Res 2002;90:918-25.

[105] Dajnowiec D, Langille BL. Arterial adaptations to chronic changes in haemodynamic function: coupling vasomotor tone to structural remodelling. Clin Sci (Lond) 2007;113:15-23.

[106] Skalak R, Growth as finite displacement field, In: Carlson DE,Shield RT (eds), Proceedings of the IUTAM Symposium on Finite Elasticity, The Hague, Martnus Nijhoff, 1981:347 - 55.

[107] Skalak R, Dasgupta G, Moss M, et al. Analytical description of growth. J Theor Biol 1982;94:555-77.

[108] Rodriguez EK, Hoger A, McCulloch AD. Stress-dependent finite growth in soft elastic tissues. J Biomech 1994;27:455-67.

[109] Taber LA. A model for aortic growth based on fluid shear and fiber stresses. J Biomech Eng 1998;120:348-54.

[110] Taber LA, Humphrey JD. Stress-modulated growth, residual stress, and vascular heterogeneity. J Biomech Eng 2001;123:528-35.

[111] Rachev A, Gleason RL, Jr. Theoretical study on the effects of pressure-induced remodeling on geometry and mechanical non-homogeneity of conduit arteries. Biomech Model Mechanobiol 2010.

[112] Alford PW, Humphrey JD, Taber LA. Growth and remodeling in a thick-walled artery model: effects of spatial variations in wall constituents. Biomech Model Mechanobiol 2008;7:245-62.

[113] Taber LA, Eggers DW. Theoretical study of stress-modulated growth in the aorta. J Theor Biol 1996;180:343-57.

[114] Rachev A, Remodeling of arteries in response to changes in their mechanical environment, In: Holzapfel G,Ogden R (eds), Biomechanics of Soft Tissues in Cardiovascular Systems, Wien New York, Springer, 2003.

[115] Rachev A, Stergiopulos N, Meister JJ. Theoretical study of dynamics of arterial wall remodeling in response to changes in blood pressure. J Biomech 1996;29:635-42.

[116] Rachev A, Stergiopulos N, Meister JJ. A model for geometric and mechanical adaptation of arteries to sustained hypertension. J Biomech Eng 1998;120:9-17.

[117] Tsamis A, Stergiopulos N. Arterial remodeling in response to hypertension using a constituent-based model. Am J Physiol Heart Circ Physiol 2007;293:H3130-9.

[118] Tsamis A, Stergiopulos N. Arterial remodeling in response to increased blood flow using a constituent-based model. J Biomech 2009;42:531-6.

[119] Humphrey JD, Rajagopal KR. A constrained mixture model for arterial adaptations to a sustained step change in blood flow. Biomech Model Mechanobiol 2003;2:109-26.

[120] Karšaj I, Humphrey JD. A multilayered wall model of arterial growth and remodeling. Mechanics of Materials 2012;44:110-9.

[121] Valentin A, Cardamone L, Baek S, et al. Complementary vasoactivity and matrix remodelling in arterial adaptations to altered flow and pressure. J R Soc Interface 2009;6:293-306.

[122] Valentin A, Humphrey JD. Evaluation of fundamental hypotheses underlying constrained mixture models of arterial growth and remodelling. Philos Transact A Math Phys Eng Sci 2009;367:3585-606.

[123] Gleason RL, Humphrey JD. Effects of a sustained extension on arterial growth and remodeling: a theoretical study. J Biomech 2005;38:1255-61.

[124] Valentin A, Humphrey JD. Modeling effects of axial extension on arterial growth and remodeling. Med Biol Eng Comput 2009;47:979-87.

[125] Valentin A, Humphrey JD. Parameter sensitivity study of a constrained mixture model of arterial growth and remodeling. J Biomech Eng 2009;131:101006.

[126] Humphrey JD. Vascular Mechanics, Mechanobiology, and Remodeling. J Mech Med Biol 2009;9:243-57.

[127] Fukutomi M, Kario K. Aging and hypertension. Expert Rev Cardiovasc Ther 2010;8:1531-9.

[128] Guyton AC, Hall JE, Textbook of medical physiology, Philadelphia, PA, Saunders, 2006.

[129] Sharma MG. Rheological properties of arteries under normal and experimental hypertension conditions. J Biomech 1976:293-300.

[130] Bashey RI, Cox R, McCann J, et al. Changes in collagen biosynthesis, types, and mechanics of aorta in hypertensive rats. J Lab Clin Med 1989;113:604-11.

[131] Vaishnav RN, Vossoughi J, Patel DJ, et al. Effect of hypertension on elasticity and geometry of aortic tissue from dogs. J Biomech Eng 1990;112:70-4.

[132] Wolinsky H. Comparison of medial growth of human thoracic and abdominal aortas. Circ Res 1970;27:531-8.

[133] Wolinsky H. Response of the rat aortic media to hypertension. Morphological and chemical studies. Circ Res 1970;26:507-22.

[134] Hansen TR, Dineen DX, Pullen GL. Orientation of arterial smooth muscle and strength of contraction of aortic strips from DOCA-hypertensive rats. Blood Vessels 1980;17:302-11.

[135] Arner A, Uvelius B. Force-velocity characteristics and active tension in relation to content and orientation of smooth muscle cells in aortas from normotensive and spontaneous hypertensive rats. Circ Res 1982;50:812-21.

[136] Matsumoto T, Hayashi K. Mechanical and dimensional adaptation of rat aorta to hypertension. J Biomech Eng 1994;116:278-83.

[137] Matsumoto T, Hayashi K. Stress and strain distribution in hypertensive and normotensive rat aorta considering residual strain. J Biomech Eng 1996;118:62-73.

[138] Munro JM, Cotran RS. The pathogenesis of atherosclerosis: atherogenesis and inflammation. Lab Invest 1988;58:249-61.

[139] Band W, Goedhard WJ, Knoop AA. Comparison of effects of high cholesterol intake on viscoelastic properties of the thoracic aorta in rats and rabbits. Atherosclerosis 1973;18:163-71.

[140] Pynadath TI, Mukherjee DP. Dynamic mechanical properties of atherosclerotic aorta. A correlation between the cholesterol ester content and the viscoelastic properties of atherosclerotic aorta. Atherosclerosis 1977;26:311-8.

[141] Sherebrin MH, Bernans HA, Roach MR. Extensibility changes of calcified soft tissue strips from human aorta. Can J Physiol Pharmacol 1987;65:1878-83.

[142] Hasegawa M, Watanabe Y. Rheological properties of the thoracic aorta in normal and WHHL rabbits. Biorheology 1988;25:147-56.

[143] Hudetz AG, Mark G, Kovach AG, et al. Biomechanical properties of normal and fibrosclerotic human cerebral arteries. Atherosclerosis 1981;39:353-65.

[144] Cox RH, Detweiler DK. Arterial wall properties and dietary atherosclerosis in the racing greyhound. Am J Physiol 1979;236:H790-7.

[145] Newman DL, Gosling RG, Bowden NL. Changes in aortic distensibility and area ratio with the development of atherosclerosis. Atherosclerosis 1971;14:231-40.

[146] Matsumoto T, Hayashi K, Ide K. Residual strain and local strain distributions in the rabbit atherosclerotic aorta. J Biomech 1995;28:1207-17.

[147] Gabella G. Complex structure of the common carotid artery of sheep. Anat Rec 1995;243:376-83.

[148] Takamizawa K, Hayashi K, Matsuda T. Isometric biaxial tension of smooth muscle in isolated cylindrical segments of rabbit arteries. Am J Physiol Heart Circ Physiol 1992;263:H30-4.

[149] Roy S, Silacci P, Stergiopulos N. Biomechanical properties of decellularized porcine common carotid arteries. Am J Physiol Heart Circ Physiol 2005;289:H1567-76.

[150] Deng LY, Schiffrin EL. Effects of endothelin-1 and vasopressin on resistance arteries of spontaneously hypertensive rats. Am J Hypertens 1992;5:817-22.

[151] Thybo NK, Korsgaard N, Eriksen S, et al. Dose-dependent effects of perindopril on blood pressure and small-artery structure. Hypertension 1994;23:659-66.

[152] Touyz RM. Molecular and cellular mechanisms regulating vascular function and structure--implications in the pathogenesis of hypertension. Can J Cardiol 2000;16:1137-46.

[153] Rachev A, Taylor WR, Vito RP. Calculation of the Outcomes of Remodeling of Arteries Subjected to Sustained Hypertension Using a 3D Two-Layered Model. Ann Biomed Eng 2013.

Chapter 1

ACTIVE AXIAL STRESS IN MOUSE AORTA

A. Agianniotis[1], A. Rachev[2], N. Stergiopulos[1]

[1] Laboratory of Hemodynamics and Cardiovascular Technology, Institute of Bioengineering, Ecole Polytechnique Fédérale de Lausanne, Lausanne, Switzerland

[2] College of Engineering and Computing, University of South Carolina, South Carolina, USA

Abstract

The study verifies the development of active axial stress in the wall of mouse aorta over a range of physiological loads when the smooth muscle cells are stimulated to contract. The results obtained show that the active axial stress is virtually independent of the magnitude of pressure, but depends predominately on the longitudinal stretch ratio. The dependence is non-monotonic and is similar to the active stress-stretch dependence in the circumferential direction reported in the literature. The expression for the active axial stress fitted to the experimental data shows that the maximum active stress is developed at longitudinal stretch ratio 1.81, and 1.56 is the longitudinal stretch ratio below which the stimulation does not generate active stress. The study shows that the magnitude of active axial stress is smaller than the active circumferential stress. There is need for more experimental investigations on the active response of different types of arteries from different species and pathological conditions. The results of these studies can promote building of refined constrictive models in vascular rheology.

Keywords

Mechanical behavior; Active stress; Mouse aorta; Vascular smooth muscle cells; Biaxial active response

Published in:

Journal of Biomechanics, 45:1924-1927, 2012

Introduction

Soft biological tissues exhibit a complex mechanical behavior. Deformation due to applied loads in total absence of vascular tone is considered as the passive response of the wall, whereas the active response of the arterial wall refers to stress developed due to the contraction of vascular smooth muscle (VSM) cells.

Rachev and Hayashi (1999) were the first who accounted for the response of the VSM within the framework of constitutive formulation of continuum mechanics. The constitutive stress-strain relation was derived by adding the active stress to the passive circumferential stress. The active circumferential stress was suggested to be a function of the length-tension relationship and of the applied stimulus according to an active tension-dose relationship obtained from isometric contraction tests (Dobrin, 1973, 1983). The model suggested by Rachev and Hayashi (1999) was adopted by many researchers thereafter and provided a satisfactory description of the active response of a broad type of arteries such as the common carotid artery (Gleason et al., 2008; Gleason et al., 2004; Gleason and Humphrey, 2004), the basilar artery (Cardamone et al., 2009; Karšaj and Humphrey, 2012; Valentin et al., 2009; Valentin and Humphrey, 2009), or the iliac artery (Humphrey and Wilson, 2003). In the model of Rachev and Hayashi and in many of the subsequent studies, the contribution of active stress was assumed to be only in the circumferential direction. There are, however, histological findings that show in some arteries the existence of two main orientations of vascular smooth muscle cells; one family of cells is oriented in the circumferential direction and the other is oriented longitudinally (Gabella, 1995). Takamizawa et al. (1992) have reported inflation-extension experiments on arterial tissue under relaxed and contracted VSM cells and showed that the isometric response of the muscle cells produced active tension in both the circumferential and axial direction. Cardamone et al. (2010) and Wagner and Humphrey (2011) proposed that the active axial stress depends on the circumferential stretch.

Based on the observation that VSM tone produces active stress in both the circumferential and axial directions, there is clearly a need for developing constitutive relations for the arterial wall, which take appropriately into account the bi-axial contribution of active stress. The goal of the present study is to describe experimentally the active stress under isometric conditions and propose an analytical expression for the active stress component in the axial direction.

Methods

Mechanical testing

Thoracic aortas from 6 mice (C57BL/6J) of both sexes 10- to 12-week-old were excised. Each artery was cleaned and mounted to our pressure myograph device (Rezakhaniha and Stergiopulos, 2008). Tests were performed in Krebs-Henseleit solution at 37 ^{o}C and at pH of 7.4 continuously bubbled with standard gas (95% O_2 + 5% CO_2). We performed extension-inflation mechanical tests at three different axial stretches, namely at λ_z = 1.6, 1.8 and 2.0, and under maximally contracted or fully relaxed state of the VSM cells. The different values of axial stretch that we imposed, allowed each vessel to be tested below, near and above its *in vivo* axial stretch. In brief, after excision we measured the unloaded length and once the artery was mounted on the testing apparatus we applied an axial stretch of 1.6. Then, we induced maximal contraction by adding in the bath phenylephrine to a final concentration of 10^{-5} M and allowed the artery to acclimate for 15 min. The pressure was increased from 0 to 150 mmHg at constant rate of approximately 1.3 mmHg/s while pressure-outer diameter and pressure-longitudinal force curves were recorded. Then, the artery was stretched to axial stretch 1.8, allowed to acclimate for 15 min and the second pair of curves was recorded. The same procedure was repeated for axial stretch 2.0. Then, to record the passive response, we stretched the artery to axial stretch 1.6, we drained and rinsed the bath, added sodium nitroprusside in a final concentration of 10^{-5} M to maximally relax the VSM, and allowed the artery to acclimate for 15 min. The artery underwent 6-7 inflation-deflation loops until the pressure-outer diameter curves became reproducible. The final ascending pressure-outer diameter curve and the corresponding pressure-axial force curve were used for data analysis. The same procedure was followed for the axial stretches 1.8 and 2.0.

The external diameter was measured using a CCD micrometer (Keyence High Accuracy CCD micrometer), the lumen pressure was measured by a pressure transducer (World Precision Instruments WPI, BLPR) and the axial force by a load-cell force transducer (World Precision Instruments WPI, FORT10). The *in vivo* axial stretch ($\lambda_{z,iv}$) was calculated as the ratio of the *in vivo* length of the mouse thoracic aorta and the *ex vivo* unloaded length. The *in vivo* length was estimated by placing a string on the surface of the aorta along its axis prior to cutting between the two dissection points and then measuring the length of the string. Similar procedure was used to measure the *ex vivo* length. After the mechanical testing, thin rings of 0.4 mm width were cut from the middle part of the artery. They were kept in Krebs-Henseleit

solution for 20 min and then the inner (R_i) and outer (R_o) radius of the rings was measured using a wide-field microscope (Leica stereomicroscope MZ16 1FA).

Biomechanical analysis

We assume that the total stress in the arterial wall can be described as the sum of the passive and the active stress. The passive stress is derived from the strain-energy density function (SEF). The total Cauchy stress tensor (**σ**) has the form

$$\boldsymbol{\sigma} = -p\mathbf{I} + \mathbf{F}\cdot\frac{\partial W}{\partial \mathbf{E}}\cdot\mathbf{F}^T + \sigma_\theta^a \mathbf{e}_\theta \otimes \mathbf{e}_\theta + \sigma_z^a \mathbf{e}_z \otimes \mathbf{e}_z \qquad (1)$$

where p is an unknown scalar function enforcing the incompressibility constraint $\det\mathbf{F} \equiv 1$, $\mathbf{F}$ is the deformation gradient tensor, $\mathbf{F}^T$ is the transpose of the deformation gradient tensor, $\mathbf{I}$ is the unit tensor, W is the SEF that describes the passive mechanics of the wall, $\mathbf{E}$ is the Green strain tensor, σ_θ^a is the active circumferential stress, σ_z^a is the active axial stress, $\mathbf{e}_\theta$ is the unit vector in circumferential direction and $\mathbf{e}_z$ is the unit vector in axial direction.

The equation of equilibrium in the axial direction of an arterial vessel that has closed ends and is subjected to a lumen pressure P and an axial force F_w is (Humphrey, 2002)

$$F_w - F_z - \pi r_i^2 P = 0 \qquad (2)$$

where F_w is the resultant axial force in the wall due to axial Cauchy stress, F_z is the recorded axial force, r_i is the inner radius of the artery and P is the lumen pressure. We calculate the undeformed cross-sectional area using measurements from the cross-section of arterial rings as

$$A_f = \pi(R_o^2 - R_i^2) \qquad (3)$$

where R_o and R_i are the undeformed outer and inner radius, respectively. Assuming incompressibility of the wall, the current inner radius can be computed from the recorded outer radius r_o, the undeformed cross-sectional area A_f and the imposed axial stretch λ_z as

$$r_i = \sqrt{r_o^2 - \frac{A_f}{\pi \lambda_z}} \tag{4}$$

The mean total axial stress is calculated as

$$\bar{\sigma}_z = \frac{F_w}{A} \tag{5}$$

where $A = \frac{A_f}{\lambda_z}$ is the current cross-sectional area of the wall.

To calculate the active axial stress we compare the axial stress in the arterial wall when the smooth muscle cells are maximally relaxed (passive arterial response) to the axial stress when the smooth muscle cells are stimulated to contract keeping identical arterial diameter and axial stretch ratio (active response under isometric contraction). Because the circumferential and axial stretch ratios are identical in both cases, the contribution of the second term in the right hand side of Eq. (1) to the total axial stress is the same. The difference in stresses is due to the contribution of the scalar function *p* (the first term in Eq.1) and to the active axial stress, if it exists, in the case of isometric contraction. Without loss of generality, the radial component of the Green strain tensor can be eliminated from the analytical form of the strain energy function by using the incompressibility condition. As was shown in (Rachev, 2003) the value of the scalar function is equal to radial stress across the wall thickness. The mean value of the radial stress in a tube inflated by an internal pressure is (Humphrey, 2002).

$$\bar{\sigma}_r = -P \frac{r_i}{r_i + r_o} \tag{6}$$

After subtraction of the axial stress resultant in the case of relaxed smooth muscle from the stress resultant for the contracted vessel, both calculated at equal arterial deformed diameters, and use of the Eqs (1), (2), (5) and (6), the following expression for the active axial stress holds valid

$$\sigma_z^a = \frac{F_{wc} - F_{wr}}{A} + \frac{r_i \left(P_c - P_r \right)}{r_i + r_o} \tag{7}$$

where the subscripts c and r stand for the cases of stimulated and relaxed smooth muscle, respectively.

To calculate the active circumferential stress we compare the circumferential stress in the arterial wall when the smooth muscle cells are maximally relaxed to the circumferential stress when the smooth muscle cells are stimulated to contract keeping identical arterial diameter and axial stretch ratio. The mean value of the circumferential stress in a tube inflated by an internal pressure is (Humphrey, 2002)

$$\bar{\sigma}_\theta = P\frac{r_i}{r_o - r_i} \tag{8}$$

After subtraction of the circumferential stress resultant in the case of relaxed smooth muscle from the stress resultant for the contracted vessel, both calculated at equal arterial deformed diameters, and use of the Eqs (1), (6) and (8), the following expression for the active axial stress holds valid

$$\sigma_\theta^a = r_i\left(\frac{1}{r_o - r_i} + \frac{1}{r_i + r_o}\right)\left(P_c - P_r\right) \tag{9}$$

where the subscripts c and r stand for the cases of stimulated and relaxed smooth muscle, respectively.

It has been experimentally established that the active stress developed by the smooth muscle cells when they are stimulated to contract depends on two main factors, namely the intrinsic capability of the cells to generate stress when activated and the configuration of contractile proteins inside the cells (Dobrin, 1973, 1983). With account for these findings and inspired by the constitutive formulation of the active circumferential stress proposed in (Rachev, 2000), the experimentally recorded data are fitted by the following expression for the active axial stress

$$\sigma_z^a = S\lambda_z\left[1 - \left(\frac{\lambda_{z,\max} - \lambda_z}{\lambda_{z,\max} - \lambda_{z,0}}\right)^2\right] \tag{10}$$

where S is the maximum stress generated by the VSM cells at axial stretch ratio $\lambda_{z,\max}$, and $\lambda_{z,0}$ is the axial stretch ratio below which the stimulation does not generate active stress. The magnitude of S depends on the intensity of stimulation and reflects the level of contractile activity of the VSM cells, which in turn depends on calcium concentration within the VSM.

Results

The morphometric measurements showed that the average unloaded dimensions of the mouse thoracic aorta were: inner radius R_i = 0.309 ± 0.024 mm, outer radius R_o = 0.385 ± 0.033 mm, and *in vivo* axial stretch ratio $\lambda_{z,iv}$ = 1.76 ± 0.08. Representative pressure-outer diameter and pressure-axial force relationships for axial stretch 1.6, 1.8 and 2.0 and pressure interval [0 – 150] mmHg are shown in Fig. 1.

Following the data processing we found that, at constant axial stretch ratio, the stimulated artery develops an active axial stress, which is virtually independent of the magnitude of pressure (Fig. 2A). This means that the active stress, at least over the range of parameters in this study, does not depend on the circumferential strain. However, the active stress varies non-monotonically with the axial stretch ratio (Fig. 2B). The experimentally recorded data were fitted by Eq. 10 with parameters S = 38.81 kPa, $\lambda_{z,\max}$ = 1.81, and $\lambda_{z,0}$ = 1.56 (Fig. 2B). Following the data processing we found that the stimulated artery develops an active circumferential stress which increases monotonically with the magnitude of pressure (Fig. 2C).

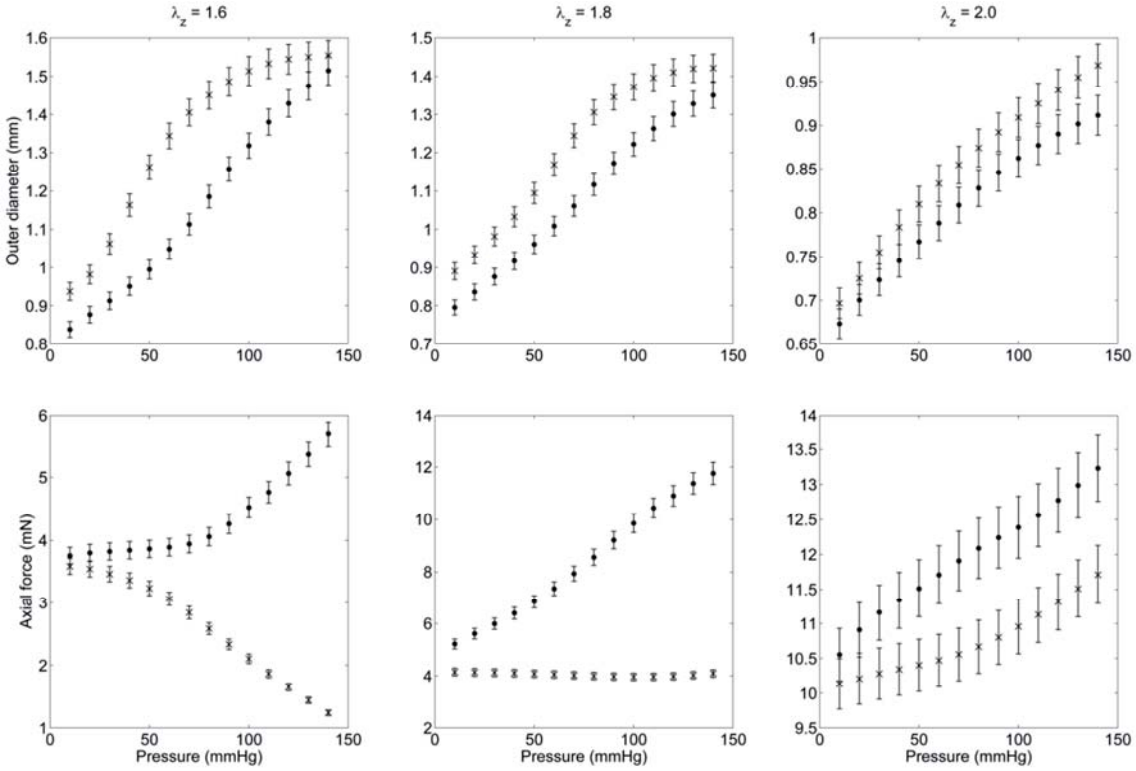

Figure 1. Representative recorded pressure-outer diameter and pressure-axial force curves for the three different axial stretches 1.6, 1.8, and 2.0. With **x** are the curves when the VSM cells are fully relaxed and with • when they are maximally contracted. Data are given as mean value with SD of the mean value.

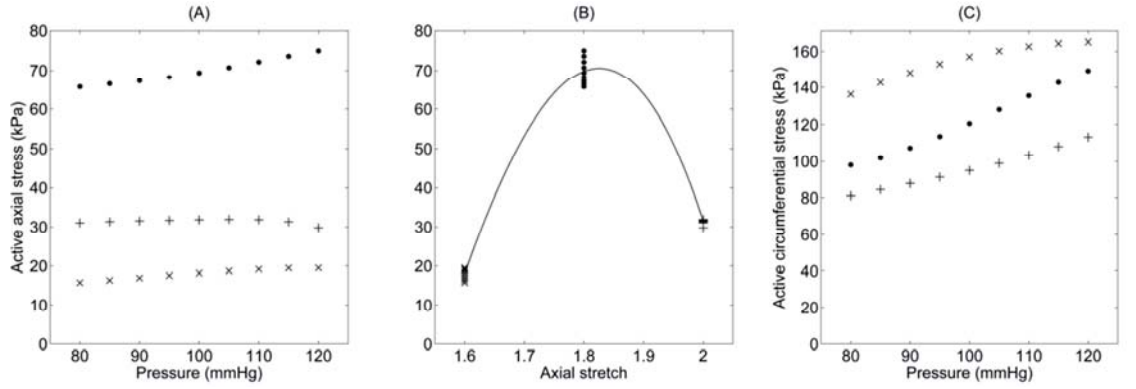

Figure 2. (A) Active axial stress as a function of pressure that corresponds to physiological loading. **x**, • and **+** correspond to axial stretch 1.6, 1.8, and 2.0. (B) Active axial stress in physiological loading for the three different axial stretches 1.6, 1.8, 2.0, and curve of the proposed model (–). (C) Active circumferential stress as a function of pressure that corresponds to physiological loading. **x**, • and **+** correspond to axial stretch 1.6, 1.8, and 2.0.

Discussion

The level of VSM activation or tone has been proposed to be a very important parameter in vascular remodeling. Hypertension or hypotension (Fridez et al., 2002; Zulliger et al., 2002), change in flow (Rachev, 2000), or change in axial extension (Valentin et al., 2009; Valentin and Humphrey, 2009) cause remodeling of the wall and alter the VSM tone in order to restore wall stress and strain toward normal values.

Development of active stress in the circumferential and axial direction in mouse thoracic aorta reported in this study is supported by the experimental findings in (Takamizawa et al., 1992) and the histological evidence that the aorta may contain axially oriented smooth muscle cells (Humphrey, 2002). The magnitude of the active axial stress is smaller than the active circumferential stress reported here and in (Gleason and Humphrey, 2004; Rachev and Hayashi, 1999). This might be explained by the fact that most of the smooth muscle cells are oriented in the circumferential direction. Existence of biaxial active response observed in our study is in agreement also with the recently proposed constitutive models of the arterial tissue in (Cardamone et al., 2010; Wagner and Humphrey, 2011), albeit Wagner and Humphrey (2011) showed that the smooth muscle cells of the common carotid artery and the basilar artery appear to be oriented primarily in the circumferential direction. While the authors of these studies have postulated that the active axial stress depends on the value of the circumferential stretch ratio, our findings show that the active stress depends rather on the axial stretch ratio. This result can be explained by the axial orientation of part of the smooth muscle cells and by the dependence of the generated stress on the length of the deformed muscle fibers. Results of our study show that the axial stretch ratio below which no active axial stress is developed is 1.56. This value is higher than the corresponding stretch ratio that refers to the development of active circumferential stress (Gleason and Humphrey, 2004; Rachev, 2000; Rachev and Hayashi, 1999). To what extent this is due to the different arrangement of the contractile filaments within the muscular cells or to a specific connection of the smooth muscle cells to the extracellular matrix fibers or to the relative number of cells oriented in axial or circumferential direction remains an open question. There is need for further experimental investigations that include imaging of the smooth muscle cells and the extracellular matrix fibers in the passive state of the muscle cells and when they are stimulated to contract.

Though development of the active stress in the circumferential, and in some cases axial direction, is not a disputable fact, the manner by which the active stresses are calculated needs better justification. It is possible that the contraction of the smooth muscle cells that causes constriction of the artery affects the orientation of the collagen fibers in a manner that even at equivalent deformed configurations the passive contribution of collagen fibers to the circumferential and axial stress is different for stimulated and relaxed smooth muscle. This hypothesis is indirectly supported by the findings that the chemical dissolution of the muscle cells in porcine common carotid arteries modifies their structure and elastic properties (Roy et al., 2005). There is need for further experimental investigations on active response of arteries that include simultaneous analysis of morphological and mechanical data.

In conclusion, we have verified the development of active axial stress in the wall of mouse aorta over a range of physiological loads when the smooth muscle cells are stimulated to contract. The results obtained show that the active axial stress depends predominately on the longitudinal stretch ratio. The dependence is non-monotonic and is similar to the active stress-stretch dependence in the circumferential direction reported in the literature. However, there is need for more experimental investigations on the active response of different types of arteries from different species and pathological conditions. Results from these studies can promote building of refined constrictive models in vascular rheology.

Acknowledgements

The authors wish to thank Dr. Luciano Capettini for valuable help in obtaining the samples. This work was supported by the Swiss National Science Foundation (Grant No. 325230-125445).

References

Cardamone, L., Valentin, A., Eberth, J.F., Humphrey, J.D., 2009. Origin of axial prestretch and residual stress in arteries. Biomechanics and Modeling in Mechanobiology 8, 431-446.

Cardamone, L., Valentin, A., Eberth, J.F., Humphrey, J.D., 2010. Modelling carotid artery adaptations to dynamic alterations in pressure and flow over the cardiac cycle. Mathematical Medicine and Biology 27, 343-371.

Dobrin, P.B., 1973. Influence of initial length on length-tension relationship of vascular smooth muscle. American Journal of Physiology 225, 664-670.

Dobrin, P.B., 1983. Vascular mechanics. In: Bohr, D.F., Somlyo, A.P., Sparks, H.V., Bethesda, J. (Eds.), Handbook of Physiology. The Cardiovascular System. Vascular Smooth Muscle. MD: American Physiological Society, pp. 65-104.

Fridez, P., Makino, A., Kakoi, D., Miyazaki, H., Meister, J.J., Hayashi, K., Stergiopulos, N., 2002. Adaptation of conduit artery vascular smooth muscle tone to induced hypertension. Annals of Biomedical Engineering 30, 905-916.

Gabella, G., 1995. Complex structure of the common carotid artery of sheep. Anatomical Record 243, 376-383.

Gleason, R.L., Dye, W.W., Wilson, E., Humphrey, J.D., 2008. Quantification of the mechanical behavior of carotid arteries from wild-type, dystrophin-deficient, and sarcoglycan-delta knockout mice. Journal of Biomechanics 41, 3213-3218.

Gleason, R.L., Hu, J.J., Humphrey, J.D., 2004. Building a functional artery: issues from the perspective of mechanics. Frontiers in Bioscience 9, 2045-2055.

Gleason, R.L., Humphrey, J.D., 2004. A Mixture Model of Arterial Growth and Remodeling in Hypertension: Altered Muscle Tone and Tissue Turnover. Journal of Vascular Research 41, 352-363.

Humphrey, J.D., 2002. Cardiovascular Solid Mechanics: Cells, Tissues, and Organs. Springer, New York.

Humphrey, J.D., Wilson, E., 2003. A potential role of smooth muscle tone in early hypertension: a theoretical study. Journal of Biomechanics 36, 1595-1601.

Karšaj, I., Humphrey, J.D., 2012. A multilayered wall model of arterial growth and remodeling. Mechanics of Materials 44, 110-119.

Rachev, A., 2000. A Model of Arterial Adaptation to Alterations in Blood Flow. Journal of Elasticity 61, 83-111.

Rachev, A., 2003. Remodeling of arteries in response to changes in their mechanical environment. In: Holzapfel, G., Ogden, R. (Eds.), Biomechanics of Soft Tissue in Cardiovascular Systems. CISM Courses and Lectures, Course and Lecture No 441. Springer, Wien New York, pp. 100-161.

Rachev, A., Hayashi, K., 1999. Theoretical study of the effects of vascular smooth muscle contraction on strain and stress distributions in arteries. Annals of Biomedical Engineering 27, 459-468.

Rezakhaniha, R., Stergiopulos, N., 2008. A structural model of the venous wall considering elastin anisotropy. Journal of Biomechanical Engineering 130, 031017.

Roy, S., Silacci, P., Stergiopulos, N., 2005. Biomechanical properties of decellularized porcine common carotid arteries. American Journal of Physiology - Heart and Circulatory Physiology 289, H1567-1576.

Takamizawa, K., Hayashi, K., Matsuda, T., 1992. Isometric biaxial tension of smooth muscle in isolated cylindrical segments of rabbit arteries. American Journal of Physiology - Heart and Circulatory Physiology 263, H30-34.

Valentin, A., Cardamone, L., Baek, S., Humphrey, J.D., 2009. Complementary vasoactivity and matrix remodelling in arterial adaptations to altered flow and pressure. Journal of the Royal Society Interface 6, 293-306.

Valentin, A., Humphrey, J.D., 2009. Modeling effects of axial extension on arterial growth and remodeling. Medical and Biological Engineering and Computing 47, 979-987.

Wagner, H.P., Humphrey, J.D., 2011. Differential passive and active biaxial mechanical behaviors of muscular and elastic arteries: basilar versus common carotid. Journal of Biomechanical Engineering 133, 051009.

Zulliger, M.A., Montorzi, G., Stergiopulos, N., 2002. Biomechanical adaptation of porcine carotid vascular smooth muscle to hypo and hypertension in vitro. Journal of Biomechanics 35, 757-765.

Chapter 2

WALL PROPERTIES OF THE APOLIPOPROTEIN E-DEFICIENT MOUSE AORTA

A. Agianniotis, N. Stergiopulos

Laboratory of Hemodynamics and Cardiovascular Technology, Institute of Bioengineering, Ecole Polytechnique Fédérale de Lausanne, Lausanne, Switzerland

Abstract

Objectives

We quantified the dysfunction of the aortic wall, determined structural and elastic properties, and provided histological data of the thoracic aortas of apolipoprotein E (apoE)-deficient mice which are used as model of atherosclerosis.

Methods

Six young 10-12 week-old (apoE)-deficient mice of both sexes were studied and six age-matched C57BL/6J wild-type mice were used as control group. We performed extension-inflation mechanical tests at three different axial stretches (λz = 1.6, 1.8, and 2.0), under maximally contracted or totally relaxed state of the vascular smooth muscle cells. Classical histology was performed on the arterial segments.

Results

Control aortas were generally more distensible than the (apoE)-deficient mouse aortas under both relaxed and contracted smooth muscle. Also, aortas from (apoE)-deficient mice were stiffer (higher incremental elastic modulus) than control aortas. Control aortas exhibited a higher active diameter response compared to (apoE)-deficient mouse aortas, despite the fact that vascular smooth muscle cell density was increased by approximately 15% in the (apoE)-deficient mouse aortas.

Conclusion

We found substantial changes in the structural and elastic properties of the wall, in the active diameter response and in the histology of (apoE)-deficient mouse aortas compared to the control group. Our data can be used in the development of constituent-based models of the arterial wall and in studying the changes in arterial wall properties in the presence of disease, such as atherosclerosis.

Keywords

Mouse aorta; Wall dysfunction; Active diameter response; Vascular smooth muscle cells; Arterial wall properties; Atherosclerosis

Published in:

Atherosclerosis, 223:314-320, 2012

Introduction

Atherosclerosis is a focal multifactorial disease. Although it is difficult to determine with certainty the specific events that lead to atherogenesis in humans, there is ample evidence that local biomechanical factors (i.e., local shear or wall stress) may play a significant role. Different animal models have been developed that mimic closely the human form of the disease. The models that are most relevant to human atherosclerotic disease include hypercholesterolemic nonhuman primates, swine, the Watanabe heritable hyperlipidemic rabbit, apolipoprotein E (apoE)-deficient mouse and the low density lipoprotein receptor-negative mouse. The characterization of biomechanical properties of arteries in these animal models is obviously a prerequisite for any subsequent analysis of the causal relationship between local stress and development of disease.

Lesions of atherosclerosis appear principally in branch points, at outflow tracts, or at bifurcations. Lesions in (apoE)-deficient mice that are fed chow diet can be detected at 10 weeks of age. Initial sites of development of lesions include the aortic root, the lesser curvature of the aortic arch, the aortic bifurcation, the renal arteries, the pulmonary artery, the right common carotid artery, the branches of the brachiocephalic artery, and the superior mesenteric artery [1]. With increasing age of mice, lesions can be detected in the descending thoracic aorta, the lower abdominal aorta, the femoral arteries, the proximal coronary, and the common iliac artery. Lesions consisting of mixture of spindle-shaped cells and foam cells develop with increasing age, and fibrous plaques appear after 20 weeks of age [1].

In the present study we analyze the biomechanical properties of the aorta of the (apoE)-deficient mouse because it is a well-established common model of atherosclerosis [2]. Specifically, the first goal of this study was to quantify the dysfunction of the aortic wall of the thoracic aorta. The second goal was to determine the mechanical properties, and to provide data that can be used in modeling the behavior of the arterial wall and in studying the growth and remodeling in the disease of atherosclerosis.

Material and methods

We studied the thoracic aortas of six 10-12 week-old (apoE)-deficient mice of both sexes. As a control group, we used thoracic aortas of six 10-12 week-old

C57BL/6J wild-type mice of both sexes. All animals were obtained from Charles River Laboratories (France) and fed non-atherosclerotic diet.

Experimental procedures

Biomechanical testing

Thoracic aortas from the (apoE)-deficient and C57BL/6J wild-type mice were excised, cleaned and mounted to our biomechanical testing device [3]. Extension – inflation mechanical tests were performed in Krebs-Hanseleit solution (in mM: 110.8 NaCl, 5.9 KCl, 25.0 $NaHCO_3$, 1.07 $MgSO_4$, 2.49 $CaCl_2$, 2.33 NaH_2PO_4 and 11.51 glucose, pH 7.4) at 37 ^oC. The tests were performed at three different axial stretches, namely at λ_z = 1.6, 1.8, and 2.0, and under maximally contracted or fully relaxed state of the VSM cells. The different values of axial stretch that we imposed, allowed each vessel to be tested below, near and above its in vivo axial stretch. Each arterial segment was first stretched to an axial stretch of 1.6. We added to the bath phenylephrine to a final concentration of 10^{-5} M to induce contraction of the VSM cells, and left the artery to acclimate for 15 min. Then, we increased the pressure from 0 to 150 mmHg (approximate rate: 1.3 mmHg/s) and external diameter data were measured with a CCD micrometer (model LS-7030MT, Keyence) while pressure was recorded with a blood pressure transducer (BLPR, World Precision Instruments). The inflation of the artery was repeated for axial stretches 1.8 and 2.0. Then we brought back the arterial segment to an axial stretch of 1.6, and drained and rinsed the bath with Krebs-Hanseleit solution. We added to the bath sodium nitroprusside in a final concentration of 10^{-5} M to induce relaxation of the VSM cells, and left the artery to acclimate for 15 min. We submitted the arterial segment to 6-7 preconditioning cycles from 0 to 150 mmHg to ensure repeatability of the curve. The procedure was repeated for axial stretches 1.8 and 2.0.

The in vivo axial stretch ratio was calculated as the ratio of the in vivo length of the artery and the ex vivo unloaded length. After the mechanical testing, arterial rings of 0.4 mm axial thickness were cut from the middle of each segment to measure the inner and outer radius. The rings were placed in a Petri dish with Krebs-Hanseleit solution at 37 ^oC and photographs were taken under an upright microscope (Leica MZ16 1FA). The remainder of the arterial segment was used for histological analysis.

Histological analysis

Immediately after we cut the arterial segments to get the arterial rings, we placed the arteries in paraformaldehyde (4% in PBS, pH 7.4). The arterial segments were prepared for classical histology and cross-section slices of 7 μm thickness were taken from both wild-type and (apoE)-deficient mice and used for histological analysis. Different sections were stained with Hematoxylin-eosin, Miller's elastic stain or Masson's trichrome stain. Optic microscopy was performed with a commercial imaging system (Olympus AX70 and UPlan FL20x/0.5 objective; Olympus, Tokyo, Japan), and pictures were acquired with an Olympus DP 70 CCD color camera. The mean VSM cell density in the media was estimated by counting the number of nuclei per unit area in Hematoxylin-eosin stained sections. The Miller's elastic stain and the Masson's trichrome stain were used to color for elastin and collagen, respectively, and elastin and collagen area-fractions were computed. Histology images were processed using ImageJ software (NIH, Bestheda, Maryland, USA).

Mechanical data analysis

Structural properties

We combine external diameter – pressure data with zero-load state data in order to calculate the inner diameter, wall area, distensibility and elastic modulus of the arterial segments. Using the inner (R_i) and outer (R_o) radius measured at the zero-load state, the axial stretch (λ_z), and assuming incompressible wall we calculate the arterial wall area (A_w) for the specific axial stretch as

$$A_w(\lambda_z) = \frac{\pi(R_o^2 - R_i^2)}{\lambda_z} \tag{1}$$

and we calculate the inner diameter of the wall as

$$d_i(p) = \sqrt{d_o^2(p) - \frac{4A_w}{\pi}} \tag{2}$$

The structural characteristics are assessed by means of the cross-sectional distensibility [4]

$$D(p) = \frac{1}{A(p)} \frac{\partial A(p)}{\partial p} \tag{3}$$

where $A = \pi d_i^2 / 4$ is the luminal cross-section area.

Elastic properties

The elastic properties of the arterial wall are expressed by means of the Hudetz incremental elastic modulus [5]

$$H_{\theta\theta}(p) = 2\left[\frac{d_o(p)d_i^2(p)}{\frac{\partial d_o(p)}{\partial p}} + pd_o^2(p)\right]\frac{1}{d_o^2(p) - d_i^2(p)} \qquad (4)$$

Active diameter response

The active diameter response of the arterial wall is expressed as the difference in diameter between pressure – outer diameter data of relaxed and contracted state at specific values of pressure. The active diameter response is a measure to assess and quantify the VSM cell dysfunction.

Statistics

All reported values are given as mean values with SD of the mean value. Two-tailed Student's t-tests were performed for comparison of the biomechanical properties, morphometric data, and histologic data of control and (apoE)-deficient mouse arteries. $P < 0.05$ was considered significant.

Results

Biomechanical analysis

Experimental pressure – outer diameter curves of (apoE)-deficient mouse and control arteries under maximally contracted and fully relaxed VSM cells for axial stretches 1.6, 1.8 and 2.0 and pressure interval [0 – 150] mmHg are presented in Fig. 1. The pressure – outer diameter curves are shifted to lower diameters at all levels of lumen pressure following activation by phenylephrine.

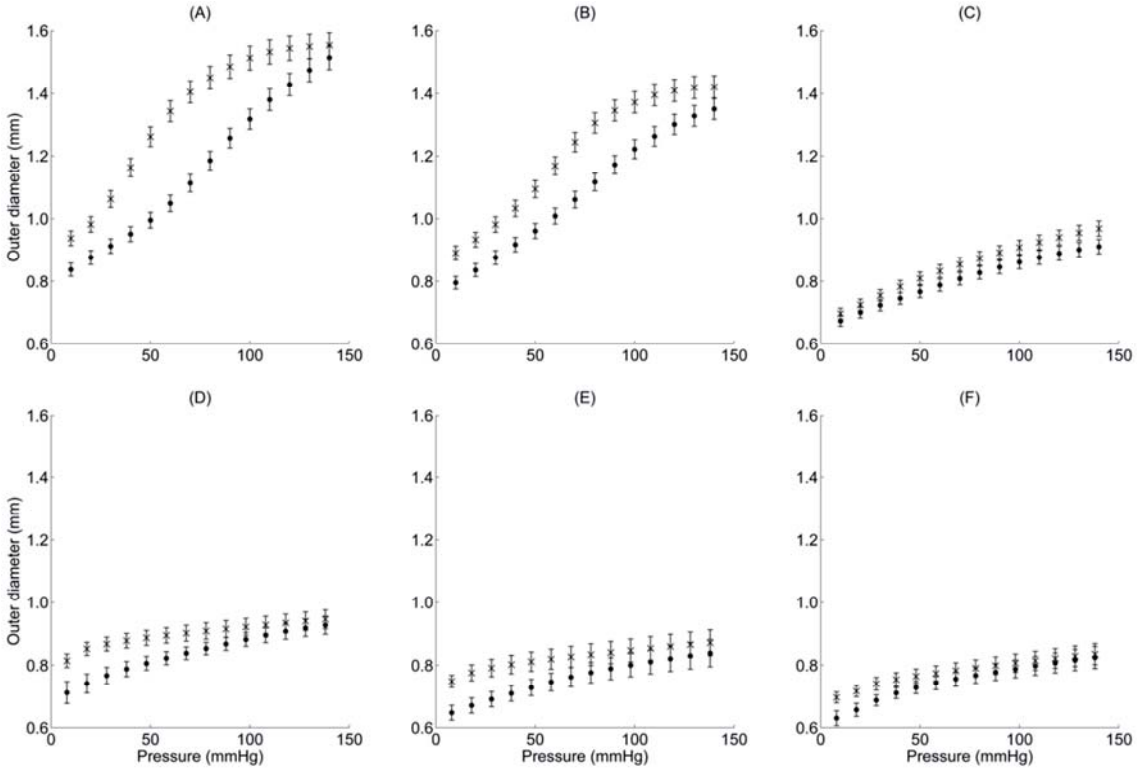

Figure 1. Experimental pressure – outer diameter curves of control (A, B, C) and (apoE)-deficient mouse (D, E, F) thoracic aortas for the three different axial stretches 1.6 (A, D), 1.8 (B, E), and 2 (C, F) when the VSM cells are fully relaxed (x) or maximally contracted (•). Data are given as mean value with SD of the mean value.

In Fig. 2 we provide a comparison of the distensibility between control and (apoE)-deficient mouse arteries. The distensibility of control arteries is higher than the distensibility of (apoE)-deficient mouse arteries for the whole range of lumen pressures in any axial stretch in the case of relaxed VSM cells. When the VSM cells are activated, the control arteries appear to be more distensible than the (apoE)-deficient mouse arteries for medium and higher pressures. In lower pressures the distensibility of the (apoE)-deficient mouse arteries is higher. The peak of the pressure – distensibility curve for the control arteries is decreased with increased axial stretch for both cases of relaxed and contracted VSM cells. The distensibility of control and (apoE)-deficient mouse arteries under relaxed or contracted state of VSM cells for the three different axial stretches at the physiological pressure of 100 mmHg is presented in table 1. Table 1 shows that the contraction of the VSM cells results in increase of the distensibility of the arteries for both control and (apoE)-deficient mouse at the physiological pressure of 100 mmHg. Also, at the same state of VSM

cells the control arteries are significantly more distensible than the (apoE)-deficient mouse arteries.

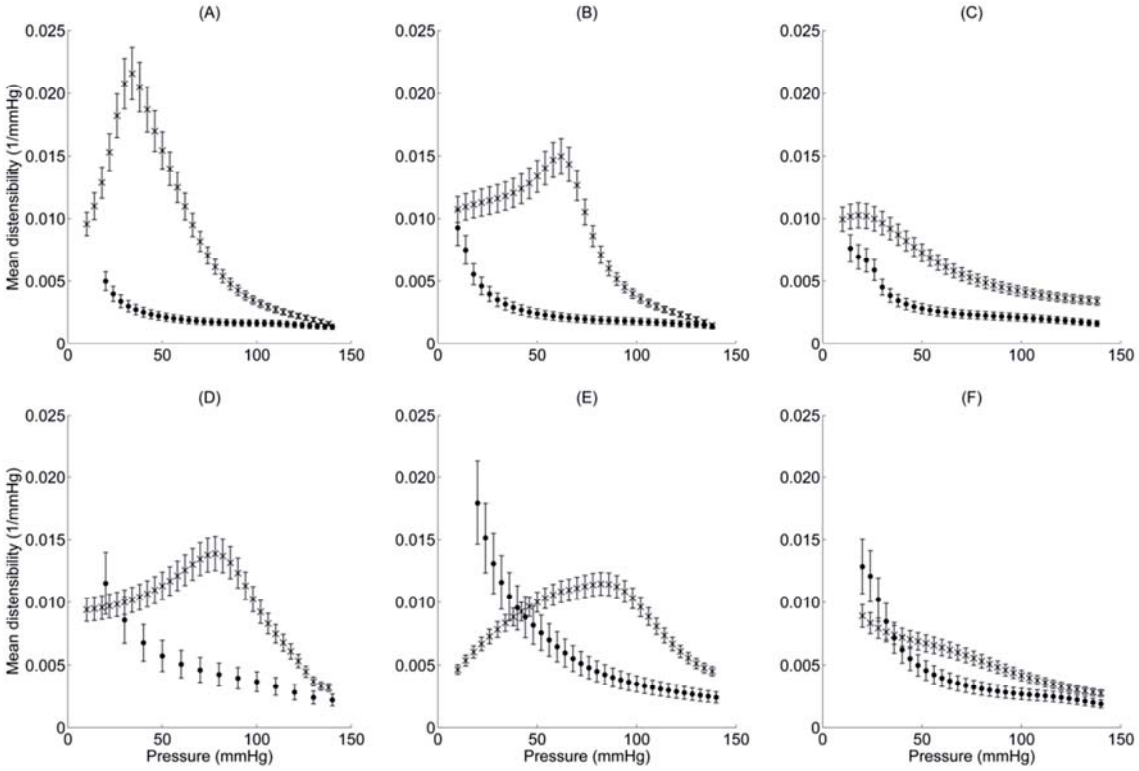

Figure 2. Distensibility – pressure curves of control (x) and (apoE)-deficient (•) mouse thoracic aortas for axial stretches 1.6 (A, D), 1.8 (B, E), and 2.0 (C, F), and for relaxed (A, B, C) and contracted (D, E, F) state of the VSM cells. Data are given as mean value with SD of the mean value.

The active diameter response of the arterial wall over a range of physiological loads is presented in Fig. 3. The values of the diameter response are normalized by the outer diameter that corresponds to the relaxed state of the VSM cells. The active diameter response of the (apoE)-deficient mouse arteries is smaller compared to the response of the control arteries for the whole range of pressures presented. At the pressure of 100 mmHg the active diameter response of the (apoE)-deficient mouse arteries is reduced about 69%, 49%, and 56% of the control value, for axial stretches 1.6, 1.8, and 2.0, respectively.

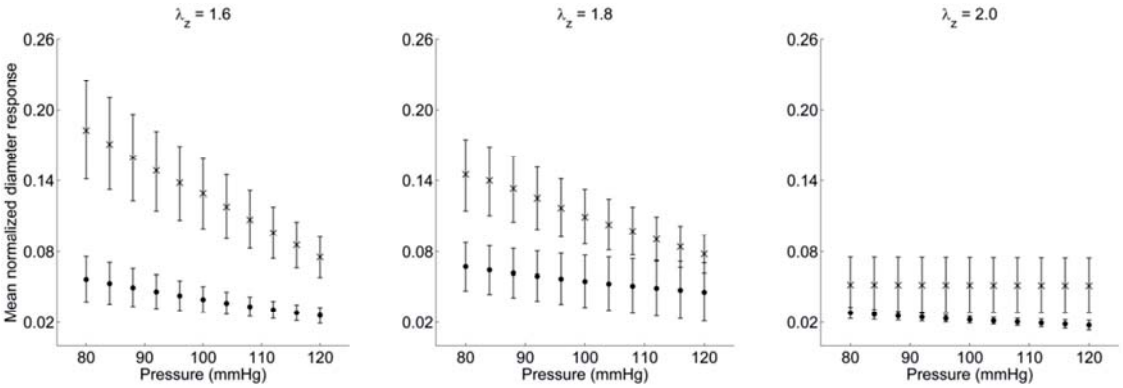

Figure 3. Active diameter response curves of control (x) and (apoE)-deficient (•) mouse thoracic aortas for axial stretches 1.6, 1.8, 2.0. Data are given as mean value with SD of the mean value.

The Hudetz incremental elastic modulus is plotted against circumferential stretch in Fig. 4. The zero-load configuration of the control and the (apoE)-deficient mouse arteries was used as the reference configuration of the control and (apoE)-deficient mouse arteries, respectively.

Table 1. Mean (SD) distensibility (1/mmHg) at physiologic pressure of 100 mmHg for control and (apoE)-deficient mouse thoracic aortas and for axial stretches 1.6, 1.8, and 2.0. At the same state of VSM cells the control arteries are significantly more distensible than the (apoE)-deficient mouse arteries.

axial stretch		1.6	1.8	2.0
Relaxed	**Control**	0.003341 (0.000644)	0.003787 (0.000722)	0.004170 (0.000798)
	apoE	0.001659 (0.000514)	0.001783 (0.000540)	0.002095 (0.000588)
Contracted	**Control**	0.009720 (0.001897)	0.008079 (0.001565)	0.004189 (0.000838)
	apoE	0.003679 (0.001576)	0.003496 (0.001298)	0.002694 (0.000913)

Morphometric data

The morphometric measurements showed that the in vivo axial stretch ratio of the control and (apoE)-deficient mouse arteries is 1.76 ± 0.08 and 1.68 ± 0.16, respectively. The mean (SD) opening angle of the control arteries is 119 ± 16 degrees and the opening angle of the (apoE)-deficient mouse arteries is 115 ± 13.4 degrees. The mean (SD) inner and outer radius of the control arteries is 309 ± 24 μm and 385 ± 33 μm, respectively. The mean (SD) inner and outer radius of the (apoE)-

deficient mouse arteries is 299 ± 35 µm and 381 ± 41 µm, respectively. No significant difference of the opening angle, the inner radius and outer radius was found between control and (apoE)-deficient mouse arteries.

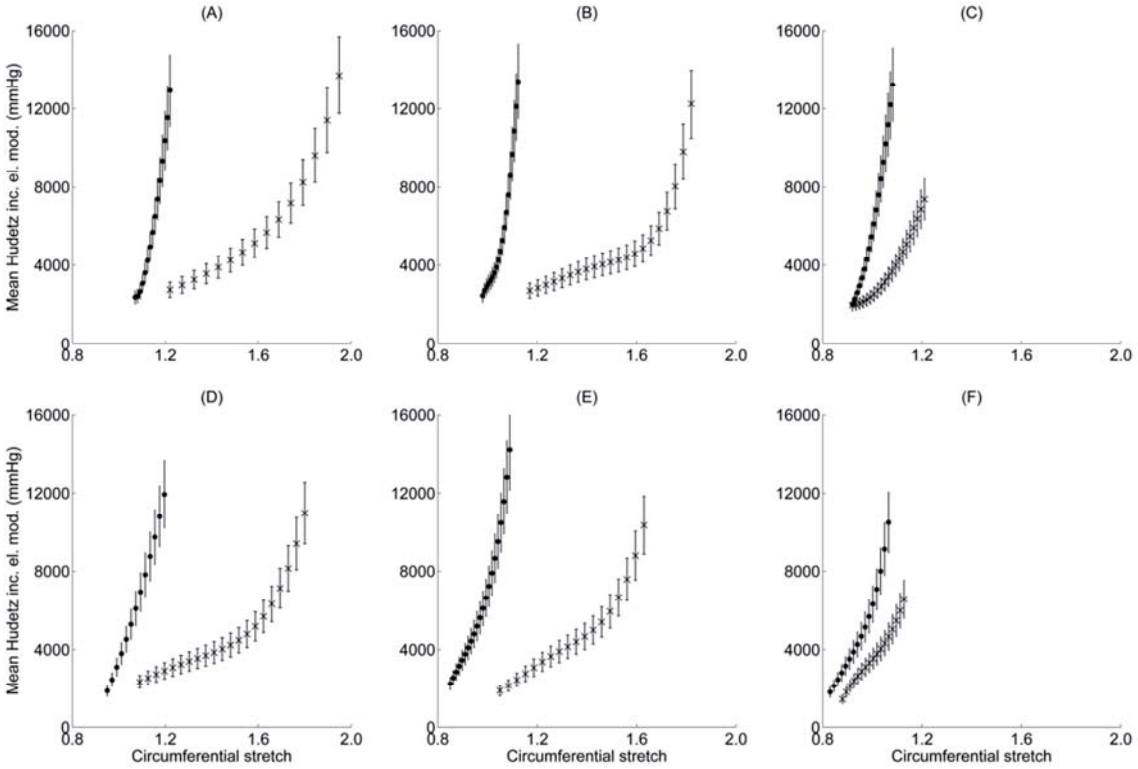

Figure 4. Hudetz inceremental elastic modulus – mean circumferential stretch curves of control (x) and (apoE)-deficient (•) mouse thoracic aortas for axial stretches 1.6 (A, D), 1.8 (B, E), 2.0 (C, F), and for relaxed (A, B, C) and contracted (D, E, F) state of the VSM cells. Data are given as mean value with SD of the mean value.

Histology

Histological sections of control and (apoE)-deficient mouse arteries stained with Hematoxylin-eosin, Miller's elastic stain and Masson's trichrome stain are shown in Fig. 5. The sections stained with Hematoxylin-eosin show higher number of nuclei in the (apoE)-deficient mouse arteries. From the image processing analysis we found that the mean cell density is 2892 nuclei/mm^2 and 3313 nuclei/mm^2 for control and (apoE)-deficient mouse arteries, respectively, which represents a non-significant higher cell density in (apoE)-deficient mouse aortas of about 15%. The image processing analysis of the sections stained with Miller's elastic stain show no significant difference in the area-fraction of elastin, which is calculated 37% and 38% for control and (apoE)-deficient mouse arteries, respectively. The analysis of sections stained with Masson's trichrome stain show significantly lower area-fraction of

collagen in (apoE)-deficient mouse arteries. The area-fraction of collagen is 20% and 7% for control and (apoE)-deficient mouse arteries, respectively.

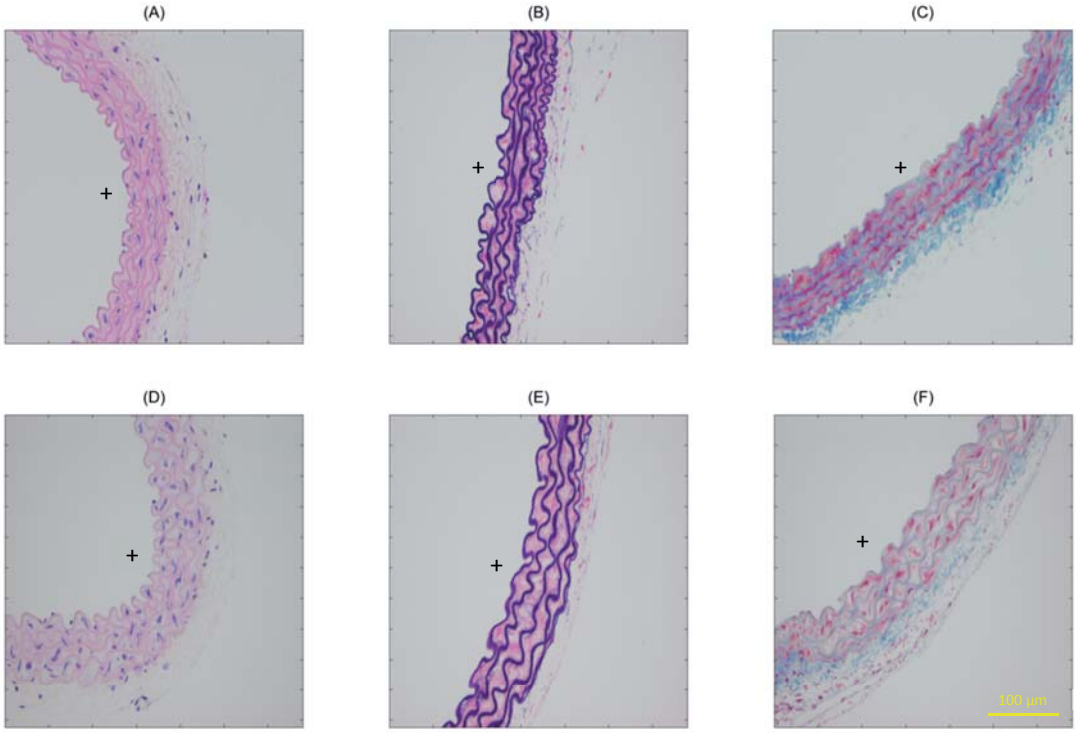

Figure 5. Histological sections of control (A, B, C) and (apoE)-deficient (D, E, F) mouse thoracic aortas. Sections A and D stained with Hematoxylin-eosin, sections B and E stained with Miller's elastic stain, and sections C and F stained with Masson's trichrome stain. The symbol "+" indicates the side of the lumen. Scale bar: 100 µm.

Discussion

Biaxial experiments providing mechanical data have been performed in arteries of various animals that are used as models of atherosclerosis. Such animals include cockerels [6], dogs [7], or rabbits [8]. Additionally, the biomechanical function of VSM cells has been studied in different animals, including dogs [7], rats [9], or rabbits [9]. Previous studies have shown that the endothelium-dependent vasodilation is attenuated by hyperlipidemia and atherosclerosis in animals. In the present study we have used a biaxial experimental device for the inflation and extension of thoracic aortas of (apoE)-deficient and wild type mice and we have provided biomechanical and histological data. The results demonstrate substantial changes in the structural and elastic properties of the wall, in the active diameter response of the wall, and in the histology of thoracic aortas of genetically engineered apolipoprotein E-deficient mice as compared to control group.

Structural properties

In contrast to control arteries, the pressure – outer diameter curves of the (apoE)-deficient mouse arteries do not have a sigmoidal shape (Fig. 1). This has as a consequence the distensibility curve to decrease monotonically with pressure (Fig. 2). Roach and Burton (1957) [10] have demonstrated that the resistance to stretch at low pressures is mainly due to elastin, whereas at high pressures collagen dominates. The results suggest that the collagen fibers are recruited at lower pressures in (apoE)-deficient mouse arteries than their control counterparts, which limits the elastic response of these arteries and results in a stiffer vessel.

When the VSM cells are activated, the peak of the distensibility – pressure curve of control arteries moves to higher pressures. This result is explained by the fact that, at given pressure, circumferential stretch of the arterial wall is reduced when the VSM cells are contracted. Therefore, the circumferential stretch for which the collagen fibers get engaged, contributing to a decrease in distensibility, is reached at higher pressures.

Elastic properties

The Hudetz incremental elastic modulus of (apoE)-deficient mouse arteries is greater than the Hudetz incremental elastic modulus of control arteries. Similar behavior was shown in [7, 11]. Hudetz et al. (1981) [11] have presented data on the incremental modulus of human carotid arteries as function of tangential stretch. In their results, the fibrosclerotic internal carotid artery has higher incremental modulus than the normal artery. Similarly, Cox and Detweiler (1979) [7] have shown that the incremental modulus of iliac and carotid arteries when expressed as a function of wall strain is higher in diet-fed dogs than in control dogs. In contrast, Hudetz et al. (1981) [11] have shown that the normal anterior cerebral artery has higher incremental modulus than the fibrosclerotic artery, and Newman et al. (1971) [6] have shown that the elastic modulus of aortas as function of pressure is higher in normal cockerels than in diet-fed cockerels.

At low stretch ratios apoE-deficient mice present stiffer aortas and this can possibly be explained by the greater fraction of elastin of (apoE)-deficient mouse arteries compared to control arteries, elastin being the main load-bearing component at low stretches. At higher circumferential stretches the incremental elastic modulus of (apoE)-deficient mouse aortas increases quite abruptly, whereas in the control artery group the elastic modulus increases more gradually. This is possibly caused by different rates of engagement of collagen between control and (apoE)-deficient

mouse arteries. To what extent this result is due to difference in the fraction of the elastic constituents between control and (apoE)-deficient mouse arteries, or due to different collagen engagement profile remains an open question.

Active diameter response

We induced the relaxation of the VSM cells using sodium nitroprusside and the contraction using phenylephrine in the same concentration for both cases of control and (apoE)-deficient mouse arteries. We observed differences in VSM mechanics between thoracic aortas of control mice and (apoE)-deficient mice. The maximum active diameter response was considerably lower in the (apoE)-deficient mouse arteries. This is in agreement with that found in [7]. Cox and Detweiler (1979) [7] have found considerably reduced active diameter response in iliac arteries of adult racing greyhounds used as atherosclerosis model. Also, it has been shown that murine models for atherosclerosis have impaired endothelium-dependent relaxation (cf. [12-13]), which may relate to an impaired contractile function as well.

The reduced active diameter response of the (apoE)-deficient mouse aortas could be explained by a) the change in the contractile function of the VSM cells, b) a different proportion of synthetic and contractile cell phenotype in the (apoE)-deficient mice, and c) by the fact that the (apoE)-deficient mouse arteries which appear stiffer may have a stiffer extracellular matrix which might limit the contractility of the VSM cells. The VSM cells exist in different phenotypes in the arterial wall. In the normal mature vessels the contractile phenotype is the predominant phenotype with major function the regulation of blood vessel diameter and blood flow [14-16] . Altered functional demands, however, can lead the VSM cells to change their phenotype to a relatively synthetic phenotype, as it is the case in early atherogenesis [17-19], and it has been shown that mouse VSM cells undergo this change of phenotype in response to a variety of atherogenic stimuli [20]. Therefore, the cells lose their contractility and instead gain the ability to secrete extracellular matrix component and divide. The change of the phenotypic state of the VSM cells from a relatively contractile to a relatively synthetic phenotype can explain the lower active diameter response of the (apoE)-deficient mouse aortas. There is need for further experimental investigations on the phenotypic state of the VSM cells.

Histology

The histological findings show differences between the control and the (apoE)-deficient mouse aortas. Hematoxylin-eosin staining reveals an increase in the number of cells per unit area in the wall of (apoE)-deficient mouse arteries. The result

is in accordance with studies which suggest that atherogenesis involves proliferation of VSM cells [21].

Limitations

We have limited our investigation on the thoracic aortas of mice because they are easy to dissect, they are relatively straight vessels and they can be attached to our experimental device to perform the biomechanical testing. We also performed the study in predefined longitudinal stretch ratios around the in vivo measured axial stretch ratio. The quantification of elastin and collagen was done through histology. This permits only qualitative measurements of elastin and collagen content, but this data are useful in the development of constituent-based models of the wall (cf. [22-23]). In the present study we used Masson's trichrome stain to visualize the collagen fibers which might fail to visualize very thin fibers. Picrosirius red which has the capacity to detect thin fibers could be used in combination with polarized light microscopy. This method, however, has also disadvantages. Collagen is not the only birefringent material in the tissue. For example, the birefringence of fibrin can equal that of the thinnest collagen fibers and that can complicate the analysis. If linearly polarized light is used, picrosirius red-stained fibers will appear dark if they are aligned parallel to the transmission axis of either of the two linearly polarized filters. Also, if circularly polarized light is used, the circular polarizers must be aligned in the crossed position, because imprecise alignment can result in orientation-dependent fiber colors and complicate the analysis [24]. We used the same reference configuration when the VSM cells are relaxed or contracted, although different reference configurations for the relaxed or the contracted state could have been used. Finally, we limited ourselves to young mice.

Conclusion

We have quantified the dysfunction of the aortic wall of (apoE)-deficient mice. Our results show that the active diameter response is considerably lower in the (apoE)-deficient mouse aortas. Additionally, these vessels have higher Hudetz incremental elastic modulus and lower distensibility. The histological analysis revealed important differences in the collagen content and the density of VSM nuclei between control and (apoE)-deficient mouse aortas. There is need for more experimental investigations on the mechanical function of VSM cells in different types of arteries and in various ages. The results of these studies can be particularly useful for developing constituent-based models and studying the changes in arterial wall properties during the atherosclerotic process.

Acknowledgements

The authors wish to thank Dr. Luciano Capettini for valuable help in obtaining the samples. This work was supported by the Swiss National Science Foundation (Grant No. 325230-125445).

References

[1] Nakashima Y, Plump AS, Raines EW, et al. ApoE-deficient mice develop lesions of all phases of atherosclerosis throughout the arterial tree. Arterioscler Thromb 1994;14:133-40.

[2] Bocan TM. Animal models of atherosclerosis and interpretation of drug intervention studies. Curr Pharm Des 1998;4:37-52.

[3] Rezakhaniha R, Stergiopulos N. A structural model of the venous wall considering elastin anisotropy. J Biomech Eng 2008;130:031017.

[4] Roy S, Silacci P, Stergiopulos N. Biomechanical properties of decellularized porcine common carotid arteries. Am J Physiol Heart Circ Physiol 2005;289:H1567-76.

[5] Hudetz AG. Incremental elastic modulus for orthotropic incompressible arteries. J Biomech 1979;12:651-5.

[6] Newman DL, Gosling RG, Bowden NL. Changes in aortic distensibility and area ratio with the development of atherosclerosis. Atherosclerosis 1971;14:231-40.

[7] Cox RH, Detweiler DK. Arterial wall properties and dietary atherosclerosis in the racing greyhound. Am J Physiol 1979;236:H790-7.

[8] Hayashi K, Ide K, Matsumoto T. Aortic walls in atherosclerotic rabbits--mechanical study. J Biomech Eng 1994;116:284-93.

[9] Cox RH. Comparison of carotid artery mechanics in the rat, rabbit, and dog. Am J Physiol 1978;234:H280-8.

[10] Roach MR, Burton AC. The reason for the shape of the distensibility curves of arteries. Can J Biochem Physiol 1957;35:681-90.

[11] Hudetz AG, Mark G, Kovach AG, et al. Biomechanical properties of normal and fibrosclerotic human cerebral arteries. Atherosclerosis 1981;39:353-65.

[12] Busse R, Fleming I. Endothelial dysfunction in atherosclerosis. J Vasc Res 1996;33:181-94.

[13] Sima AV, Stancu CS, Simionescu M. Vascular endothelium in atherosclerosis. Cell Tissue Res 2009;335:191-203.

[14] Thyberg J, Hedin U, Sjolund M, et al. Regulation of differentiated properties and proliferation of arterial smooth muscle cells. Arteriosclerosis 1990;10:966-90.

[15] Stegemann JP, Hong H, Nerem RM. Mechanical, biochemical, and extracellular matrix effects on vascular smooth muscle cell phenotype. J Appl Physiol 2005;98:2321-7.

[16] Rudijanto A. The role of vascular smooth muscle cells on the pathogenesis of atherosclerosis. Acta Med Indones 2007;39:86-93.

[17] Campbell GR, Campbell JH. Smooth muscle phenotypic changes in arterial wall homeostasis: implications for the pathogenesis of atherosclerosis. Exp Mol Pathol 1985;42:139-62.

[18] Chamley-Campbell J, Campbell GR, Ross R. The smooth muscle cell in culture. Physiol Rev 1979;59:1-61.

[19] Campbell GR, Chamley-Campbell JH. Invited review: the cellular pathobiology of atherosclerosis. Pathology 1981;13:423-40.

[20] Doran AC, Meller N, McNamara CA. Role of smooth muscle cells in the initiation and early progression of atherosclerosis. Arterioscler Thromb Vasc Biol 2008;28:812-9.

[21] Schwartz SM, Ross R. Cellular proliferation in atherosclerosis and hypertension. Prog Cardiovasc Dis 1984;26:355-72.

[22] Tsamis A, Stergiopulos N, Rachev A. A structure-based model of arterial remodeling in response to sustained hypertension. J Biomech Eng 2009;131:101004.

[23] Alford PW, Humphrey JD, Taber LA. Growth and remodeling in a thick-walled artery model: effects of spatial variations in wall constituents. Biomech Model Mechanobiol 2008;7:245-62.

[24] Rich L., Whittaker P. Collagen and picrosirius red staining: a polarized light assessment of fibrillar distribution. Braz. J. morphol. Sci. 2005;22:97-104.

Chapter 3

STRUCTURE BASED CONSTITUTIVE FORMULATION OF ARTERIAL TISSUES CONSIDERING THE LINK BETWEEN SMOOTH MUSCLE CELLS AND ELASTIN

A. Agianniotis[1], A. Rachev[2], N. Stergiopulos[1]

[1] Laboratory of Hemodynamics and Cardiovascular Technology, Institute of Bioengineering, Ecole Polytechnique Fédérale de Lausanne, Lausanne, Switzerland

[2] College of Engineering and Computing, University of South Carolina, South Carolina, USA

Abstract

A novel structure-based constitutive model of arterial tissue is proposed. We consider the arterial tissue as a constrained mixture of elastin, collagen, and smooth muscle cells. The model considers a plausible link between part of the elastin and the smooth muscle of the arterial wall. One type of elastin is bonded to the smooth muscle cells, and the other part of elastin bears loads in concert with the collagen fibers. The opened-up configuration obtained from a circular ring after performing a radial cut is considered as a natural state of the vessel, but in this configuration the wall constituents are prestretched. We quantify the prestretch ratios of the wall constituents by using data from normal and decellularized artery, we explain experimental findings reported in the literature, and we verify the model by comparing theoretically predicted against experimentally recorded pressure – radius curves. Finally, we perform sensitivity analysis of the prestretch ratios of the constituents.

Keywords

Arterial wall biomechanics; Collagen; Elastin; Prestretch ratio; Decellularized artery; Extracellular matrix

To be submitted to:

Annals of Biomedical Engineering

Introduction

Quantification of the constitutive equations of arterial tissue is needed for formulating and solving boundary value problems in vascular mechanics that provide predictive results, processing experimental data, and motivating new kinds of experimental research. The constitutive description of the passive mechanical properties of arterial tissue, i.e., when the contribution of the contractile activity of the vascular smooth muscle (VSM) on the vessel geometry and stress state is not taken into account, can be described in the framework of the theory of finite elasticity. Therefore, the constitutive stress – strain relations are derived from a strain energy density function (SEF), the analytical form and material constants of which are determined from at least two-dimensional mechanical tests. Recently, the phenomenological approach for quantification of the SEF, which is based on a best fit between the experimentally recorded and theoretically predicted mechanical response (cf. [1]), is replaced by specifying a structure motivated and structure based SEF. This approach accounts for the amount and individual mechanical properties of elastin and collagen which are the major load-bearing constituents of the arterial tissue (cf. [2]). A step towards a more profound constitutive modeling of arterial tissues is made by considering the tissue as a constrained mixture of elastin and collagen, each having an individual zero-stress configuration such that in the zero-stress configuration of the artery the mixture contains locally self-equilibrated partial stresses borne by the elastin and collagen due to the different strains that they experience. This approach has been proposed in the mid 80-ties [3]. Recently its complete 3D formulation and implementation to study arterial growth and remodeling was developed independently [4-6]. Focused on the consequences of the constrained mixture model of prestretched constituents for the growth and remodeling of arteries as a result of changes in pressure and flow, these studies do not provide methodology for experimental quantification of the strains of each specific constituent of the mixture in the zero-stress configuration of the artery. The major difficulty is the fact that the individual zero-stress configurations of elastin and collagen are not experimentally recordable.

The adoption of the model of a constrained mixture of prestretched constituents seems reasonable and the identification of the constituent-specific strains experimentally feasible for a passive arterial tissue subjected to decellularization as described in [7]. Briefly, after the smooth muscle of porcine common carotid arteries has been functionally inactivated, the muscle cells were physically removed from the tissue by a detergent-enzymatic procedure that

preserves extracellular matrix scaffold. The internal diameter, external diameter, and length were measured by optical microscopy on neighboring histological sections before and after decellularization. The decellularized arteries appear with higher inner diameter, decreased wall thickness and larger length compared to the control arteries in the zero-load state. Additionally, it has been shown that the opening angle that characterizes the shape that appears after a radial cut of the traction-free arterial ring segment, is significantly smaller in the decellularized arteries than in the control vessels. The authors suggested that part of elastin is bonded to the vascular smooth muscle cells and is under compression. Geometrical changes are interpreted as elastic deformations that are released after the link between smooth muscle cells and elastin is eliminated by decellularization procedure. In the present study we build a constitutive model of arterial tissue which accounts for a plausible link between part of the elastin and the smooth muscle, and propose a method for determining the model parameters by using data from decellularized arteries.

Theoretical framework

We consider first a structure-based constitutive formulation of the arterial tissue taking into account for the contribution of both initially prestretched parts of elastin; the part of elastin that is bonded to the VSM cells and the part of elastin that bears loads in concert with the collagen fibers. Afterwards, we present a methodology for quantification of the model parameters using data from mechanical tests and histological studies of decellularized arteries. Finally, the model is verified by comparing model predictions to experimental data given in [7].

Constitutive modeling

Arterial tissue is considered as a constrained mixture of three constituents, elastin, collagen, and VSM cells. The tissue constituents are elastic and incompressible and under physiological loads undergo finite deformations. In this study we focus on the passive response of the arterial tissue which occurs when the VSM cells are maximally relaxed and do not generate stress. Though the VSM cells do not manifest a contractile response, they are physically present in the vascular tissue. Motivated by the histological observations and the mechanical response of decellularized arteries given in [7], we consider two types of elastin that are involved in load bearing. One type of elastin, ESM, is bonded to the smooth muscle cells. The other part of elastin, EC, bears loads in concert with the collagen fibers.

Following Chuong and Fung [8] the opened-up configuration β_0, (Fig. 1), taken by an unloaded circular ring after performing a radial cut, is considered as a natural state for the intact vessel. It has the form of a circular sector of inner radius R_i, wall thickness H, and opening angle Φ, as defined in Fig. 1. Under applied arterial pressure and longitudinal extension to *in situ* length, the artery undergoes axisymmetric finite elastic deformation to configuration β, which represents a circular ring of inner radius r_i and outer radius r_o (Fig. 1). The mapping of β_0 into β is described by the deformation gradient tensor

$$[F] = diag\{\lambda_r, \lambda_\theta, \lambda_z\} = diag\left\{\left(\frac{dr}{dR}\right), \left(\frac{\chi r}{R}\right), \lambda\right\} \tag{1}$$

where λ_r, λ_θ, and λ_z are the stretch ratios in the radial, circumferential and longitudinal direction, respectively. r and R is the current radius in β and β_0, respectively; $\chi = \pi/(\pi - \Phi)$; λ is the prescribed value of the longitudinal stretch ratio. Because of incompressibility of the material

$$\frac{dr}{dR}\frac{\chi r}{R}\lambda = 1 \tag{2}$$

which after integration yields

$$r = \sqrt{\frac{R^2}{\lambda \chi} + R_i^2\left(\mu^2 - \frac{1}{\lambda \chi}\right)}, \quad \mu = \frac{r_i}{R_i} \tag{3}$$

Considering the tissue as a constrained mixture, the constitutive equations for the arterial tissue represent sums of the individual constitutive equations for elastin, collagen, and smooth muscle, weighted by their individual mass fraction (cf. [4, 9]). We speculate that the effects of smooth muscle on the passive mechanical properties of the tissue are due to the deformation of ESM. The constitutive equations for each structural constituent are derived from the corresponding SEF, which depends on the strain measures defined with respect to the natural configuration of the individual constituent. Though the opened-up configuration β_0 is a natural (zero-stress) configuration for the mixture, this does not hold true for the elastin and collagen. We assume that in this configuration ESM is extended, while EC is compressed. Further we assume that the collagen fibers are oriented in the

circumferential direction and follow the deformation of EC and because of their undulated configuration they do not produce stress in the opened-up configuration. Therefore, the deformation gradient tensors that describe mapping of the individual zero-stress configurations $\tilde{\beta}$ (Fig. 1) into the deformed configuration β due to the applied load are

$$\begin{aligned}
\left[F_{ESM}\right] &= diag\left\{\lambda_{rESM}\lambda_r, \lambda_{\theta ESM}\lambda_\theta, \lambda_{zESM}\lambda\right\} = diag\left\{\lambda_{rESM}\left(\frac{dr}{dR}\right), \lambda_{\theta ESM}\left(\frac{\chi r}{R}\right), \lambda_{zESM}\lambda\right\} \\
\left[F_{EC}\right] &= diag\left\{\lambda_{rEC}\lambda_r, \lambda_{\theta EC}\lambda_\theta, \lambda_{zEC}\lambda\right\} = diag\left\{\lambda_{rEC}\left(\frac{dr}{dR}\right), \lambda_{\theta EC}\left(\frac{\chi r}{R}\right), \lambda_{zEC}\lambda\right\} \\
\left[F_{C}\right] &= diag\left\{\lambda_{rC}\lambda_r, \lambda_{\theta C}\lambda_\theta, \lambda_{zC}\lambda\right\} = diag\left\{\lambda_{rC}\left(\frac{dr}{dR}\right), \lambda_{\theta C}\left(\frac{\chi r}{R}\right), \lambda_{zC}\lambda\right\}
\end{aligned} \tag{4}$$

where the subscripts *ESM*, *EC*, and *C* refer to the ESM, EC, and collagen, respectively. It must be noted that while both configurations β_0 and β are measurable, the individual natural configurations of elastin and collagen $\tilde{\beta}$ are not observable. We account for their existence via stretch ratios required for mapping the individual natural configurations into the opened-up configuration β_0. According to the introduced assumptions and using the material incompressibility, the prestretch ratios are: $\lambda_{\theta ESM} > 1$, $\lambda_{zESM} > 1$, $\lambda_{rESM} = \left(\lambda_{\theta ESM}\,\lambda_{zESM}\right)^{-1}$, $0 < \lambda_{\theta EC} < 1$, $0 < \lambda_{zEC} < 1$, $\lambda_{rEC} = \left(\lambda_{\theta EC}\,\lambda_{zEC}\right)^{-1}$, $0 < \lambda_{\theta C} < 1$, $\lambda_{rC} = \lambda_{zC} = \left(\lambda_{\theta C}\right)^{-1/2}$. Given the strain energy density functions for elastin, W_E, and collagen, W_C, and making use of the rule-of-mixture, the components of the total Cauchy stress tensor in the arterial wall can be calculated as follows

$$\begin{aligned}
\sigma_r &= \varphi_{ESM}\lambda_{rESM}\lambda_r \frac{\partial W_E}{\partial\left(\lambda_{rESM}\lambda_r\right)} + \varphi_{EC}\lambda_{rEC}\lambda_r \frac{\partial W_E}{\partial\left(\lambda_{rEC}\lambda_r\right)} + p \\
\sigma_\theta &= \varphi_{ESM}\lambda_{\theta ESM}\lambda_\theta \frac{\partial W_E}{\partial\left(\lambda_{\theta ESM}\lambda_\theta\right)} + \varphi_{EC}\lambda_{\theta EC}\lambda_\theta \frac{\partial W_E}{\partial\left(\lambda_{\theta EC}\lambda_\theta\right)} + \varphi_C\lambda_{\theta C}\lambda_\theta \frac{\partial W_C}{\partial\left(\lambda_{\theta C}\lambda_\theta\right)} + p \\
\sigma_z &= \varphi_{ESM}\lambda_{zESM}\lambda_z \frac{\partial W_E}{\partial\left(\lambda_{zESM}\lambda_z\right)} + \varphi_{EC}\lambda_{zEC}\lambda_z \frac{\partial W_E}{\partial\left(\lambda_{zEC}\lambda_z\right)} + p
\end{aligned} \tag{5}$$

where $\lambda_{\theta C} = \lambda_{\theta EC}$, and φ_{ESM}, φ_{EC}, and φ_C are mass fractions defined as follows

$$\varphi_{ESM} = \frac{M_{ESM}}{M}, \quad \varphi_{EC} = \frac{M_{EC}}{M}, \quad \varphi_C = \frac{M_C}{M}, \quad M = M_{ESM} + M_{EC} + M_C + M_{SM} \tag{6}$$

M is the total mass and M_{ESM}, M_{EC}, M_C, and M_{SM} are the mass of ESM, EC, collagen, and vascular smooth muscle, respectively. It is assumed that the constituents are uniformly distributed across the wall thickness. p is unknown scalar function due to the incompressibility of the constituents. The function p has to be determined from the equations of equilibrium and the boundary conditions.

Equations (5) represent the general form of the constitutive equations of the passive arterial tissue considered as a constrained mixture of two groups of elastin, and collagen, each of which has an individual stress-free configuration. Accounting for the incompressibility of elastin, the equations contain four unknown parameters, namely the prestretch ratios $\lambda_{\theta ESM}$, λ_{zESM}, $\lambda_{\theta EC}$ and λ_{zEC}. If $\lambda_r = \lambda_\theta = \lambda_z = 1$, which corresponds to the opened-up configuration β_0 (Fig. 1), all components of the total stress are equal to zero. As stated above the collagen does not contribute to the total stress in this configuration. Both types of elastin, however, are under stress. The stresses are balanced and result in a zero total stress in the mixture. After setting $\lambda_r = \lambda_\theta = \lambda_z = 1$ in Eqs. (5), eliminating *p*, and accounting for the material incompressibility, the following two equations hold true

$$\begin{aligned}
&\varphi_{ESM}\left[\lambda_{\theta ESM}\frac{\partial W_E}{\partial \lambda_{\theta ESM}} - \lambda_{rESM}\frac{\partial W_E}{\partial \lambda_{rESM}}\right] + \varphi_{EC}\left[\lambda_{\theta EC}\frac{\partial W_E}{\partial \lambda_{\theta EC}} - \lambda_{rEC}\frac{\partial W_E}{\partial \lambda_{rEC}}\right] = 0 \\
&\varphi_{ESM}\left[\lambda_{zESM}\frac{\partial W_E}{\partial \lambda_{zESM}} - \lambda_{rESM}\frac{\partial W_E}{\partial \lambda_{rESM}}\right] + \varphi_{EC}\left[\lambda_{zEC}\frac{\partial W_E}{\partial \lambda_{zEC}} - \lambda_{rEC}\frac{\partial W_E}{\partial \lambda_{rEC}}\right] = 0
\end{aligned} \tag{7}$$

where $\lambda_{rESM} = \left(\lambda_{\theta ESM}\ \lambda_{zESM}\right)^{-1}$ and $\lambda_{rEC} = \left(\lambda_{\theta EC}\ \lambda_{zEC}\right)^{-1}$.

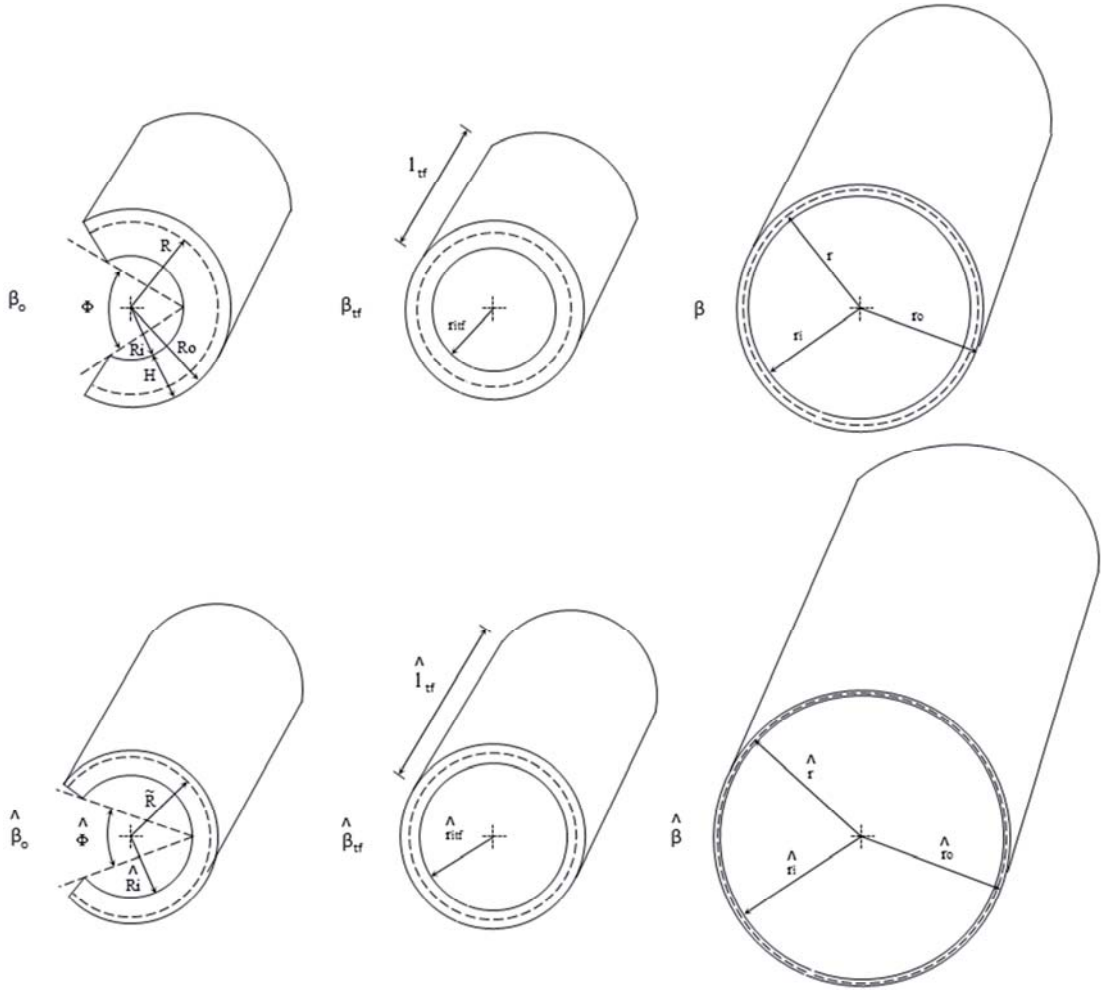

Figure 1. Configurations of arterial cross sections. β_0, β_{tf} and β are the zero-stress configuration, the traction-free configuration and a loaded configuration of the normal artery, respectively. $\hat{\beta}_0$, $\hat{\beta}_{tf}$ and $\hat{\beta}$ are the zero-stress configuration, the traction-free configuration and a loaded configuration of the decellularized artery, respectively. β_0: Φ, opening angle; R, radius; R_i, inner radius of curvature; R_o, outer radius of curvature; H, wall thickness. β_{tf}: l_{tf}, length of the artery; r_{itf}, inner radius. β: r, radius; r_i, inner radius; r_o, outer radius. $\hat{\beta}_0$: $\hat{\Phi}$, opening angle; $\tilde{R}$, radius; $\hat{R}_i$, inner radius of curvature; $\hat{R}_o$, outer radius of curvature; $\hat{\beta}_{tf}$: $\hat{l}_{tf}$, length of the artery; $\hat{r}_{itf}$, inner radius. $\hat{\beta}$: $\hat{r}$, radius; $\hat{r}_i$, inner radius; $\hat{r}_o$, outer radius.

Identification of model functions and parameters

Except for mass fractions, which can be measured from histological studies, the strain energy density functions for elastin and collagen and the prestretch ratios of both groups of elastin have to be determined from mechanical experiments. The general method for identifying a strain energy density function is based on the

selection of a certain analytical form of the function motivated by some preliminary mechanical studies and information about the structure of the tissue, followed by determination of the values of material constants. The common procedure is based on seeking the best fit values that minimize the discrepancy between the loads of inflation and axial extension that are needed to produce a deformation, as defined by Eq. (1), and the experimentally recorded values of pressure and axial force applied to an arterial segment tested *in vitro*. After using the equations of equilibrium and boundary conditions that pressure *P* is applied at the inner arterial surface while the outer surface is traction-free, the loads that produce the deformation described by Eq. (1) are [10]

$$P = \int_{r_i}^{r_o} \left(\sigma_\theta - \sigma_r\right)\frac{dr}{r}, \quad F = \pi \int_{r_i}^{r_o} \left(2\sigma_z - \sigma_r - \sigma_\theta\right) r dr \tag{8}$$

where F is the resultant of the axial stress.

Equations (8) contain as unknown parameters the deformation parameter μ and the four prestretch ratios $\lambda_{\theta ESM}$, λ_{zESM}, $\lambda_{\theta EC}$ and λ_{zEC}; they have to satisfy Eqs. (7). We derive two additional equations for the prestretch parameters using part of the experimental results from the mechanical response of a decellularized artery. When the VSM cells are physically removed from the arterial tissue, the elastin that is bonded to them is not under tensile stress, the compressed EC is not equilibrated, and an unloaded tubular segment changes its dimensions. The traction-free (unloaded) configuration β_{tf} of an arterial segment of inner radius r_{itf} and length l_{tf} changes to the traction-free configuration $\hat{\beta}_{tf}$ of the decellularized segment of inner radius $\hat{r}_{itf}$ and length $\hat{l}_{tf}$ (Fig. 1). Hereafter the symbol “hat” is used for parameters that refer to the decellularized artery. The experimental data reported in [7] showed that the decellularized segment has bigger inner radius, thinner wall and larger length. In fact, these findings were the rationale for accepting that the EC is compressed in the normal vessel.

It is reasonable to accept that decellularization completely releases the compressive stress in EC acting in the longitudinal direction and we can calculate the longitudinal prestretch ratio from experimentally measurable data as $\lambda_{zEC} = l_{tf} / \hat{l}_{tf}$. This assumption is justified by the following facts. The configuration $\hat{\beta}_{tf}$ is not stress-free and contains residual strain and stress. It is accepted that they are released after

a radial cut of the unloaded segment, which results in the deformation of configuration $\hat{\beta}_{tf}$ into configuration $\hat{\beta}_0$ of inner radius $\hat{R}_i$ and opening angle $\hat{\Phi}$ (Fig. 1). The bending deformation that follows a radial cut of an unloaded arterial segment does not virtually affect the length of the segment [8, 11-12].

To determine the prestretch of EC in the circumferential direction, $\lambda_{\theta EC}$, we use the information about the opening angle $\hat{\Phi}$ in configuration $\hat{\beta}_0$. Because the arterial tissue is considered to be an elastic material, the configuration $\hat{\beta}_0$ can also be reached after decellularization of the intact artery when the intact artery is in its opened-up configuration β_0 that has opening angle Φ. Following the approach used in [13], we consider first a more general mapping of β_0 to $\hat{\beta}_0$, without imposing the requirement that the configuration $\hat{\beta}_0$ is stress-free. It is described by the deformation gradient tensor

$$\left[\tilde{F}\right] = diag\left\{\tilde{\lambda}_r, \tilde{\lambda}_\theta, \tilde{\lambda}_z\right\} = diag\left\{\left(\frac{d\tilde{R}}{dR}\right), \left(\frac{\tilde{\chi}\tilde{R}}{R}\right), \tilde{\lambda}\right\} \tag{9}$$

where $\tilde{R}$ is the current radius in $\hat{\beta}_0$; $\tilde{\chi} = \left(\pi - \hat{\Phi}\right)/\left(\pi - \Phi\right)$ and $\tilde{\lambda}$ is the prescribed longitudinal stretch ratio. Accounting for material incompressibility, similarly to Eq. (3) we have

$$\tilde{R} = \sqrt{\frac{R^2}{\tilde{\lambda}\,\tilde{\chi}} + R_i^2\left(\tilde{\mu}^2 - \frac{1}{\tilde{\lambda}\,\tilde{\chi}}\right)}, \quad \tilde{\mu} = \frac{\hat{R}_i}{R_i} \tag{10}$$

and the stretch ratios associated with the prescribed deformation are

$$\tilde{\lambda}_\theta = \sqrt{\frac{\tilde{\chi}}{\tilde{\lambda}} + \frac{\tilde{\chi}^2 R_i^2}{R^2}\left(\tilde{\mu}^2 - \frac{1}{\tilde{\chi}\,\tilde{\lambda}}\right)}, \quad \tilde{\lambda}_z = \tilde{\lambda}, \quad \tilde{\lambda}_r = \left(\tilde{\lambda}_\theta\,\tilde{\lambda}_z\right)^{-1} \tag{11}$$

If $\tilde{\mu} = \left(\tilde{\lambda}\,\tilde{\chi}\right)^{-\frac{1}{2}}$, the stretch ratios are constant across the wall thickness and $\tilde{\lambda}_\theta = \sqrt{\frac{\tilde{\chi}}{\tilde{\lambda}}}$. Let specify the additional deformation that is imposed on the configuration β_0 by choosing $\tilde{\lambda} = 1/\lambda_{zEC}$ and $\tilde{\lambda}_\theta = 1/\lambda_{\theta EC}$ and eliminating ESM, due

to the decellularization of the artery, as a member that equilibrates EC. Because EC is initially compressed in configuration β_0, the specified additional deformation makes the total deformation be $\lambda_\theta = \lambda_z = \lambda_r = 1$. This indicates that the configuration $\hat{\beta}_0$ is stress-free and represents the opened-up configuration of the decellularized artery. Making use of the expressions for $\tilde{\lambda}_\theta$ defined above, the circumferential prestretch ratio of EC can be calculated from the opening angles of the intact and decellularized artery and the longitudinal prestretch ratio as follows

$$\lambda_{\theta EC} = \sqrt{\frac{\pi - \Phi}{\lambda_{zEC}\left(\pi - \hat{\Phi}\right)}} \tag{12}$$

Given the SEF for elastin and its mass fractions, and having calculated the prestretch ratios of EC, Eqs. (7) allow calculation of the prestretch ratios of ESM. Thus, the constitutive equations (5) do not contain unknown parameters.

$\hat{\beta}$ is a loaded configuration of the decellularized artery (Fig. 1). It represents a circular ring of inner radius $\hat{r}_i$ and outer radius $\hat{r}_o$. Similar to the mapping of β_0 into β, the mapping of $\hat{\beta}_0$ into $\hat{\beta}$ yields

$$\hat{r} = \sqrt{\frac{\tilde{R}^2}{\hat{\lambda}\,\hat{\chi}} + \hat{R}_i^2\left(\hat{\mu}^2 - \frac{1}{\hat{\lambda}\,\hat{\chi}}\right)}, \quad \hat{\mu} = \frac{\hat{r}_i}{\hat{R}_i} \tag{13}$$

where $\hat{r}$ and $\tilde{R}$ is the current radius in $\hat{\beta}$ and $\hat{\beta}_0$, respectively; $\hat{\lambda}$ is the axial stretch ratio of the decellularized artery; $\hat{\chi} = \dfrac{\pi}{\pi - \hat{\Phi}}$.

The determined constitutive equations have to be verified by comparing the solutions of appropriate boundary value problems against experimentally recorded data that had not been used for calculating model parameters. The predictive power of the constitutive formulation can be tested by comparing the theoretically predicted and experimentally recorded pressure – inner radius relationships of the intact and decellularized artery at a constant longitudinal stretch ratio.

Illustrative Results

To quantify the prestretch ratios in the arterial wall and illustrate the predictive capability of the proposed structure-based biomechanical model, we use the experimental data for the intact and decellularized porcine carotid artery given in [7]. Based on recorded increase by 12% of the length of the artery after decellularization, the longitudinal prestretch ratio of the EC is taken to be $\lambda_{zEC} = 0.88$. Using the recorded opening angles 55^o and 20^o of the intact and decellularized artery, respectively, Eq. (12) yields $\lambda_{\theta EC}$=0.946. Equations (7) cannot be used for calculation of the prestretch ratios of ESM until the analytical form and the material constants of the SEF are specified. We use the pressure – diameter experimental data given in [7] simultaneously with Eqs. (7) to determine the strain energy density function and the prestretch ratios of ESM. The analytical form of the SEF is selected as follows.

$$W = \varphi_E W_E + \varphi_C W_C \tag{14}$$

where W_E is the neo-Hookean SEF [14]

$$W_E = C_{el}(I_1 - 3), \quad I_1 = \lambda_\theta^2 + \lambda_z^2 + \lambda_r^2 \tag{15}$$

and W_C is the SEF for collagen proposed in [15]

$$W_C = \frac{C_{coll}}{2} \int_0^{E_\theta} x^2 \frac{b^k k \left(E_\theta - x\right)^{k-1}}{[b^k + (E_\theta - x)^k]^2} dx \tag{16}$$

C_{el} is the material constant of elastin, C_{coll} is the material constant of collagen, k and b are parameters of the collagen engagement distribution, $\varphi_E = \varphi_{ESM} + \varphi_{EC}$ is the total mass fraction of elastin and φ_C is the mass fraction of collagen. We neglect the SEF for the passive properties of the VSM cells because it has been reported that its contribution is about one order of magnitude less than that of the SEF for elastin [16-17]. The mass fraction of collagen and the total mass fraction of elastin are measured from histology. Because of lack of available data for the mass fractions of the specific arterial tissue used to obtain the normal and the decellularized curves, we choose mass fractions that are close to values reported for other types of tissues (cf. [10]). In the present illustrative example we choose $\varphi_{EC} + \varphi_{ESM} = 0.24$ and $\varphi_C = 0.36$ (by dry weight). The mass fractions of EC and ESM are not measurable; nevertheless, the sum of the mass fractions of EC and

ESM is the total mass fraction of elastin in the normal artery. The elastic constant of collagen, C_{coll}, is chosen 200 MPa which is a reasonable value [18-19] and is previously used by Zulliger et al. [20].

We determine the parameters of the SEF by seeking best fit values that minimize the discrepancy between the pressures needed to produce deformation and experimentally recorded pressures that produce the same deformation to a normal arterial segment tested in vitro under constant axial stretch 1.3 [7]. The longitudinal and circumferential prestretch ratios of ESM, $\lambda_{z\,ESM}$ and $\lambda_{\theta\,ESM}$, respectively, have to satisfy equations (7). The minimization of the discrepancy between the theoretically derived and experimentally recorded pressures with constraints given by equations (7) is performed by using the algorithm "fmincon" of the commercially available software MATLAB (Release R2009b from MathWorks Inc., USA). The parameters of the model are presented in Table 1.

Table 1. Values of model parameters

Fixed parameters	Mass fraction of collagen	$\varphi_C = 0.36$
	Mass fraction of ESM, decell.	$\hat{\varphi}_{ESM} = 0$
	Mass fraction of EC, decell.	$\hat{\varphi}_{EC} = 0.116$
	Mass fraction of C, decell.	$\hat{\varphi}_C = 0.313$
	Axial stretch ratio, normal	$\lambda = 1.3$
	Axial stretch ratio, decell.	$\hat{\lambda} = 1.3$
	Opening angle, normal	$\Phi = 55^o$
	Opening angle, decell.	$\hat{\Phi} = 20^o$
	Collagen constant	$C_{coll} = 200$ MPa
Free parameters	Circ. prestretch ratio of ESM	$\lambda_{\theta\,ESM} = 1.128$
	Axial prestretch ratio of ESM	$\lambda_{z\,ESM} = 1.196$
	Circ. prestretch ratio of EC	$\lambda_{\theta\,EC} = 0.946$
	Axial prestretch ratio of EC	$\lambda_{z\,EC} = 0.88$
	Collagen distribution param.	$k = 0.74$
	Collagen distribution param.	$b = 31.46$
	Mass fraction of ESM, normal	$\varphi_{ESM} = 0.104$
	Mass fraction of EC, normal	$\varphi_{EC} = 0.136$
	Elastin constant	$C_{el} = 163.95$ kPa

Roy et al. [7] reported that the decellularization of the artery led to an increase of the wall volume. The difference in volume of the artery after and before the decellularization was higher than the volume of the cells that have been removed due

to filling of the decellularized artery with bathing solution. This resulted in a decrease of the mass fractions of elastin and collagen in the decellularized arterial tissue. Due to lack of precise data we assume that the increase in the total volume of the wall is 15% [7]. In addition, the effective mass fraction of elastin in the decellularized artery is further reduced because only EC contributes to bearing the load and therefore $\hat{\varphi}_{ESM} = 0$. For the illustrative example we use $\hat{\varphi}_{EC} = 0.116$ and $\hat{\varphi}_{C} = 0.313$.

The model is verified by comparing the predicted response of decellularized artery to the experimentally recorded response under constant axial extension of 1.3 and inflation from 10 to 140 mmHg. The experimental pressure – inner radius curve and the prediction of the model are presented in Fig. 2.

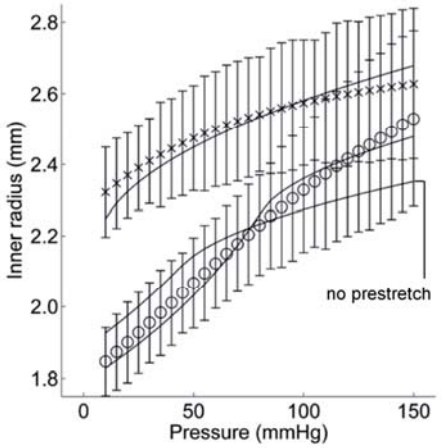

Figure 2. Experimental pressure – inner radius curves of normal (o) and decellularized (x) artery and theoretical pressure – inner radius curves (—). The theoretical curve of the normal artery is obtained after fitting the model to the data points of the experimental curve of the normal artery with constraints given by equations (7). The theoretical curve of the decellularized artery is the prediction of the model and is compared to the experimental curve of the decellularized artery. We also plot the pressure – inner radius curve of normal artery in the case of no prestretch. The axial stretch ratio is 1.3 for both normal and decellularized artery. The bars are SD of the mean (from [7]).

Sensitivity analysis of prestretch ratios

We perform sensitivity analysis of the prestretch ratios of ESM. For the sensitivity analysis of the longitudinal prestretch ratio of ESM, we vary the value of $\lambda_{z\,ESM}$ between 80% and 120% of the value calculated from the parameter

identification procedure (i.e., 1.196), while keeping $\lambda_{\theta ESM}$ constant to 1.128. For the sensitivity analysis of the circumferential prestretch of ESM, we vary the value of $\lambda_{\theta ESM}$ between 80% and 120% of the value calculated from the parameter identification procedure (i.e., 1.128), while keeping λ_{zESM} constant to 1.196. In both cases of sensitivity analysis, the prestretch ratios of EC, λ_{zEC} and $\lambda_{\theta EC}$, are calculated from Eq. (7). For the sensitivity analysis, the values of all the rest parameters related to the normal artery are the ones used in the parameter identification procedure. Given the prestretch ratios λ_{zEC} and $\lambda_{\theta EC}$, and the opening angle Φ of the normal artery, we calculate from Eq. (12) the opening angle $\hat{\Phi}$ of the decellularized artery. We present the curves pressure – inner radius of normal artery and circumferential and axial prestretch ratio of ESM – normalized opening angle of decellularized artery in Fig. 3, and pressure – circumferential stress of normal artery and pressure – axial stress of normal artery in Fig. 4. The opening angle of decellularized artery is normalized with respect to the opening angle of the normal artery.

Further, we calculate the prestretch ratios of EC using Eq. (7) when one of the prestretch ratios of ESM is kept constant while the other varies between 80% and 120% of its value. The values of the mass fractions and the parameters of the SEFs are the ones used in the identification parameter procedure. We vary the axial and circumferential prestretch ratio of ESM around its reference value (1.196 and 1.128, respectively) and we present the curves axial prestretch of ESM – circumferential prestretch of EC, axial prestretch of ESM – axial prestretch of EC, circumferential prestretch of ESM – circumferential prestretch of EC and circumferential prestretch of ESM – axial prestretch of EC in Fig. 5.

We calculate the distribution of the residual stresses and strains in the arterial wall of the normal artery for the different cases of sensitivity analysis. We vary the values of the axial and circumferential prestretch ratios of ESM ±20% of the values calculated from the parameter identification procedure (λ_{zESM}=1.196 and $\lambda_{\theta ESM}$ =1.128, respectively) and we plot the residual circumferential stress, residual axial stress, residual radial stress, residual circumferential stretch, residual axial stretch and residual radial stretch in Figs. 6 and 7, respectively.

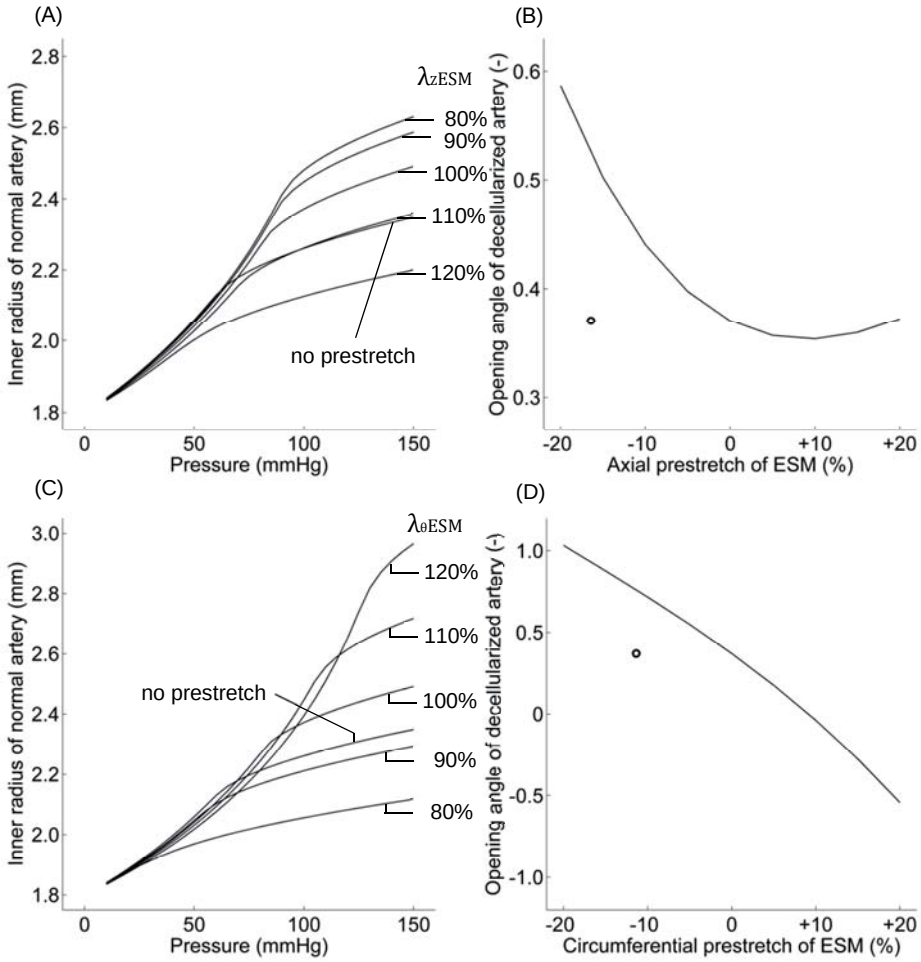

Figure 3. Sensitivity analysis of the prestretch ratios $\lambda_{z\,ESM}$ (A, B) and $\lambda_{\theta\,ESM}$ (C, D). The values of the prestretch ratios vary ±10% and ±20% of the value calculated from the parameter identification procedure ($\lambda_{z\,ESM}$ =1.196, $\lambda_{\theta\,ESM}$ =1.128). We plot the curves pressure – inner radius of normal artery (A, C) and axial and circumferential prestretch of ESM – normalized opening angle of decellularized artery (B, D). The opening angle of decellularized artery is normalized with respect to the opening angle of the normal artery. We also plot the curves that correspond to the case of no prestretch (A, C). The open circle (o) corresponds to the case of no prestretch (B, D).

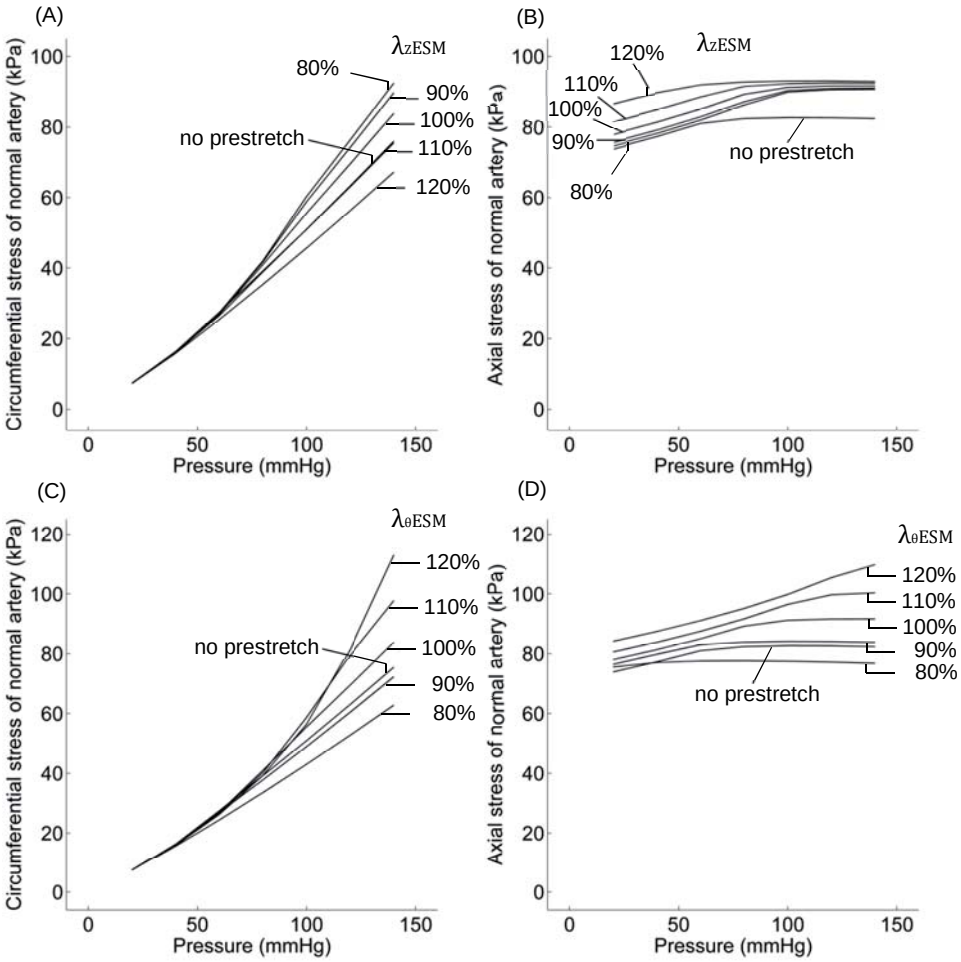

Figure 4. Sensitivity analysis of the prestretch ratios $\lambda_{z\,ESM}$ (A, B) and $\lambda_{\theta\,ESM}$ (C, D). The values of the prestretch ratios vary ±10% and ±20% of the value calculated from the parameter identification procedure ($\lambda_{z\,ESM}$ =1.196, $\lambda_{\theta\,ESM}$ =1.128). We plot the curves pressure – circumferential stress of normal artery (A, C) and pressure – axial stress of normal artery (B, D). We also plot the curves that correspond to the case of no prestretch.

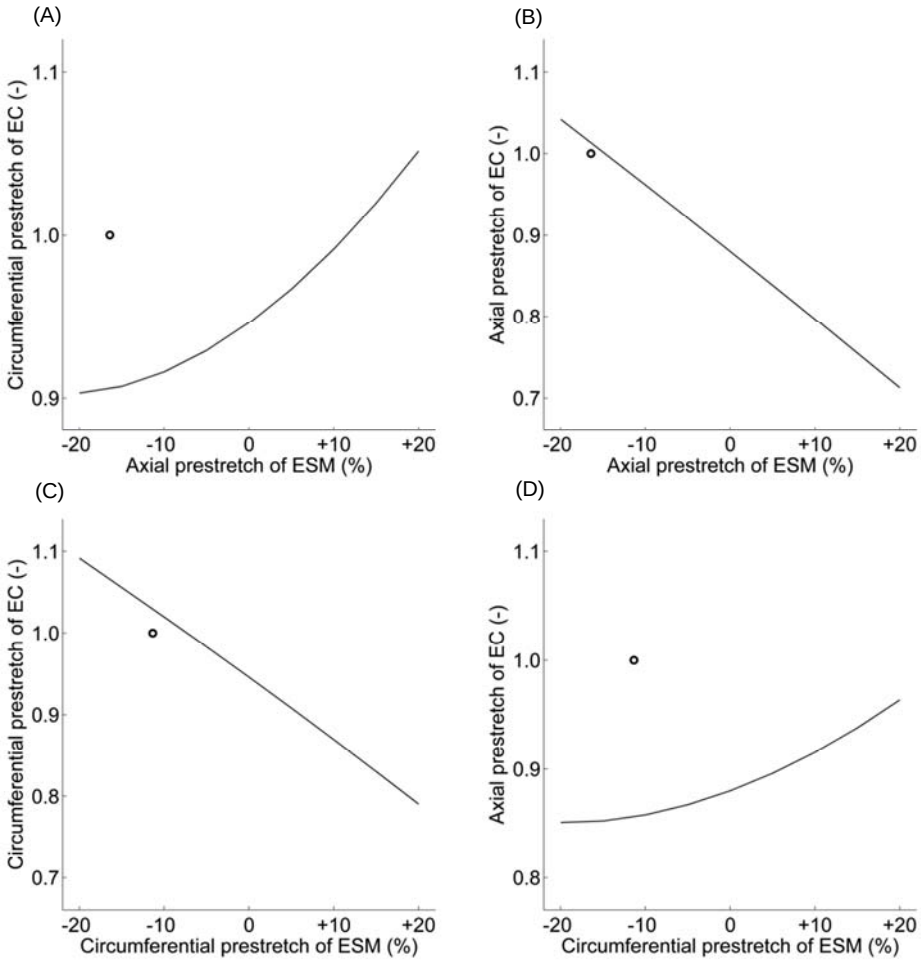

Figure 5. We vary the values of the axial (A, B) and circumferential (C, D) prestretch ratios of ESM ±20% of the values calculated from the parameter identification procedure (λ_{zESM} =1.196, $\lambda_{\theta ESM}$ =1.128) and we plot the prestretch ratios of EC. We plot the curves axial prestretch of ESM – circumferential prestretch of EC (A), axial prestretch of ESM – axial prestretch of EC (B), circumferential prestretch of ESM – circumferential prestretch of EC (C), and circumferential prestretch of ESM – axial prestretch of EC (A). The open circle (o) corresponds to the case of no prestretch.

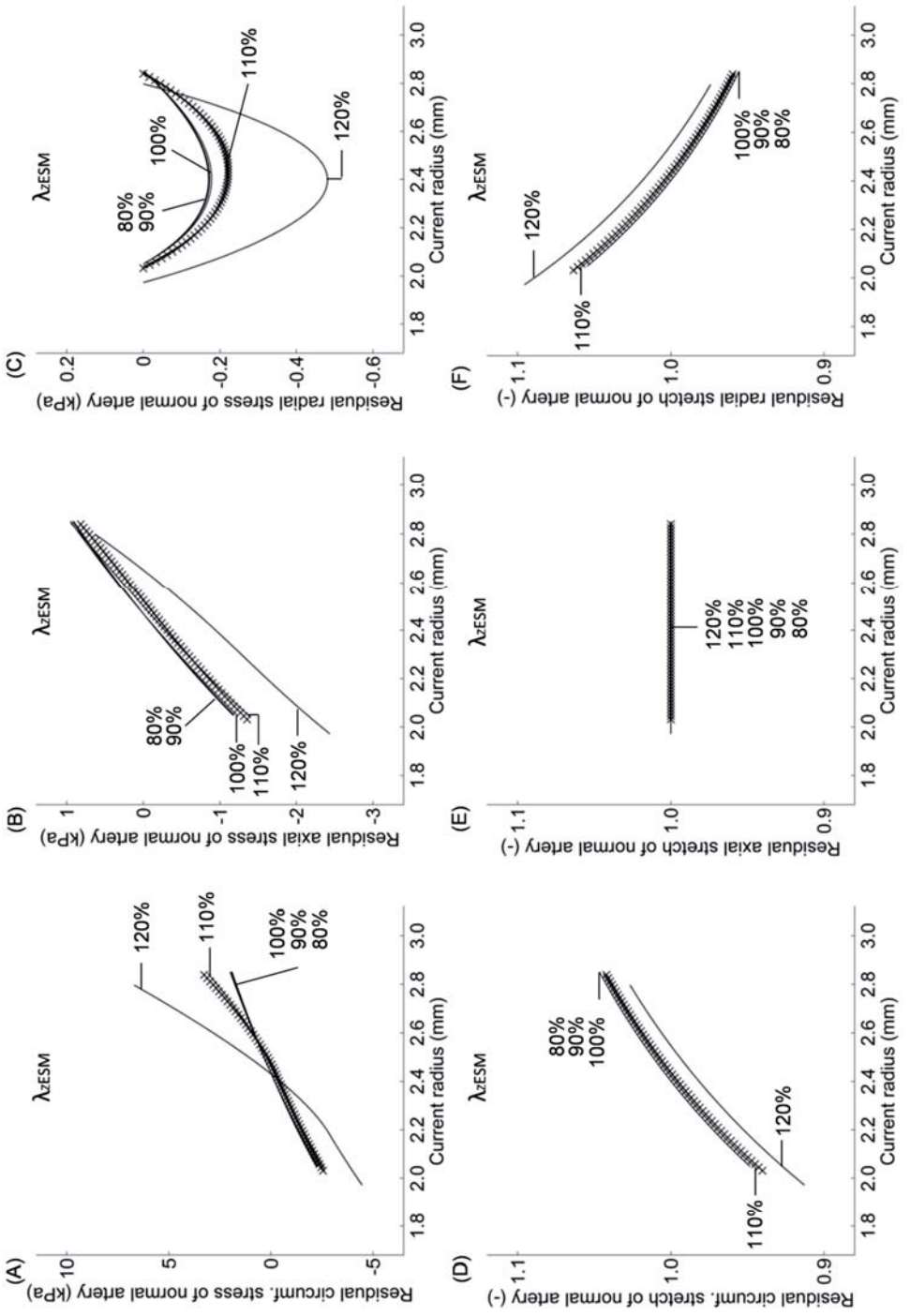

Figure 6. We vary the values of the axial prestretch ratio of ESM ±20% of the value calculated from the parameter identification procedure ($\lambda_{z\,ESM}$ =1.196) and we plot the distribution of the residual stresses and stretches in the wall of the normal artery. We plot the curves current radius – residual circumferential stress (A), current radius – residual axial stress (B), current radius – residual radial stress (C), current radius – residual circumferential stretch (D), current radius – residual axial stretch (E) and current radius – residual radial stretch (F). The curve (x) corresponds to the case of no prestretch.

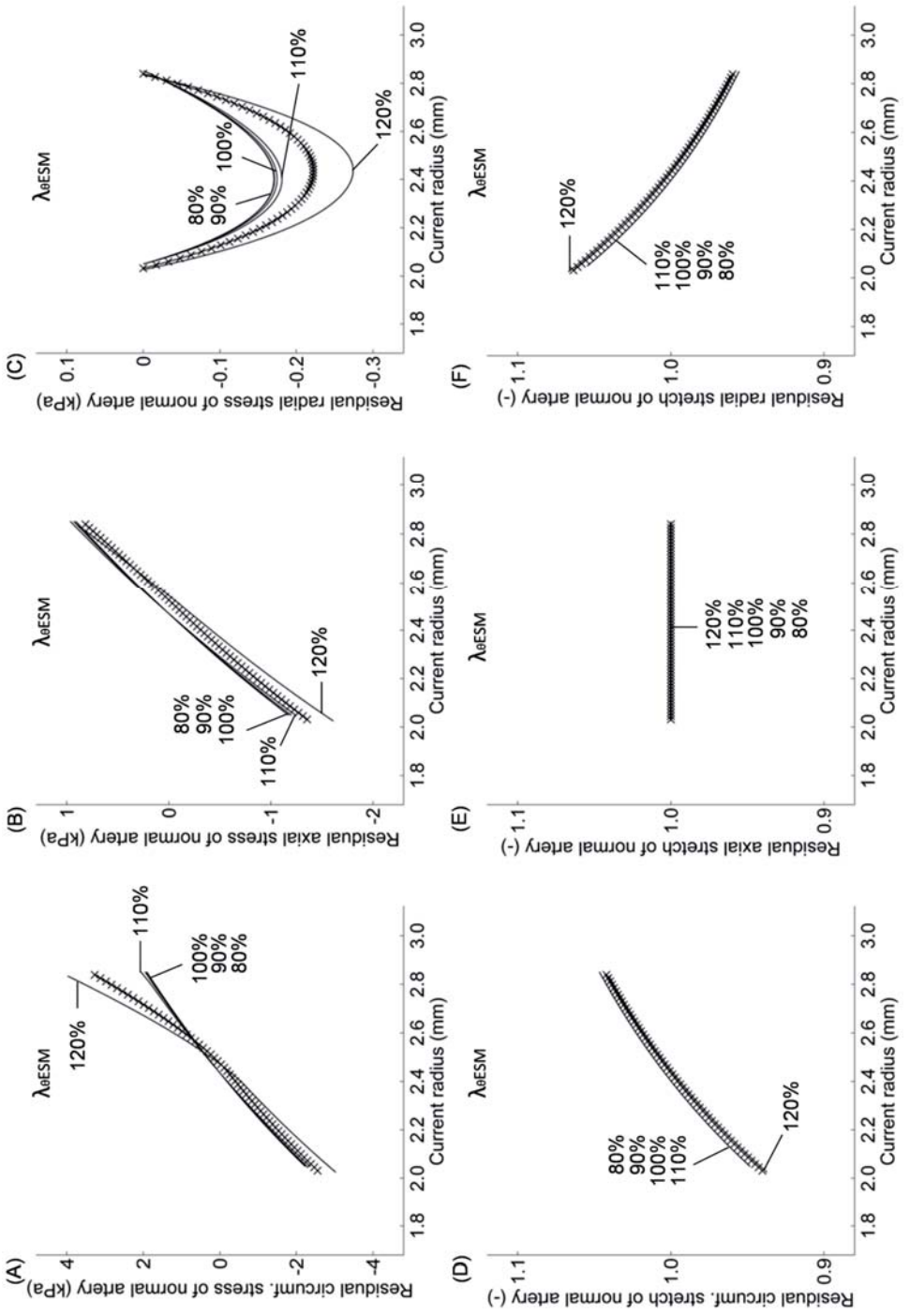

Figure 7. We vary the value of the circumferential prestretch ratio of ESM ±20% of the value calculated from the parameter identification procedure ($\lambda_{\theta ESM}$ =1.128) and we plot the distribution of the residual stresses and stretches in the wall of the normal artery. We plot the curves current radius – residual circumferential stress (A), current radius – residual axial stress (B), current radius – residual radial stress (C), current radius – residual circumferential stretch (D), current radius – residual axial stretch (E) and current radius – residual radial stretch (F). The curve (x) corresponds to the case of no prestretch..

Discussion

We have proposed a novel structure-based biomechanical model for the passive behavior of the arterial tissue. The new model considers the link between elastin and VSM cells, quantifies the prestretch ratios of the different constituents of the arterial wall and predicts the response of arteries after the chemical dissolution of the VSM cells. The arterial tissue is considered as a mixture of elastin, collagen, and VSM cells. The constituents of the tissue are incompressible and elastic and undergo finite deformations under physiological loads. In the proposed model we consider two groups of elastin; ESM is the part of elastin that is bonded to the VSM cells and EC is the part of elastin that bears load in concert with the collagen fibers. Using the results of the illustrative example we compare the model predictions with results of previous studies and offer credible explanations for some experimental findings reported in the literature.

The biomechanical model suggests profound changes in the geometry of the artery when the link between the VSM cells and the elastin is disrupted. In agreement with the experimental finding of Roy et al. [7] the model predicted increased inner diameter of the wall and increased arterial length. The values of the elastic constant of elastin, C_{el}, and the parameters k and b which are associated with the engagement distribution of collagen are predicted by the model and are in the order of previously reported values [9, 20].

The model quantifies the mass fractions of the two parts of elastin, EC and ESM. The ESM could be considered as the part of elastin associated with the VSM cell-to-elastin attachments and inter-lamellar elastin fibers forming links between elastin lamina and VSM cells that have been qualitatively observed by Clark et al. [21] and Rezakhaniha et al. [22]. Further, the model predicts that the mass fraction of ESM is less than the mass fraction of EC. ESM needs to be stretched more than EC for the equilibrium to be achieved at the zero-stress configuration of the artery and therefore the level of prestretch of ESM is greater than the level of prestretch of EC.

It has been observed that the lumen diameter at the zero-load configuration of the human aorta increases with age [23] and that the *in situ* axial stretch ratio decreases with age [24]. We could speculate that these happen due to the earlier mechanical fatigue failure of ESM compared to EC when the arterial tissue is subjected to pulsatile wall strain over the number of cardiac cycles during lifetime. This is reasonable if one takes into account for the different prestretch ratios between

EC and ESM. During loading of the arterial tissue, ESM experiences higher stretch ratios compared to EC and therefore higher stress. When the artery is subjected to pulsatile wall strain, ESM which experiences higher stress will disrupt at lower number of cardiac cycles, that is, earlier in lifetime, compared to EC. This will result EC to be the only part of elastin which will bear load and therefore to increased lumen diameter and increased length of the artery at its zero-stress configuration or decreased *in situ* axial stretch ratio if we consider constant length of loaded artery, as we showed with our model. There is a need for further experimental investigations on the mechanical fatigue failure of elastin during progressing age.

The sensitivity analysis of the axial and circumferential prestretch ratios of ESM shows a dependence of the inner radius, the circumferential stress and the axial stress developed in the arterial wall of the normal artery on the level of the prestretch ratios. For larger value of $\lambda_{z\,ESM}$, the increase in the inner radius of the artery and the circumferential stress between 100 mmHg and 140 mmHg is smaller. Because the deviation of the circumferential stress and the inner radius from the baseline values due to increase of pressure could initiate hypertension-induced remodeling, a sufficient high value of the axial prestretch ratio of ESM could possibly prevent the artery from remodeling. Further, the sensitivity analysis shows that the inner radius and the circumferential stress are sensitive to change in the values of $\lambda_{z\,ESM}$ and $\lambda_{\theta\,ESM}$ for higher values of pressure. The axial stress is sensitive to change in the value of $\lambda_{\theta\,ESM}$ for higher values of pressure, and to change in the value of $\lambda_{z\,ESM}$ for lower values of pressure. The opening angle has been suggested to be a measure of the residual stress in the arterial wall [8]. The sensitivity analysis shows that lower prestretch ratios of ESM result in higher opening angle of the decellularized artery, and thus higher residual stress in that artery. Further experimental investigations are needed to study the relation between the prestretch ratios of the constituents and the remodeling of arteries.

Limitations

Several aspects affecting the passive behavior of the arterial tissue have not been taken into account. In the present work we have assumed that the VSM cells are linked only with elastin fibers. However, the link between other constituents cannot be excluded. Future biomechanical models might assume the link between collagen and VSM or collagen and elastin based on appropriate experimental

observations. Because the mass fractions of ESM and EC are not measurable, one of them has to be left as free parameter that can be determined by fitting other available experimental data. We have assumed that the collagen fibers are oriented in the circumferential direction, whereas considering angular dispersion and waviness of collagen fibers would be more realistic [25-26]. In the present work we used as strain energy density function for elastin the Neo-Hookean SEF although elastin may play a role also in the anisotropic behavior of the tissue [22, 27]. We disregarded the multilayer structure of the arterial wall by modeling the artery as one-layered tube. Also, the effect of the composition and structure of different collagen types is not taken into account in the present model. Finally, the contribution of the VSM cells in their relaxed state has been neglected.

Conclusion

In conclusion, we developed a structure-based biomechanical model that considers the link between VSM cells and elastin. The model assumes the existence of two groups of elastin, one of which is bonded to VSM cells. The opened-up configuration obtained from a circular ring after performing a radial cut is considered as natural state for the vessel, but in this configuration the wall constituents are prestretched. We proposed a method to quantify the prestretch ratios of the wall constituents by using data from normal and decellularized artery. Finally, the model was verified by comparing theoretically predicted against experimentally recorded pressure – radius curves of decellularized artery and sensitivity analysis of the prestretch ratios of ESM was performed.

Acknowledgements

This work was supported by the Swiss National Science Foundation (Grant No. 325230-125445).

References

[1] Demiray H, Vito RP. A layered cylindrical shell model for an aorta. International Journal of Engineering Science 1991;29:47-54.

[2] Holzapfel GA, Gasser TC, Ogden RW. A new constitutive framework for arterial wall mechanics and a comparative study of material models. Journal of Elasticity 2000;61:1-48.

[3] Brankov G, Rachev A, Stoychev S, A composite model of large blood vessels, In: Brankov G (ed), Mechanics of Biological Solid: Proceedings of the Eurimech colloguium, Varna, Publishing House of the Bulgarian Academy of Sciences, 1975:71-8.

[4] Gleason RL, Humphrey JD. A Mixture Model of Arterial Growth and Remodeling in Hypertension: Altered Muscle Tone and Tissue Turnover. Journal of Vascular Research 2004;41:352-63.

[5] Gleason RL, Taber LA, Humphrey JD. A 2-D model of flow-induced alterations in the geometry, structure, and properties of carotid arteries. J Biomech Eng 2004;126:371-81.

[6] Humphrey JD, Rajagopal KR. A constrained mixture model for arterial adaptations to a sustained step change in blood flow. Biomech Model Mechanobiol 2003;2:109-26.

[7] Roy S, Silacci P, Stergiopulos N. Biomechanical properties of decellularized porcine common carotid arteries. Am J Physiol Heart Circ Physiol 2005;289:H1567-76.

[8] Chuong CJ, Fung YC. On residual stresses in arteries. J Biomech Eng 1986;108:189-92.

[9] Zulliger MA, Rachev A, Stergiopulos N. A constitutive formulation of arterial mechanics including vascular smooth muscle tone. Am J Physiol Heart Circ Physiol 2004;287:H1335-43.

[10] Humphrey JD, Cardiovascular Solid Mechanics: Cells, Tissues, and Organs, New York, Springer-Verlag, 2002.

[11] Kang T, Humphrey JD, Finite deformation of an inverted artery, In: Vanderby R (ed), Advances in Bioengineering, New York, ASME, 1991.

[12] Cardamone L, Valentin A, Eberth JF, et al. Origin of axial prestretch and residual stress in arteries. Biomech Model Mechanobiol 2009;8:431-46.

[13] Rachev A, Hayashi K. Theoretical study of the effects of vascular smooth muscle contraction on strain and stress distributions in arteries. Ann Biomed Eng 1999;27:459-68.

[14] Watton PN, Ventikos Y, Holzapfel GA. Modelling the mechanical response of elastin for arterial tissue. J Biomech 2009;42:1320-5.

[15] Zulliger MA, Stergiopulos N. Structural strain energy function applied to the ageing of the human aorta. J Biomech 2007;40:3061-9.

[16] Bergel DH. The static elastic properties of the arterial wall. J Physiol 1961;156:445-57.

[17] VanDijk AM, Wieringa PA, van der Meer M, et al. Mechanics of resting isolated single vascular smooth muscle cells from bovine coronary artery. Am J Physiol 1984;246:C277-87.

[18] Burton AC. Relation of structure to function of the tissues of the wall of blood vessels. Physiol Rev 1954;34:619-42.

[19] Milnor WR, Hemodynamics, Baltimore, William & Wilkins, 1989.

[20] Zulliger MA, Fridez P, Hayashi K, et al. A strain energy function for arteries accounting for wall composition and structure. J Biomech 2004;37:989-1000.

[21] Clark JM, Glagov S. Structural integration of the arterial wall. I. Relationships and attachments of medial smooth muscle cells in normally distended and hyperdistended aortas. Lab Invest 1979;40:587-602.

[22] Rezakhaniha R, Fonck E, Genoud C, et al. Role of elastin anisotropy in structural strain energy functions of arterial tissue. Biomech Model Mechanobiol 2010.

[23] Langewouters GJ, Visco-elasticity of the human aorta in vitro in relation to pressure and age, Amsterdam, Vrije Universiteit te Amsterdam, 1982.

[24] Wenn CM, Newman DL. Arterial tortuosity. Australas Phys Eng Sci Med 1990;13:67-70.

[25] Agianniotis A, Rezakhaniha R, Stergiopulos N. A structural constitutive model considering angular dispersion and waviness of collagen fibres of rabbit facial veins. Biomed Eng Online 2011;10:18.

[26] Rezakhaniha R, Agianniotis A, Schrauwen JT, et al. Experimental investigation of collagen waviness and orientation in the arterial adventitia using confocal laser scanning microscopy. Biomech Model Mechanobiol 2012;11:461-73.

[27] Rezakhaniha R, Stergiopulos N. A structural model of the venous wall considering elastin anisotropy. J Biomech Eng 2008;130:031017.

Chapter 4

THEORETICAL SIMULATION OF ADAPTIVE AND MALADAPTIVE REMODELING IN RESPONSE TO HYPERTENSION

A. Agianniotis[1], N. Stergiopulos[1], R. P. Vito[2], T. Shazly[3], A. Rachev[2,3]

[1] Laboratory of Hemodynamics and Cardiovascular Technology, Institute of Bioengineering, Ecole Polytechnique Fédérale de Lausanne, Lausanne, Switzerland

[2] George W. Woodruff School of Mechanical Engineering, Georgia Institute of Technology, Georgia, USA

[3] College of Engineering and Computing, University of South Carolina, South Carolina, USA

Abstract

We perform theoretical simulations of adaptive and maladaptive remodeling in response to hypertension. We consider an artery to be a thick-walled cylindrical tube made of nonlinear, elastic, incompressible material. First we solve the direct problem of arterial wall mechanics and we determine the baseline mechanical environment. Then we solve the inverse problem of arterial wall mechanics and determine the outcomes of remodeling of the artery in response to hypertension. We determine the altered zero-stress state and deformed geometry in two different cases of remodeling; perfect adaptation and maladaptive inward remodeling. We use two parameters associated with the vascular tone and the arterial mass. Data from experimental animal models of hypertension that are inspired by vascular solid mechanics, together with theoretical studies can enable development of adequate mathematical models of remodeling and promote better understanding of the physiology and pathophysiology of arteries.

Keywords

Hypertension; Arterial remodeling; Maladaptive remodeling; Perfect adaptation

To be submitted to:

Journal of Biomechanics

Introduction

Hypertension is a major risk factor for many cardiovascular diseases, including atherosclerosis, aneurysm, stroke, and heart and kidney failure. The sustained increase in pressure causes remodeling in arteries, which results in long-term changes in the geometrical dimensions, in the mechanical properties, and in the mass of the vascular tissue.

The remodeling of arteries can be manifested in different manners depending on possible change in mass and diameter [1]. When increased, decreased, or constant mass is observed, the remodeling is termed hypertrophic, hypotrophic, or eutrophic, respectively. When the diameter is increased, or decreased, the remodeling is termed outward, or inward, respectively. Due to the multi-factorial and complex nature of remodeling, it is exceedingly difficult to evaluate the relative importance of any one factor in isolation in bench-top or animal studies. Predictive mathematical models based on continuum mechanics are powerful tools for studying the mechanical and remodeling response of blood vessels. Until now most theoretical studies have addressed adaptive remodeling in response to hypertension (cf. [2]). An adaptive response manifests as preservation of the normotensive deformed diameter, change in residual strains and axial stretch ratio, and thickening of the arterial wall, such that the tensile wall stress and the flow-induced shear stress remain at baseline values [3-4]. Maladaptive remodeling is characterized by the incomplete restoration of the baseline mechanical environment and could result from a variety of dysfunctional biological processes [5-8].

There are animal models that show that hypertension regulates the production of nitric oxide (NO), which is a vasodilating substance, and thus the vascular tone [9]. In one form of hypertension, the increased production of vasoconstrictor factors leads to increased synthesis of NO. Thus, the vasoconstrictor influences are opposed by NO production which acts as a protective mechanism [10]. In another form of hypertension, however, a decrease production of NO occurs, and the vasoconstrictor activity in the wall is unopposed [11].

There is clearly a need for understanding the mechanisms by which the structural and functional changes occur in the vascular wall and evaluating the relative importance of certain geometrical and mechanical factors in the remodeling response to hypertension. In the present study we perform theoretical simulations of adaptive and inward maladaptive remodeling.

Theoretical framework

We consider an artery as a thick-walled cylindrical tube made of nonlinear, elastic, incompressible material. Under applied internal pressure and *in situ* axial stretching, the artery undergoes finite axisymmetric deformations in the state of plain strain. Residual stresses exist in the traction-free configuration of an arterial segment. The residual stresses are released by a radial cut [12-13]. For an incompressible wall, the stretch ratios in the radial, circumferential, and axial directions are, respectively,

$$\lambda_r = \frac{R}{\lambda\chi r}, \quad \lambda_\theta = \frac{\chi r}{R}, \quad \lambda_z = \lambda \tag{1}$$

and the Green strains are

$$\mathrm{E}_i = \frac{1}{2}\left(\lambda_i^2 - 1\right), \quad i = r, \theta, z \tag{2}$$

$$r = \sqrt{\frac{R^2}{\lambda\chi} + R_i^2\left(\mu^2 - \frac{1}{\lambda\chi}\right)}, \quad \mu = \frac{r_i}{R_i}, \quad \lambda = \frac{l}{L}, \quad \chi = \frac{\pi}{\pi - \Phi} \tag{3}$$

where r and R are radii in a loaded configuration and zero-stress configuration, respectively, r_i and R_i are the inner radii in a loaded configuration and zero-stress configuration, respectively, μ, χ, and λ are the deformation parameters, l and L are the deformed and undeformed axial lengths, respectively, and Φ is the opening angle.

The nonzero components of the Cauchy stress are

$$\begin{aligned}
\sigma_r &= \int_{r_i}^{r}\left(\sigma_\theta^\alpha + \lambda_\theta^2\frac{\partial W}{\partial E_\theta} - \lambda_r^2\frac{\partial W}{\partial E_r}\right)\frac{dr}{r} - P \\
\sigma_\theta &= \sigma_r + \lambda_\theta^2\frac{\partial W}{\partial E_\theta} - \lambda_r^2\frac{\partial W}{\partial E_r} + \sigma_\theta^\alpha \\
\sigma_z &= \sigma_r + \lambda_z^2\frac{\partial W}{\partial E_z} - \lambda_r^2\frac{\partial W}{\partial E_r}
\end{aligned} \tag{4}$$

where σ_θ^α is the active circumferential stress, P is the arterial pressure applied at the inner surface and is calculated as

$$P = \int_{r_i}^{r_o} \left(\sigma_\theta^\alpha + \lambda_\theta^2 \frac{\partial W}{\partial E_\theta} - \lambda_r^2 \frac{\partial W}{\partial E_r} \right) \frac{dr}{r} \tag{5}$$

W is the strain energy function (SEF), and r_o is the outer deformed radius.

The linearized overall mechanical response of an artery around certain deformed states is expressed by using the pressure – strain elastic modulus, known as Peterson's elastic modulus [14],

$$E_p = r_o \frac{\Delta P}{\Delta r_o} \tag{6}$$

Direct problem of Arterial Wall Mechanics

Under normotensive pressure, *in situ* axial stretch ratio, and basal tone of the vascular smooth muscle cells, the stress distribution in the arterial wall and the deformed radius reflect baseline values. The baseline values are determined by solving the following problem. We assume as known the geometrical parameters of the zero-stress configuration (Φ^N, R_i^N, R_o^N), the axial stretch ratio λ^N, and the parameters of the SEF. R_o^N is the outer diameter of the zero-stress configuration, and "N" denotes normotensive values. We solve the equation

$$\int_{r_i}^{r_o} \left(\sigma_\theta^\alpha + \lambda_\theta^2 \frac{\partial W}{\partial E_\theta} - \lambda_r^2 \frac{\partial W}{\partial E_r} \right) \frac{dr}{r} - P^N = 0 \tag{7}$$

where P^N is the normotensive pressure. The only unknown is the deformation parameter μ^N. Then we calculate $\sigma_{\theta i}^N$, $\sigma_{\theta o}^N$, and $\bar{\sigma}_z^N$, which are the normotensive circumferential stress at the inner surface, the normotensive circumferential stress at the outer surface, and the average normotensive axial stress, respectively, from Eqs. (4), and the normotensive Peterson's modulus from Eq. (6).

Inverse problem of Arterial Wall Mechanics

In the inverse problem we determine some model parameters from observed data or prescribed outcomes of the model. Following the methodology proposed in [15] we determine the outcomes of adaptive and inward maladaptive remodeling, given the parameters of the SEF. Unknowns are the parameters that describe the

zero-stress configuration (Φ^H, R_i^H, R_o^H), the deformation parameter μ^H, and the axial stretch ratio λ^H, where "H" denotes hypertensive values.

In the case of perfect adaptation we solve the system of equations

$$\begin{aligned} P - P^H &= 0 \\ \mu_i^H R_i^H - \mu_i^N R_i^N &= 0 \\ \sigma_{\theta i} - \sigma_{\theta i}^N &= 0 \\ \sigma_{\theta o} - \sigma_{\theta o}^N &= 0 \\ \bar{\sigma}_z - \bar{\sigma}_z^N &= 0 \end{aligned} \tag{8}$$

The first equation takes into account for the radial equation of equilibrium and the boundary condition that pressure applied at the inner surface is P^H, where P^H is the hypertensive pressure. The second equation results in restoration of the deformed inner radius. The third and fourth of Eqs. (8) result in restoration of the distribution of circumferential stress, and the fifth of Eqs. (8) results in restoration of the axial stress. Assuming Poiseuille flow, the shear stress at the inner arterial surface is

$$\tau = \frac{4\eta Q}{\pi r_i^3} \tag{9}$$

where Q is the volumetric blood flow and η is the blood viscosity. Assuming unchanged blood viscosity and flow rate in remodeling due to hypertension, the restoration of deformed inner radius essentially results in restoration of the shear stress at the inner surface.

In the case of maladaptive adaptation we solve the system of equations

$$\begin{aligned} P - P^H &= 0 \\ a^H - k_a a^N &= 0 \\ \sigma_{\theta i} - \sigma_{\theta i}^N &= 0 \\ \sigma_{\theta o} - \sigma_{\theta o}^N &= 0 \\ \bar{\sigma}_z - \bar{\sigma}_z^N &= 0 \end{aligned} \tag{10}$$

It differs from the system of equations (8) in the second equation which now describes the change in area due to remodeling. The normotensive and hypertensive area is calculated as

$$a^k = (\pi - \Phi^k)(R_o^{k2} - R_i^{k2}), \quad k = N, H \tag{11}$$

k_a is a coefficient of proportionality.

We determine the growth index and the remodeling index for the adaptive and maladaptive remodeling. The growth index refers to the percentage change in wall cross-sectional area and is calculated as [1]

$$GI = \frac{a^H - a^N}{a^N} 100\% \tag{12}$$

The remodeling index refers to the percentage change in lumen area and is calculated as [1]

$$RI = \frac{a^H_{lumen} - a^N_{lumen}}{a^N_{lumen}} 100\% \tag{13}$$

where the normotensive and hypertensive lumen area is calculated as

$$a^k_{lumen} = \pi r_i^{k2}, \quad k = N, H \tag{14}$$

Among vessels made of identical material, there is an infinite number of zero-stress, and respectively deformed configurations that have identical stress distributions for given pressure and activation parameter S. The inverse problem is single valued after specification of the cross-section area via the parameter k_a. In the case of maladaptive remodeling, the shear stress at the inner surface may not be restored to normotensive value due to non-restoration of the deformed inner radius.

All governing equations in the reverse problem are coupled and represent a highly nonlinear system of equations. First we solve the direct problem for normotensive pressure 100 mmHg. Then we solve the inverse problem for hypertensive pressure ranging from 100 up to 160 mmHg with variation of the muscular tone via the activation parameter $S^H = k_s S^N$, where k_s is a coefficient of proportionality, and the cross-section area via the coefficient k_a. The algorithms that solve the direct problem and the inverse problem in adaptive and maladaptive remodeling are implemented in a commercially available solver (Maple™ 16 from Maplesoft™, Canada).

Illustrative example

We specify the model parameters and solve the governing equations numerically. We use a four-fiber family strain energy function to model the passive behavior of the artery [16]

$$W = c\left(I_1 - 3\right) + \sum_{k=1,2,3,4} \frac{b_{1k}}{4b_{2k}} \left\{ \exp\left[b_{2k} \left(\lambda_k^2 - 1 \right)^2 \right] - 1 \right\} \tag{15}$$

where I_1 is the first invariant of the right Cauchy-Green tensor, c, b_{1k}, b_{2k} are material constants; k denotes a family of collagen fibers oriented at mean angle a_k with respect to the longitudinal axis; $\lambda_k = \sqrt{\lambda_\theta^2 \sin^2 a_k + \lambda_z^2 \cos^2 a_k}$ is the stretch ratio of k -th family of collagen fibers due to deformation.

We account for the active stress generated by the vascular smooth muscle cells. The active circumferential stress is [17]

$$\sigma_\theta^\alpha = S\lambda_\theta \left[1 - \left(\frac{\lambda_M - \lambda_\theta}{\lambda_M - \lambda_o} \right)^2 \right] \tag{16}$$

where S is the activation parameter related to the intensity of stimulation, λ_M is the circumferential stretch ratio at which the active stress is maximum, and λ_o is the circumferential stretch ratio below which the stimulation does not generate active stress.

We perform the simulations using data for a common carotid artery of New Zealand white rabbit that are available in the literature [16]. The normotensive values of the active circumferential stress where chosen in order to give reasonable active stress and are in the level of previously reported values for common carotid arteries [16, 18]. The values of the model parameters for the passive and active behavior and the geometrical parameters of the zero-stress configuration are as follows. c = 15.90 kPa, b_{11} = 0.44 kPa, b_{21} = 0.83, b_{12} = 7.79 kPa, b_{22} = 0.187, b_{13} = 0.21 kPa, b_{14} = 0.21 kPa, b_{23} = 1.10, b_{24} = 1.10, a_3 = 45.45°, a_4 = 45.54°, S^N = 10 kPa, λ_M = 1.4, λ_o = 0.8, R_i^N = 2.749 mm, R_o^N = 3.524 mm, and Φ^N = 96.6°.

We present the thickness, the inner radius and the outer radius of the zero-stress configuration, the opening angle, and the deformed inner radius for adaptive

and maladaptive remodeling (Fig. 1). The results of maladaptive remodeling with varying k_S at $P^H = 160$ mmHg are normalized with respect to the normotensive values (Fig. 2). The maladaptive response of the artery to increased pressure results in values of thickness and inner radius of the zero-stress configuration and deformed inner radius that are below the values of adaptive response. The values for maladaptive remodeling drop with increase of the vascular smooth muscle tone. For values of k_a < 1.7, both the deformed inner radius and wall thickness are smaller than those of adaptive remodeling and insignificantly depend on the magnitude of the tone. The opening angle decreases with the increase of the tone and does not depend on the change in the arterial mass. Similar tendency holds for the Peterson's modulus (Fig. 3A). Due to geometrical changes the Peterson's modulus increases in hypertension, indicating a structural stiffening of the artery (Fig. 3A). The axial stretch ratio changes insignificantly with changes in pressure, muscular tone, and cross-section area (results not shown). The growth and remodeling index for perfect adaptation and maladaptive adaptation, respectively, are shown in Fig. 3B and 3C, respectively.

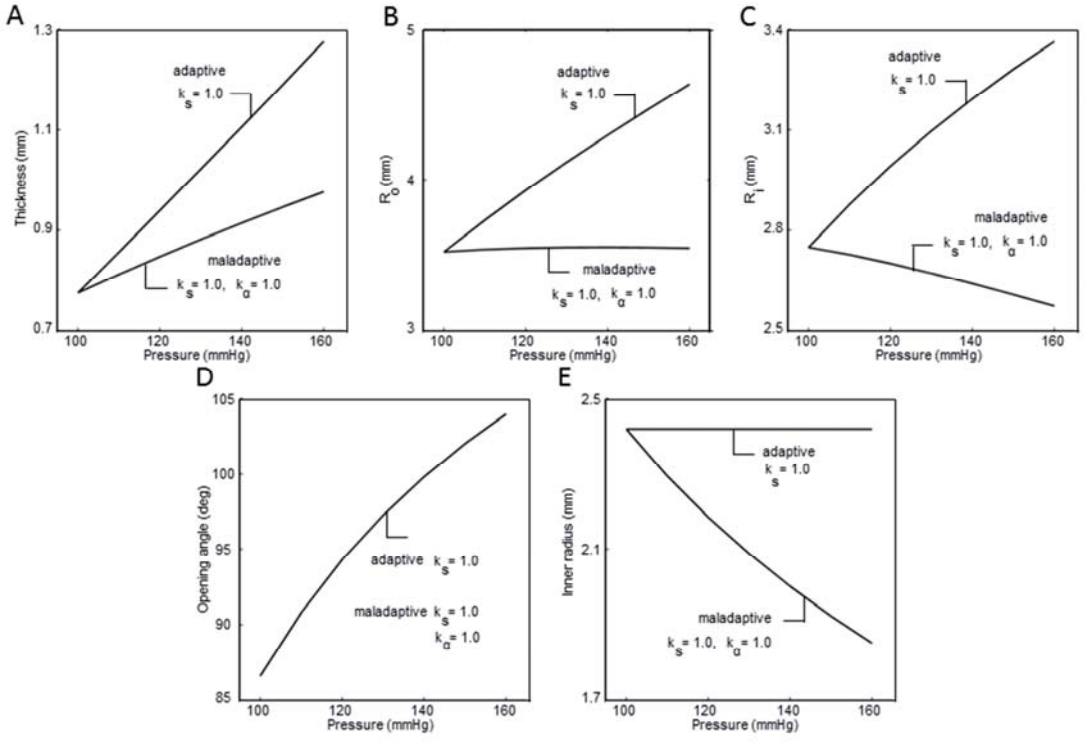

Figure 1. Thickness of zero-stress configuration (A), outer radius of zero-stress configuration (B), inner radius of zero-stress configuration (C), opening angle (D), and deformed inner radius (E) vs. pressure, for adaptive and maladaptive remodeling in response to hypertension.

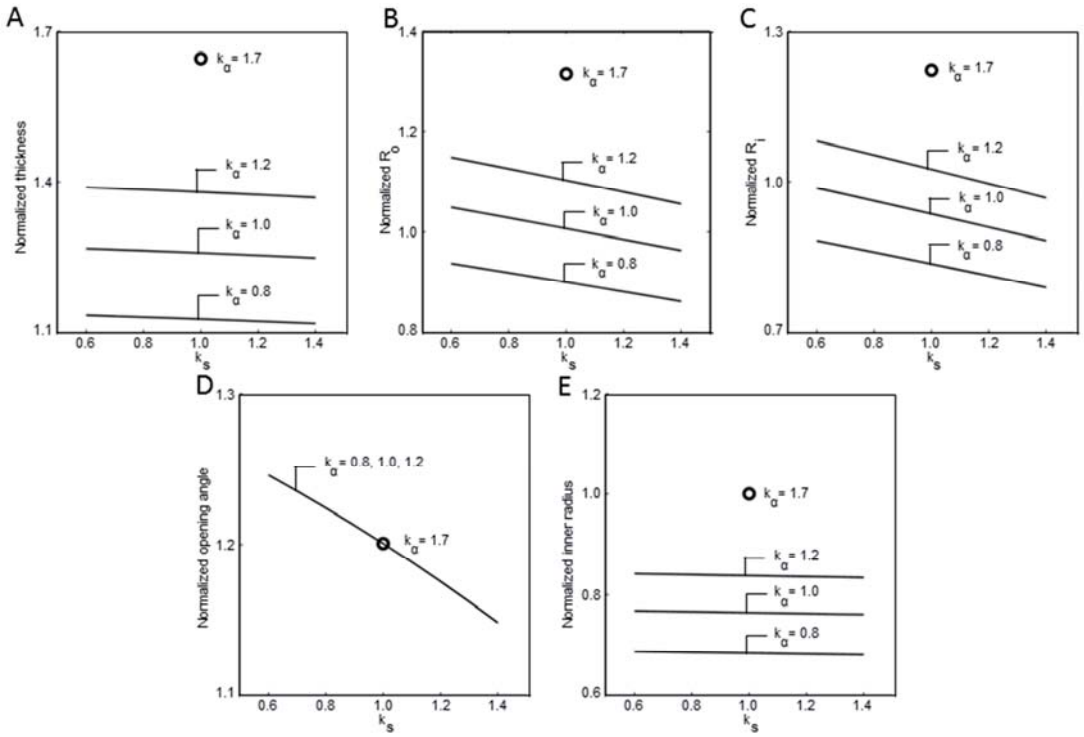

Figure 2. Thickness of zero-stress configuration (A), outer radius of zero-stress configuration (B), inner radius of zero-stress configuration (C), opening angle (D), and deformed inner radius (E) vs. vascular smooth muscle cells activation parameter k_s for the case of maladaptive remodeling at P = 160 mmHg. The opened circle corresponds to the case of adaptive remodeling. The results are normalized with respect to the normotensive values.

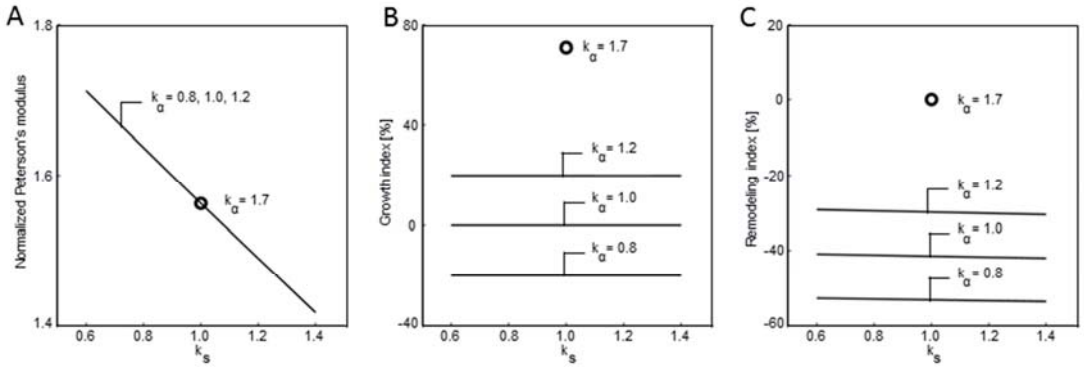

Figure 3. Peterson's elastic modulus (A), growth index (B) and remodeling index (C) vs. vascular smooth muscle cells activation parameter k_s for the case of maladaptive remodeling at P = 160 mmHg. The opened circle corresponds to the case of adaptive remodeling. The values of the Peterson's elastic modulus are normalized with respect to the normotensive value.

Discussion

The sustained increase in pressure causes remodeling in arteries, which results in long-term changes in the geometrical dimensions, in the mechanical properties, and in the mass of the vascular tissue. Motivated by animal models that show that hypertension regulates the production of vasodilating nitric oxide and thus the vascular tone, we performed theoretical simulation of adaptive and inward maladaptive remodeling with varying the vascular smooth muscle tone and the mass of the remodeled tissue. The aim of the study was to evaluate the relative importance of certain geometrical and mechanical factors in the remodeling response to hypertension.

The changes in the geometrical dimensions, in the mechanical properties, and in the mass of the vascular tissue due to hypertension are associated with humoral and mechanical factors, and can result in altered function of the artery. The adaptive remodeling process restores the deformed inner radius of the artery to normotensive values and therefore keeps the flow-induced shear stress at the endothelium at normotensive values [19]. In the inward remodeling, however, the inner radius is under-restored (Fig. 1E) which results in increased shear stress at the endothelium. Similar to the predictions of previous theoretical models, the wall stress is restored to baseline values (cf. [20]), and the zero-stress configuration parameters deviate from their baseline values, as it has been experimentally observed [12].

It could be speculated that there exists a causal link between the change in the tone and the mass of the artery resulting from maladaptive remodeling. The muscular tone is regulated via shear stress-dependent production of NO by the endothelial cells, whereas the synthetic activity and hypertrophy of the VSM cells is responsible for the mass production. In terms of biological categories, maladaptive remodeling is associated with impaired ability of the endothelial cells to synthesize NO, impaired contractile or synthetic activity of the VSM cells, or combinations of these events. It has been suggested that NO inhibits growth factor stimulated proliferation of VSM cells [21] and extracellular matrix production [22]. Radicals, oxidized low-density lipoprotein, or activated renin-angiotensin system by enhanced angiotensin converting enzyme activity may be involved in the development of endothelial dysfunction and reduced production of NO [23]. This causes an increase in vascular tone in concert with elevated pressure, reduced deformed radius and increased shear stress at the endothelium. The function of the endothelial cells appears to be sensitive to shear stress [24], which would mediate the release of

endothelium-derived NO and lead to reduction of muscular tone and the artery would reach a state of equilibrium. In the case of impaired synthetic activity of the VSM cells, the remodeling-induced mass may not be sufficient to restore the baseline deformed radius and the healthy endothelial cells experience higher shear stress. This results in up-regulation of the NO synthesis leading to reduction of the muscular tone. If the reduction of muscular tone is sufficient, it could lead to restoration of the deformed radius to baseline values. Further experimental investigations of the effect of the muscular tone and mass production on the remodeling of arteries are needed.

Due to geometrical changes the hypertension-induced remodeling results in higher circumferential stretch of the artery at the operating pressure of 160 mmHg compared to the normotensive artery at the operating pressure of 100 mmHg (results not shown). In higher circumferential stretch more collagen fibers are possibly engaged and thus the hypertensive artery is stiffer (higher Peterson's modulus, Fig. 3A) compared to the normotensive artery.

The model predicts insignificantly increased axial stretch ratio as has also been predicted in [20]. It has been observed that hypertension-induced remodeling of the descending thoracic aorta of dog reduced the *in situ* axial stretch ratio [25]. The axial stretch ratio depends mainly on the axial stress, which in turn depends on the contribution of a) elastin, b) collagen fibers, and c) vascular smooth muscle cells. In the present study we have considered only the circumferential contribution of the VSM cells to the generation of stress. A model for the active axial stress developed by the VSM cells has been proposed recently [26]. Including into the model the active axial stress could reduce the axial stretch ratio.

There are aspects that can affect remodeling, and have not been taken into account in the present study. First, we neglected the contribution of VSM cells to the development of active axial stress, which can affect the axial stretch ratio. Second, we did not consider the multilayer structure of the arterial wall because we modeled the artery as a homogeneous one-layer tube. Third, we assumed that the collagen fibers belong to families with specific orientation (circumferential, axial and at angle $a_{3,4}$). A statistical distribution of fiber orientations would be more realistic [27-28]. Finally, we did not consider the contribution of the different collagen types of the arterial wall.

In conclusion, we performed simulations of adaptive and maladaptive remodeling in response to hypertension with variation of the muscular tone and the

cross-sectional area. The approach is supported by animal models that show that hypertension regulates the production of NO, and thus the vascular tone. There is a pressing need for understanding the mechanisms by which the structural and functional changes occur in the vascular wall. Data from experimental animal models of hypertension that are inspired by vascular solid mechanics, together with theoretical studies can enable development of adequate mathematical models of remodeling and promote better understanding of the physiology and pathophysiology of arteries.

Acknowledgements

This work was supported by the Swiss National Science Foundation (Grant No. 325230-125445).

References

[1] Mulvany MJ, Baumbach GL, Aalkjaer C, et al. Vascular remodeling. Hypertension 1996;28:505-6.

[2] Tsamis A, Stergiopulos N. Arterial remodeling in response to hypertension using a constituent-based model. Am J Physiol Heart Circ Physiol 2007;293:H3130-9.

[3] Fung YC, Biomechanics: Motion, Flow, Stress, and Growth, New York, Springer Verlag, 1990.

[4] Langille BL, Blood Flow-Induced Remodeling of the Artery Wall, In: Bevan JA, Kaley G,Rubanyi GM (eds), Flow-Dependent Regulation of Vascular Function, New York, Oxford University Press, 1995:277-99.

[5] Touyz RM. Molecular and cellular mechanisms regulating vascular function and structure--implications in the pathogenesis of hypertension. Can J Cardiol 2000;16:1137-46.

[6] Heagerty AM, Aalkjaer C, Bund SJ, et al. Small artery structure in hypertension. Dual processes of remodeling and growth. Hypertension 1993;21:391-7.

[7] Deng LY, Schiffrin EL. Effects of endothelin-1 and vasopressin on resistance arteries of spontaneously hypertensive rats. Am J Hypertens 1992;5:817-22.

[8] Thybo NK, Korsgaard N, Eriksen S, et al. Dose-dependent effects of perindopril on blood pressure and small-artery structure. Hypertension 1994;23:659-66.

[9] Nava E, Luescher TF, Hypertension, In: Rubanyi GM (ed), Pathophysiology and Clinical Applications of Nitric Oxide, Amsterdam, Harwood Academic Publishers, 1999:251 - 66.

[10] Risler NR, Cruzado MC, Miatello RM. Vascular Remodeling in Experimental Hypertension. ScientificWorldJournal 2005;5:959-71.

[11] Moncada S. Nitric oxide: discovery and impact on clinical medicine. J R Soc Med 1999;92:164-9.

[12] Fung YC, Liu SQ. Change of residual strains in arteries due to hypertrophy caused by aortic constriction. Circ Res 1989;65:1340-9.

[13] Vaishnav RN, Vossoughi J. Residual stress and strain in aortic segments. J Biomech 1987;20:235-9.

[14] Peterson LH, Jensen RE, Parnell J. Mechanical Properties of Arteries in Vivo. Circulation Research 1960;8:622-39.

[15] Rachev A, Taylor WR, Vito RP. Calculation of the Outcomes of Remodeling of Arteries Subjected to Sustained Hypertension Using a 3D Two-Layered Model. Ann Biomed Eng 2013;41:1539-53.

[16] Wagner HP, Humphrey JD. Differential passive and active biaxial mechanical behaviors of muscular and elastic arteries: basilar versus common carotid. J Biomech Eng 2011;133:051009.

[17] Rachev A. A Model of Arterial Adaptation to Alterations in Blood Flow. Journal of Elasticity 2000;61:83-111.

[18] Gleason RL, Dye WW, Wilson E, et al. Quantification of the mechanical behavior of carotid arteries from wild-type, dystrophin-deficient, and sarcoglycan-delta knockout mice. J Biomech 2008;41:3213-8.

[19] Zarins CK, Zatina MA, Giddens DP, et al. Shear stress regulation of artery lumen diameter in experimental atherogenesis. J Vasc Surg 1987;5:413-20.

[20] Tsamis A, Stergiopulos N, Rachev A. A structure-based model of arterial remodeling in response to sustained hypertension. J Biomech Eng 2009;131:101004.

[21] Cornwell TL, Arnold E, Boerth NJ, et al. Inhibition of smooth muscle cell growth by nitric oxide and activation of cAMP-dependent protein kinase by cGMP. Am J Physiol 1994;267:C1405-13.

[22] Murrell GA, Jang D, Williams RJ. Nitric oxide activates metalloprotease enzymes in articular cartilage. Biochem Biophys Res Commun 1995;206:15-21.

[23] Feliciano L, Henning RJ. Coronary artery blood flow: physiologic and pathophysiologic regulation. Clin Cardiol 1999;22:775-86.

[24] Carew TE, Patel DJ. Effect of tensile and shear stress on intimal permeability of the left coronary artery in dogs. Atherosclerosis 1973;18:179-89.

[25] Vaishnav RN, Vossoughi J, Patel DJ, et al. Effect of hypertension on elasticity and geometry of aortic tissue from dogs. J Biomech Eng 1990;112:70-4.

[26] Agianniotis A, Rachev A, Stergiopulos N. Active axial stress in mouse aorta. J Biomech 2012;45:1924-7.

[27] Gasser TC, Ogden RW, Holzapfel GA. Hyperelastic modelling of arterial layers with distributed collagen fibre orientations. Journal of the Royal Society Interface 2006;3:15-35.

[28] Agianniotis A, Rezakhaniha R, Stergiopulos N. A structural constitutive model considering angular dispersion and waviness of collagen fibres of rabbit facial veins. Biomed Eng Online 2011;10:18.

Summary, conclusions and perspectives

SUMMARY, CONCLUSIONS AND PERSPECTIVES

Cardiovascular diseases, such as hypertension and atherosclerosis, contribute to the morbidity and mortality worldwide. Local mechanical factors are supposed to play a significant role in the initiation and development of cardiovascular diseases. Increased knowledge of the vascular mechanics in both physiological and pathological vascular tissue could help a) comprehend the way through which the mechanical environment affects the adaptation of the vascular tissue under healthy and diseased conditions, b) suggest approaches for the prevention of development of cardiovascular diseases, and c) develop suitable treatment approaches.

The aim of the thesis is to contribute to the field of biomechanics, with particular focus on providing experimental data and modeling the arterial wall based on the organization of the components of the wall that include elastin, collagen, and vascular smooth muscle. The level of the vascular smooth muscle tone has been supposed to be an important parameter in vascular remodeling. The majority of prior theoretical studies have considered the development of active stress only in the circumferential direction when the vascular smooth muscle cells are stimulated to contract. There are experimental observations, however, that vascular smooth muscle tone produces active stress in both the circumferential and axial direction. We have experimentally verified the development of active axial stress in the wall of mouse aorta. Further, we proposed a method for the calculation of the active stresses in the circumferential and axial directions. We found that the active axial stress is smaller than the active circumferential stress. This might be explained by the fact that most of the vascular smooth muscle cells are oriented in the circumferential direction. Our findings show that the active axial stress depends mainly on the axial stretch ratio. The dependence is non-monotonic and is similar to the stretch-stress dependence in circumferential direction. Further, we found that the axial stretch ratio below which no active axial stress is developed is higher than the corresponding stretch ratio that refers to the development of circumferential active stress. This could be explained by the different arrangement of the contractile filaments within the muscular cells, a specific connection of the smooth muscle cells to the extracellular matrix fibers, or the relative number of cells oriented in circumferential or axial direction.

In the present thesis we analyzed the mechanical properties of the aorta of apolipoprotein E-deficient mice. We found that the distensibility of the mouse aortas

decreased monotonically with pressure, which suggests that the collagen fibers are recruited at lower pressure in (apoE)-deficient mouse arteries than in the control arteries. We also found that the Hudetz incremental elastic modulus of the (apoE)-deficient mouse aortas was greater compared to control values. Further, we analyzed the differences in vascular smooth muscle mechanics between control and (apoE)-deficient mice. We found that the active diameter response was lower in the (apoE)-deficient mouse arteries in agreement with findings in the literature. This finding could be explained by the change in the contractile function of the vascular smooth muscle cells, a different proportion of synthetic and contractile cell phenotype, and a possibly stiffer extracellular matrix in the (apoE)-deficient mouse arteries which might limit the contractility of the muscle cells. We also found differences in the collagen content and the density of the vascular smooth muscle nuclei between control and (apoE)-deficient mouse aortas.

In the third part of this thesis we proposed a novel structure-based model for the passive behavior of the arterial tissue. The arterial tissue is considered as a constrained mixture of two groups of elastin, collagen and smooth muscle cells. The model considers the link between one group of elastin and vascular smooth muscle cells. Each constituent has individual zero-stress configuration. The zero-stress configuration of the mixture is the result of locally self-equilibrated stresses borne by the two parts of elastin due to the different strains that they experience. We proposed a method to quantify the prestretch ratios of the wall constituents by using data from normal and decellularized arteries. The model suggests that the prestretch ratios of the constituents are constant across the wall thickness; thus, they do not affect the homogenization of the stress distribution in the arterial wall, and ensure the optimal performance of arteries as thick-wall structures that bear loads.

The final part of this thesis is about remodeling of arterial tissue in response to hypertension. An adaptive response manifests as preservation of the normotensive deformed diameter, change in residual strains and axial stretch ratio, and thickening of the arterial wall, such that tensile wall stress and the flow-induced shear stress remain at baseline values. A maladaptive response is characterized by the incomplete restoration of the baseline mechanical environment, and could result from a variety of dysfunctional processes. The approach followed in this work is supported by animal models that show that hypertension regulates the production of the vasodilator nitric oxide, and thus the vascular tone. The simulations showed that the maladaptive response of the artery to hypertension results in values of thickness and inner radius of the zero-stress configuration and deformed inner radius that are

below the values of adaptive response. Further, the values of maladaptive remodeling drop with increase of the vascular smooth muscle tone. Due to geometrical changes, the Peterson's modulus increases, indicating a structural stiffening of the artery.

In this thesis we have made considerable improvements over previous theoretical and experimental investigations. First, we described experimentally the active stress developed by the vascular smooth muscle cells under isometric conditions, and proposed an analytical expression for the active stress component in axial direction. Second, we quantified the dysfunction of the aortic wall, determined structural and elastic properties and provided histological data of thoracic aortas of apolipoprotein E-deficient mice. Third, we proposed a method to quantify the prestretch ratios of the wall constituents by using data of normal and decellularized arteries, and we proposed a model that considers the bonding of part of the wall elastin with the vascular smooth muscle cells. Fourth, we performed theoretical simulations of maladaptive remodeling in response to hypertension, and evaluated the relative importance of certain geometrical and mechanical factors in the remodeling response of the artery.

Several limitations have been addressed throughout the chapters. Aspects that could constitute a follow-up of this work are the following. First, a statistical distribution of collagen fiber orientation and undulation would be more realistic. Second, future theoretical models and experimental investigations should consider the effect of different collagen types in the arterial wall. Third, future theoretical models could take into account the multi-layer structure of the arterial wall. Fourth, future experimental investigations could include imaging of the smooth muscle cells and extracellular matrix fibers in the passive state of the muscle cells and when they are stimulated to contract. Fifth, the vascular smooth muscle cells might be bonded to other arterial wall constituents in addition to elastin. Sixth, growth factors involved in the remodeling of the arterial wall could be considered in future models. Seventh, the contribution of the vascular smooth muscle cells in their relaxed state could be taken into account. Finally, the mathematical models proposed in this thesis could be introduced in a finite element context; this would allow for structure-based analysis of geometrically complicated cases in health and disease, for example in studying the formation of aneurysms.